Check for updates

Small

NANO · MICRO small
www.small-journal.com

REVIEW

Enhancing Thermal Stability of Perovskite Film for durable Solar Cells

Hao Huang[1] | Meng Wan[1] | Jingyuan Zhang[1] | Hanlin Xiong[1] | Jinxi Zheng[1] | Guanggen Zeng[2] | Shengqiang Ren[2] | Peng Cui[1] | Meicheng Li[1]

[1]State Key Laboratory of Alternate Electrical Power System with Renewable Energy Sources, School of New Energy, North China Electric Power University, Beijing, China | [2]College of Materials Science & Engineering and Engineering Research Center of Alternative Energy Materials & Devices Ministry of Education Sichuan University, Chengdu, China

Correspondence: Meicheng Li (mcli@ncepu.edu.cn)

Received: 30 December 2025 | **Revised:** 16 April 2026 | **Accepted:** 15 May 2026

Keywords: heat | ion migration | PSCs | thermal stability | thermal stress

ABSTRACT

The practical application of metal halide PSCs (PSCs) is badly impeded by their long-term stability concerns, with the issues primarily rooted in the perovskite film. In real-service environments, PSCs endure multiple external factors, light, heat, humidity, and oxygen. Among them, thermal instability represents a particularly severe and fundamental challenge, since heat acts not only as a direct degradation driver but also as a potent accelerator of other degradation pathways. Herein, this review discusses the thermal degradation mechanisms of perovskite from the perspectives of phase transition, materials decomposition, thermal stress, passivation failure and thermal coupled effect, with the latter two aspects emphasized. Then, the review outlines the effective strategies for enhancing the thermal stability of perovskite film and corresponding solar cells, including A-site cation component engineering, crystal facet engineering, dimensional engineering, stress regulation and ion migration inhibition. Finally, perspectives on the future researches for advancing the development of thermally stable devices are proposed, aiming to offer referable routes for accelerating the PSCs industrialization.

1 | Introduction

The development and industrialization of cost-efficient photovoltaic technologies serve as the core pillar for advancing global energy transition and addressing environmental and energy challenges, with metal halide PSCs (PSCs) emerging as the spotlight in next-generation photovoltaic technologies [1–5]. Since the first report of PSCs in 2009, the power conversion efficiency has surged from the initial 3.8% [6] to 27.2% [7], which is comparable to the highest efficiency of silicon-based solar cells [8]. Furthermore, PSCs are transitioning from the laboratory stage to industrialization, achieving breakthrough progress in area scaling (with a PCE of 24% for 100 cm^2) [9] and high-efficiency perovskite/silicon tandem solar cells (with a PCE exceeding 34%) [10], demonstrating enormous commercialization potential. However, the long-term stability of PSCs has become a core bottleneck restricting their practical applications. Although significant progress in stability enhancement has been achieved by researchers through various strategies such as component regulation [11], interface engineering [12] and encapsulation optimization [13], there remains a substantial gap from the long-term reliability requirements imposed by the industry on commercial devices.

During the actual operation, the device temperature can rise to 60°C–85°C or even higher (70°C measured in Chania, Greece [14], 76.8°C (Baghdad, Iraq) [15] and even 85°C–95°C measured in Arizona, the United States of American [16, 17]). Significant diurnal temperature swings also occur, ranging from 0°C to 70°C in the southern U.S. desert [18] and from 5°C to 50°C in Sede Boker,

All rights reserved, including rights for text and data mining and training of artificial intelligence technologies or similar technologies.
© 2026 Wiley-VCH GmbH

Israel [19]. This temperature range triggers thermal degradation processes of perovskite materials, including the volatilization of organic cations, migration of halide ions, phase transition of crystal structures and interfacial reactions with charge transport layers. Meanwhile, in practical operation, the high-temperature environment can further couple with UV illumination, humidity, electric fields and other factors, significantly accelerating the degradation of perovskite materials and devices. The direct and indirect working effects of heat on perovskites render it a critical factor governing the stability of PSCs. Regarding the thermal stability, Zai et al. integrated wafer-scale continuous monolayer molybdenum disulfide (MoS_2) buffer layers on both the top and bottom of the perovskite layer, endowing the device with an efficiency decay of less than 4% after continuous operation at 85°C for 1200 h [20]. Li et al. combined the ultrahigh rigidity of graphene with the excellent flexibility of polymers, integrating polymers and graphene on the surface of perovskite films to regulate strain. The resultant devices retained more than 97% of their initial efficiency after continuous illumination under AM 1.5G solar light at 90°C for over 3670 h [21]. In the research on PSC stability, despite rapid progress in thermal stability enhancement, a critical gap remains between laboratory-scale results and industrial qualification benchmarks. As for the industrial standards represented by IEC 61646 that involves combined heat-humidity-cycling stresses (85°C/85% RH, 1000 h) that closely mimic real outdoor environments, the importance of thermal stability lies not only in its direct impact on the long-term reliability of devices but also in its coupling with other factors, forming a "thermal acceleration effect" [22–24]. Furthermore, in novel structures such as perovskite-silicon tandem solar cells, the mismatch in thermal expansion coefficients between the perovskite layer and the silicon substrate under high-temperature conditions can further induce interfacial defects and mechanical stress, exacerbating device performance degradation [25]. Therefore, systematic and in-depth research of thermal degradation mechanism of perovskite film and PSCs, and development of targeted strategies hold irreplaceable core value for advancing their commercialization.

In this review, we systematically summarize the recent in-depth investigation into the thermal degradation mechanisms and the effective strategies for enhancing the device thermal stability. To establish a clear and industrially relevant descriptor for long-term operational durability, this review defines durable PSCs as devices that retain more than 80% of their initial performance for at least 1000 h under continuous operation at approximately 85°C. According to recent quantitative correlations between laboratory accelerated aging and outdoor field behavior, the actual operating temperature of PSCs under service can reach 40°C–50°C above ambient temperature, indicating that 85°C represents a representative condition capable of reflecting realistic operational lifetime. As presented in Figure 1, the review begins with a brief introduction to the basic physical properties of metal halide perovskite materials and their superb application in photovoltaics; then, the thermal degradation mechanisms of perovskite film from the perspective of phase transition, film decomposition, thermal strain, thermal induced passivation failure and thermal coupled effect are discussed. Following that, we outline the effective strategies for enhancing the thermal stability of perovskite film and corresponding solar cells, including A-site cation component engineering, crystal facet engineering, dimensional engineering,

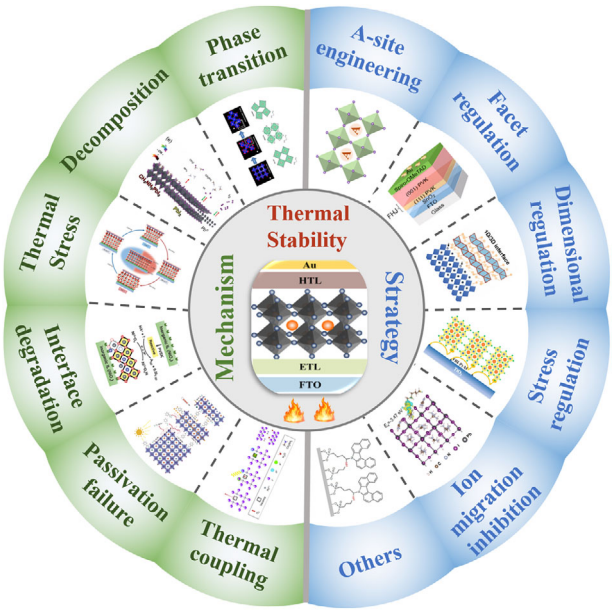


FIGURE 1 | Schematic summary of perovskite thermal degradation mechanism and corresponding enhancement strategies.

stress regulation, ion migration inhibition. Finally, we provide our insight and perspective on future research regarding how to advance the thermally stable device. We expect this review to provide a comprehensive discussion and shed new light on prospective research directions for enhancing the PSCs' thermal stability, thus laying a solid theoretical foundation to accelerate the commercialization of perovskite-based devices.

2 | Brief Introduction to Perovskite Materials and Solar Cells

Perovskite, a mineral first identified in the Ural Mountains of Russia in 1839 by the German mineralogist Gustav Rose, is named after the Russian mineralogist Lev Perovski [26]. In contemporary materials science, the term "perovskite" broadly encompasses compounds crystallizing in the ABX_3 structure. Among them, metal halide perovskites, exemplified by formamidinium lead iodide ($FAPbI_3$), have emerged as a preeminent class of semiconductors for photovoltaics. This prominence is attributed to their exceptional optoelectronic properties, including high absorption coefficients, low exciton binding energies, long charge carrier diffusion lengths, and widely tunable bandgaps [27]. Consequently, PSCs have undergone rapid development, with device architectures diversifying to single-junction, tandem, ultra-thin flexible, bifacial configurations and so on. Remarkable progress has been made in PCE with current certificated value more than 27% [7], showcasing significant industrialization application potential.

2.1 | Fundamental Crystal Structure of Perovskites

As illustrated in Figure 2a, the prototypical perovskite structure adopts an ideal cubic phase (space group *Pm-3m*). This structure exhibits notable composition flexibility. The A-site is

16136829, 0, Downloaded from https://onlinelibrary.wiley.com/doi/10.1002/smll.202514991 by Meicheng Li - North China Electric Power University Beijing , Wiley Online Library on [25/05/2026]. See the Terms and Conditions (https://onlinelibrary.wiley.com/terms-and-conditions) on Wiley Online Library for rules of use; OA articles are governed by the applicable Creative Commons License

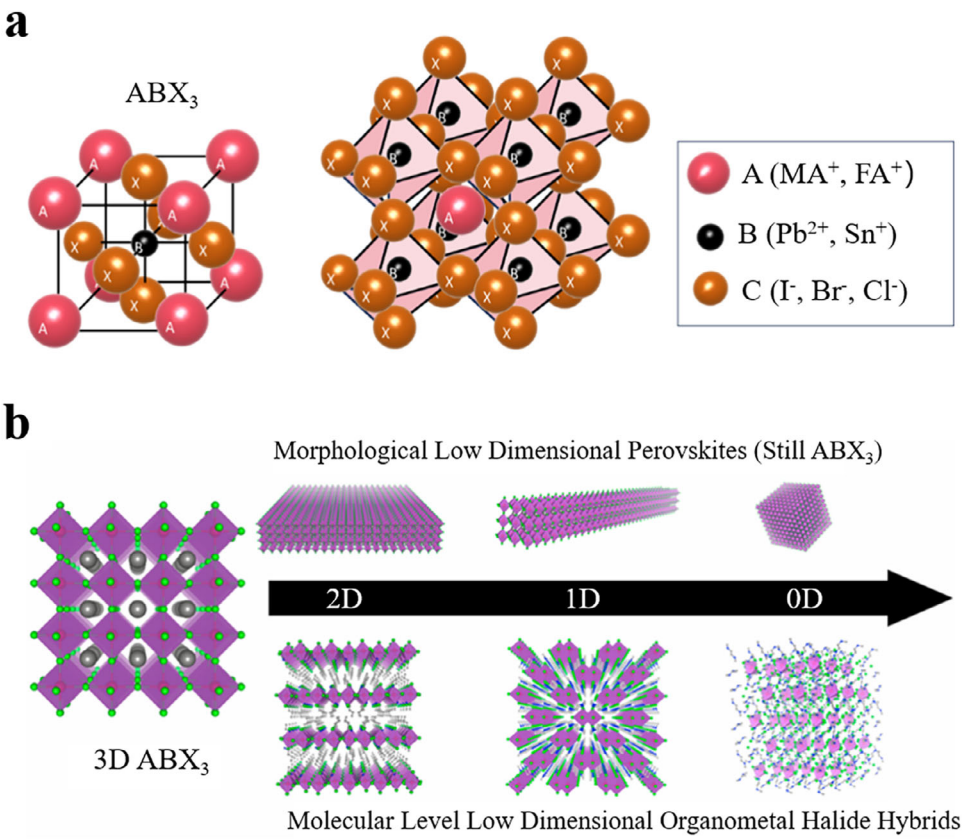


FIGURE 2 | (a) The crystal structure of perovskite. (b) Crystal Structures of perovskites with different dimensions. Reproduced with permission [30]. Copyright 2019, Elsevier.

occupied by a monovalent cation, which can be organic (e.g., methylammonium, MA^+; formamidinium, FA^+) or inorganic (e.g., Cs^+). The B-site hosts a divalent metal cation, typically Pb^{2+} or Sn^{2+}. The X-site is normally filled by halide anions (I^-, Br^-, Cl^-). The crystal framework is built from corner-sharing $[BX_6]4^-$ octahedra, forming a 3D network. The A-site cations reside in the cuboctahedra cavities formed by this network, providing structural stability [28]. However, this 3D network is susceptible to distortion under external stimuli. Temperature variations, in particular, can induce transitions from the high-symmetry cubic phase to lower-symmetry tetragonal or orthorhombic structures, often accompanied by degradation of optoelectronic properties. The structural stability of the ABX_3 perovskite is commonly assessed by the Goldschmidt tolerance factor (t) and it is defined as below.

$$t = \frac{r_A + r_X}{\sqrt{2}(r_B + r_X)} \quad (1)$$

In the above equation, r_A, r_B, and r_X are the effective ionic radii of the respective ions. A t value in the range of 0.8 to 1 favors the formation of the ideal cubic phase. It is suggested that elevated temperatures can exacerbate lattice thermal expansion and atomic vibrations, altering effective ionic radii and promoting structural distortion and phase instability.

Additionally, perovskites exhibit a certain degree of structural versatility, which enables deliberate dimensional engineering. The structures of different dimensions of perovskites are shown in Figure 2b. Incorporating large, bulky organic cations can disrupt the 3D network, yielding low-dimensional derivatives. 2D perovskites feature layered structures where inorganic octahedral sheets are separated by organic spacers, creating natural quantum wells with enhanced environmental stability and tunable optoelectronic properties. 1D perovskites consist of chains of edge- or corner-sharing octahedra, exhibiting anisotropic charge transport useful for specialized optoelectronics. When isolated $[BX_6]4^-$ octahedra are fully surrounded by organic ligands, 0D perovskite quantum dots are formed. Due to their superior moisture resistance and thermal stability, low-dimensional perovskites are frequently employed as passivating layers or components in composite structures to enhance the performance and durability of 3D perovskite-based devices [29, 30].

2.2 | Optoelectronic Properties of Perovskites

The distinctive crystal structure of perovskite confers exceptional optoelectronic characteristics. First, perovskites are direct-bandgap semiconductors, indicating the valence band maximum and conduction band minimum are aligned in momentum space, which facilitates efficient photon absorption and carrier generation. Coupled with their tunable bandgap achieved via cation alloying or halide mixing, perovskites exhibit broad and strong light absorption. This allows for the fabrication of highly efficient light-harvesting layers with thicknesses of only a few hundred nanometers, enabling lightweight and flexible device architectures [31]. In particular, precise bandgap tunability

16136829, 0, Downloaded from https://onlinelibrary.wiley.com/doi/10.1002/smll.202514991 by Meicheng Li - North China Electric Power University Beijing , Wiley Online Library on [25/05/2026]. See the Terms and Conditions (https://onlinelibrary.wiley.com/terms-and-conditions) on Wiley Online Library for rules of use; OA articles are governed by the applicable Creative Commons License

is advantageous for constructing high-efficiency tandem solar cells.

Second, perovskites demonstrate excellent photoluminescence quantum yields and low non-radiative voltage losses, indicative of their innate potential for high-performance optoelectronics. This stems from their favorable defect physics and electronic structure. The corner-sharing $[BX_6]4^-$ octahedral network facilitates highly dispersive band edges, leading to small effective masses and high charge carrier mobilities. Crucially, many intrinsic point defects in perovskite form shallow energy levels within the bandgap. Carriers trapped at shallow defects can be thermally released back to the band edges, thereby suppressing non-radiative recombination [32]. This property is often termed intrinsic defect tolerance, which is a key factor enabling high photovoltaic efficiencies. The synergistic combination of strong and tunable absorption with efficient emission underpins the remarkable performance of perovskite optoelectronics.

These properties, attainable via low-temperature, solution-processable methods on diverse substrates, have not only driven progress in photovoltaics but also enabled novel applications such as semi-transparent solar cells, colored glazing in building integrated photovoltaic, indoor photovoltaics, and integrated light-emitting devices.

2.3 | PSCs

PSCs are a revolutionary thin-film photovoltaic technology whose active layer is based on organic-inorganic hybrid perovskite semiconductors. A typical device stack comprises a transparent conductive oxide (TCO) front electrode, an electron transport layer (ETL), the perovskite absorber, a hole transport layer (HTL), and a metal back contact. The meteoric rise of PSCs, from an initial efficiency of less than 4% [6] at the beginning to certified values exceeding 27% [7] today, is a direct consequence of the outstanding material properties of perovskites.

The field of PSCs is currently characterized by intensive innovation across multiple fronts. Architecturally, extensive research is being pursued on both regular (n-i-p) and inverted (p-i-n) device configurations, alongside sophisticated tandem structures [33, 34]. From an application standpoint, the low-temperature fabrication process, compatibility with flexible substrates, and potential for transparency are paving the way for transformative applications beyond conventional rigid panels, including lightweight portable chargers, building-integrated components, internet-of-things power sources and so on.

Despite these extraordinary advances, the pathway to widespread commercialization is still impeded by long-term stability concerns [35]. Under real-world conditions, devices are subjected to a complex interplay of stressors including light, heat, humidity, and oxygen, leading to rapid performance degradation. Among these, thermal instability represents a particularly severe and fundamental challenge. Heat acts not only as a direct degradation driver—inducing phase transitions, ion migration, and chemical decomposition—but also as a potent accelerator of other degradation pathways. Therefore, a comprehensive understanding of thermal instability and its coupling with other factors is paramount for developing commercially viable PSCs. This review aims to systematically analyze the mechanisms of thermal degradation and summarize corresponding mitigation strategies.

3 | Mechanisms of Thermal Induced Perovskite Degradation

The poor thermal stability of PSCs badly hinders their commercialization, representing an issue that urgently needs to be addressed in the current field [36]. The origins of thermal instability are complex, constituting a multi-faceted problem involving physics and chemistry, and interacting with factors such as light, moisture, and oxygen. A thorough understanding of its mechanisms is crucial for developing effective solutions.

As an ionic compound, perovskite materials possess low ionic bond energy, which lies at the root of their thermal instability. The weak binding between ions facilitates ion migration, leading to lattice distortion, phase transition, and ultimately material degradation. External temperature fluctuations, ion migration from other functional layers within the device, and cracks induced by internal stress in the perovskite material can all accelerate the above processes. Hence, this section will systematically analyze the thermally-induced degradation mechanisms of perovskite materials and devices. In particular, we will focus on the stability mechanisms under the coupling of heat and other factors, as this represents the actual scenario in real-world applications (Figure 3).

3.1 | Phase Transition

In general, 3D perovskite exhibit the α phase, β phase, γ phase, and δ phase. The Table 1 summarizes the properties and characteristics of the phases mentioned above. The α phase is normally regarded as the most desirable perovskite structure for photovoltaics. In this phase, the $[BX_6]4^-$ octahedra shares vertices in a well-ordered arrangement, resulting in high symmetry and weak anisotropy. These structural features contribute to its excellent photovoltaic performance. As the $[BX_6]4^-$ octahedra undergoes cooperative tilting and rotation, it turns into β and γ phases which exhibit lower symmetry and inferior optoelectronic performance. In the δ-phase, the connection pattern of the octahedra changes, which results in a noticeably widened bandgap and a significant decline in optoelectronic performance.

As for the classical metal halide perovskite of $MAPbI_3$, its stable phase at room temperature is the tetragonal phase (I4/mcm). This phase features an inorganic framework with out-of-phase octahedral tilting and the continuous reorientation of the MA^+ cations inside the framework. Upon heating to approximately 57°C, the decrease in structural order and increase in entropy drive the transformation to the cubic phase (Pm-3m) (Figure 4a) [37]. According to density functional theory (DFT) calculations, the phase transition sets in as the tilting of the inorganic $[PbI_6]4^-$ framework eases, followed by the reorientation of the organic MA^+ cations. During this process, hydrogen bonding between the organic cation and the halogens modulates the octahedral tilt angle, which in turn influences the orientation and binding

16136829, 0, Downloaded from https://onlinelibrary.wiley.com/doi/10.1002/smll.202514991 by Meicheng Li - North China Electric Power University Beijing , Wiley Online Library on [25/05/2026]. See the Terms and Conditions (https://onlinelibrary.wiley.com/terms-and-conditions) on Wiley Online Library for rules of use; OA articles are governed by the applicable Creative Commons License

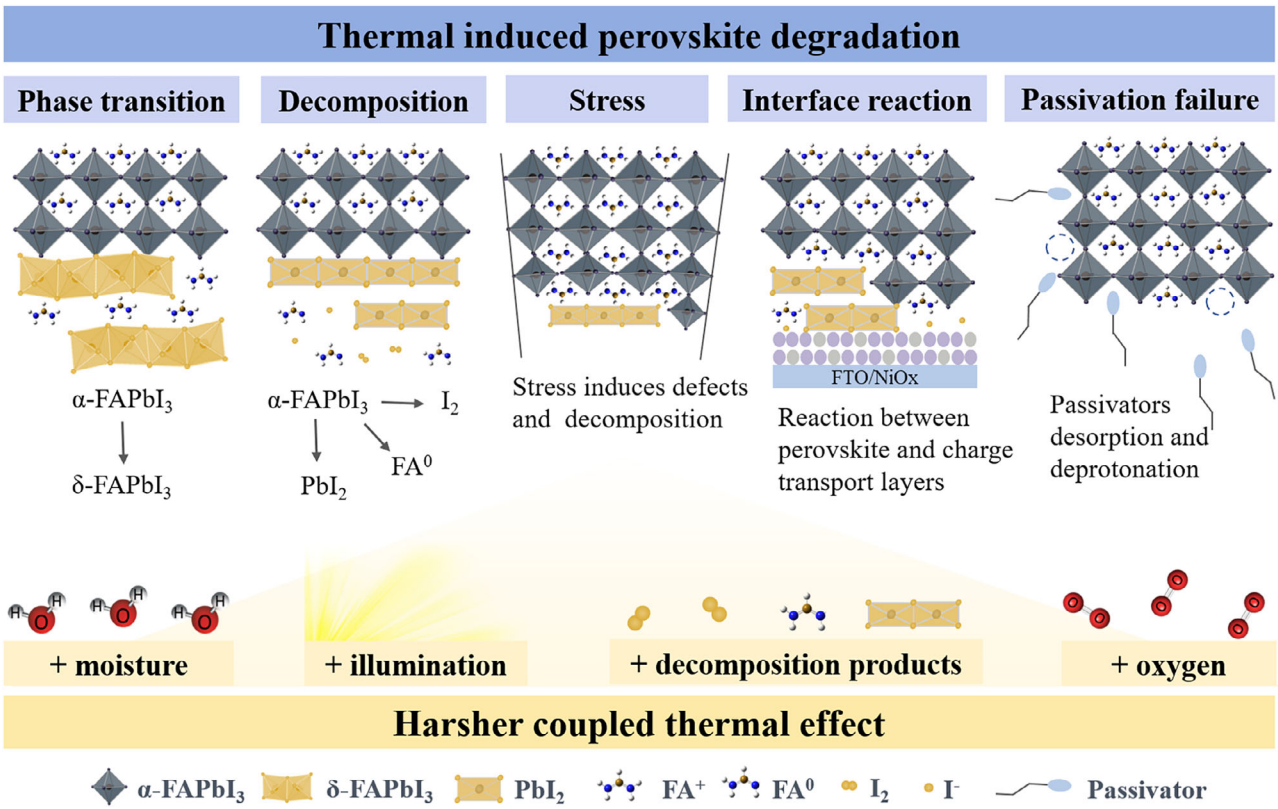


FIGURE 3 | The illustration of thermal degradation mechanisms of perovskite films

TABLE 1 | The phases of perovskite.

	α phase	β phase	γ phase	δ phase
Crystal structure	Cubic	Tetragonal	Orthorhombic	Hexagonal
Symmetry	High	Relatively high	Relatively low	Low (non-perovskite phase)
$[BX_6]4^-$	Corner-sharing,	Slightly distorted, corner-sharing	Severely distorted, corner-sharing	Edge-sharing or even face-sharing
Bandgap	1.5–1.6 eV	larger than α phase	Larger than β phase	>2 eV
Optoelectronic properties	Superior	Moderate	Inferior	Poor

state of MA^+, thereby governing the transition pathway and energy barrier [38]. Figure 4b reveals that inverse participation ratio (IPR) values of both electron and hole increase, indicating higher charge carrier localization in the higher-temperature phases [39]. This phase and temperature-dependent localization suggests that charge transport is impeded due to reduced mobility, ultimately compromising charge collection efficiency and device performance.

Regarding to the popular absorber of $FAPbI_3$ in current research, its phase transition mechanism differs significantly from that of $MAPbI_3$ due to the larger ionic radius of the FA^+ cation (~253 pm). Such a large size raises the tolerance factor slightly above 1 [40]. Consequently, $FAPbI_3$'s thermodynamically stable phase at room temperature is the hexagonal δ phase, which is not photoactive. In contrast, the photoactive black α-phase (cubic/trigonal) is metastable and resides at a higher energy level (Figure 4c). Although the α phase possesses higher internal energy ($H_\alpha > H_\delta$), the disordered rotation of FA^+ contributes substantial entropy ($S_\alpha >> S_\delta \approx 0$). This entropic contribution ($-TS_\alpha$) overwhelmingly lowers G_α, thereby stabilizing the α-phase. At lower temperatures, about 165°C [97], the entropic term diminishes, making the δ-phase with its lower enthalpy (G_α) the thermodynamically stable phase, which drives the α→δ transition. Common point defects such as iodine interstitials create low-energy pathways for atomic rearrangement, significantly lowering the activation energy and accelerating the transformation (Figure 4d) [41]. Thermal-expansion mismatch and internal stress gradients can also directly drive the α→δ transition.

16136829, 0, Downloaded from https://onlinelibrary.wiley.com/doi/10.1002/smll.202514991 by Meicheng Li - North China Electric Power University Beijing , Wiley Online Library on [25/05/2026]. See the Terms and Conditions (https://onlinelibrary.wiley.com/terms-and-conditions) on Wiley Online Library for rules of use; OA articles are governed by the applicable Creative Commons License

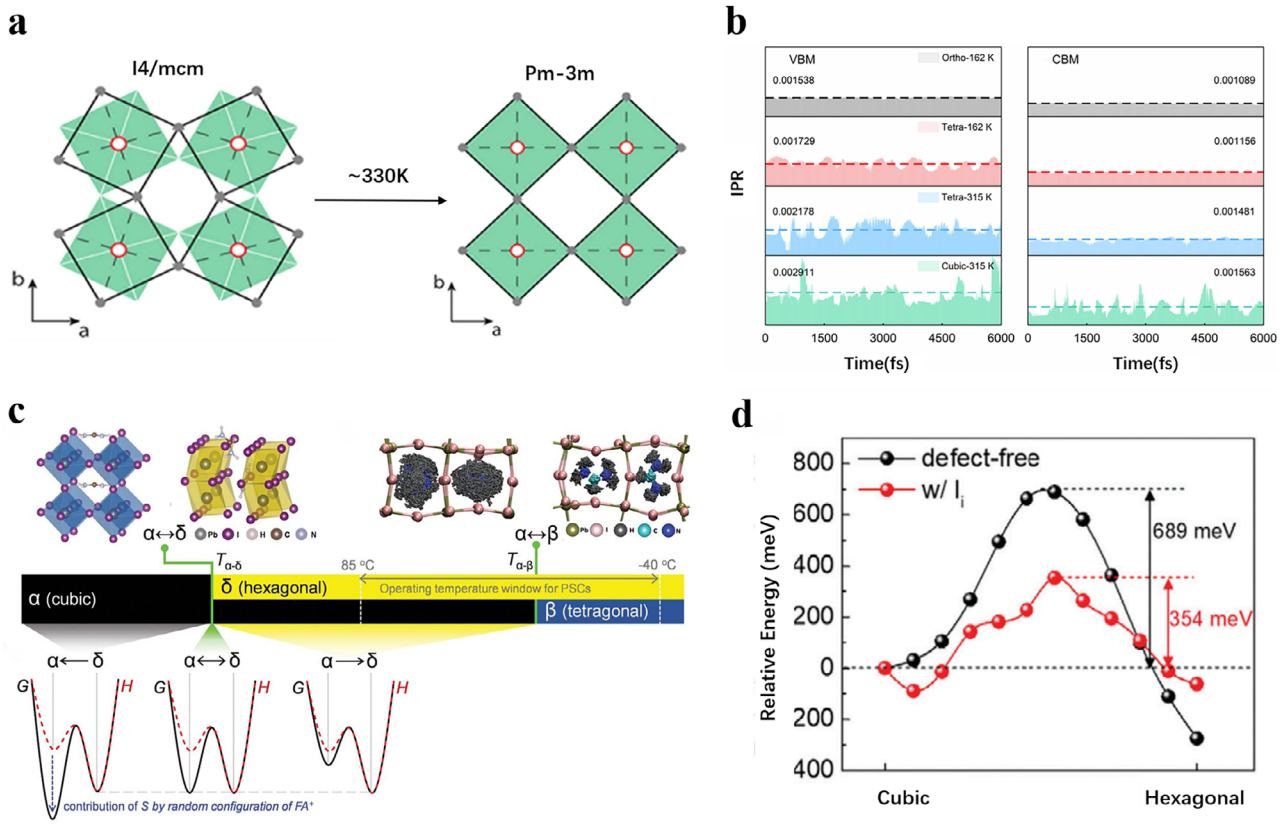


FIGURE 4 | (a) Continuous phase transitions from the tetragonal phase (I4/mcm, ≈160-330 K) to the cubic phase (Pm3m, >330 K). Adapted under the terms of the CC-BY 4.0 license [37]. Copyright 2016, P. S. Whitfiel et al. (b) Evolution of the inverse participation ratio (IPR) for VBM and CBM in the Ortho-162 K, Tetra-162 K, Tetra-315 K, and Cubic-315 K $MAPbI_3$ systems. Reproduced with permission [39]. Copyright 2022, American Chemical Society. (c) Schematic illustration of the Gibbs free energy for the α-phase and δ-phase, revealing the physical origin of their stability reversal. The black solid line represents the free energy G, and the red dashed line denotes the enthalpy H [41] (d) Simulated energy barrier for the phase transition from cubic to hexagonal structure depending on the presence of iodine interstitial defects(I_i). Reproduced under the terms of the CC-BY 3.0 license [41]. Copyright 2025, H.-S. Kim et al.

Research on the phase transition pathways and stabilization mechanisms of perovskite materials has achieved systematic understanding, which provides the theoretical feasibility for designing multi-cation perovskite solar cells. Nan et al. successfully isolated and identified the key intermediate phase 8H, whose structure simultaneously contains both corner-sharing and face-sharing $[PbX_6]4^-$ octahedra, integrating multiple structural cage types. The evolution sequence from the photoactive cubic phase (3C, α-phase) to the non-photoactive hexagonal phase (2H, δ-phase) was further revealed to be 3C → 8H → 6H → 4H → 2H. Based on Pauling's rules, smaller halide ions (e.g., Br^-) tend to occupy corner-sharing sites due to repulsive forces, thereby stabilizing the corner-sharing network. Besides, smaller cations (e.g., Cs^+, MA^+) preferentially enter the energetically favorable smaller cubic cages rather than the larger oblate cages due to better size matching [42]. From a kinetic perspective, the essential role of cations in multi-cation systems lies in suppressing the collective rotation of $[PbI_6]4^-$ octahedra. Cs^+ doping induces lattice contraction, which reduces the Pb-I-Pb bond angle, making the large-amplitude rotations necessary to trigger phase transitions more difficult. Concurrently, Cs^+ also restricts the free rotation of FA^+ cations within the lattice voids, confining their orientational dynamics to more localized orientations [43–45].

Halogen atoms also significantly influence phase transitions. Bromine incorporation introduces local lattice strain at the atomic scale, which lowers the formation activation energy for halide vacancies (particularly bromine vacancies). This substantially reduces the energy barrier for material decomposition, making phase transitions more facile. Consequently, the phase transition pathway for bromine-doped samples differs markedly from that of the pure iodide system, in which PbI_2 formation begins at a lower temperature of 100°C, and the decomposition pathway shifts toward the accumulation of PbI_2 rather than the formation of 4H-$FAPbI_3$, indicating that bromine doping reduces thermodynamic phase stability [44].

In a word, heat can directly induce phase transitions in perovskite materials; meanwhile, it can synergistically couple with defects, internal stress and other intrinsic factors to accelerate the phase transition process, complicate the phase transition pathways, ultimately leading to reduced photoactivity of perovskite materials and irreversible device failure. Among these, while the chemical nature of B-site metals and the electronegativity of X-site halides significantly influence the localized chemical environment, the A-site cation acts as the primary determinant of the overall phase equilibrium. For instance, the transition from the photoactive α-phase to the non-perovskite δ-phase in

16136829, 0, Downloaded from https://onlinelibrary.wiley.com/doi/10.1002/smll.202514991 by Meicheng Li - North China Electric Power University Beijing , Wiley Online Library on [25/05/2026]. See the Terms and Conditions (https://onlinelibrary.wiley.com/terms-and-conditions) on Wiley Online Library for rules of use; OA articles are governed by the applicable Creative Commons License

$FAPbI_3$ is intrinsically linked to the rotational entropy and size of the FA^+ cation. Even with the participation of halide ions in modulating the lattice strain, the choice and combination of A-site cations define the fundamental thermodynamic barrier for such phase transitions, effectively setting the upper limit for the film's thermal robustness. Moreover, thermally induced phase transitions usually occur prior to high-temperature driven material decomposition, and this process proceeds at a faster rate than the material degradation caused by long-term defect accumulation and stress build-up. Therefore, elucidating the material degradation mechanisms induced by thermally triggered phase transitions is essential and highly meaningful.

3.2 | Thermal Decomposition

The fundamental cause of thermal decomposition lies in the breaking of chemical bonds. When temperature exceeds a critical threshold, the vibration energy of lattice atoms overcomes the bonds' dissociation energy barrier, causing bond breakage and perovskite degradation.

Taking the classic $MAPbI_3$ as an example, its formation energy is relatively low (0.11–0.14 eV), indicating poor thermal stability. The chemical equation of the perovskite's decomposition process is as follows:

$$CH_3NH_3PbI_3 \xrightarrow{\Delta} PbI_2 + CH_3NH_3I \xrightarrow{\Delta} CH_3NH_2 + HI \quad (2)$$

In this equation, both CH_3NH_2 and HI are volatile species. Under thermal influence, they readily desorb from the lattice and escape from the device (Figure 5a) [46]. According to Le Chatelet's principle, this shifts the chemical equilibrium away from the perovskite phase and instead favors the decomposition pathway. Therefore, upon heating to a certain temperature, PbI_2 can be detected in the perovskite film by XRD, as a decomposition product of $MAPbI_3$ (Figure 5b) [47]. Thermogravimetric analysis also confirms the perovskite decomposition through the release of HI and CH_3NH_2, showing a mass loss of approximately 26% when heated from room temperature to 420°C (Figure 5c) [47]. Consequently, the originally black photoactive perovskite gradually transforms into a yellow non-perovskite phase (PbI_2).

Throughout this process, the continuous outgassing of volatile products repeatedly stresses the stability of the perovskite's cubic framework. The cavities left by the escaping A-site organic cations, the most prone to thermal desorption, directly undermine local support for the $[PbI_6]4^-$ octahedral network, inducing tilting and even collapse. Moreover, the thermal desorption of A-site cations creates vacancy defects, which provides pathways for ion migration, a process that is already sensitive to external factors, and disrupts the bonding network between the organic cations and halide ions. This not only undermine the structural stability but also disrupt the charge balance, causing changes in the local electric field. With the halide ions less constrained, the destabilization of the perovskite is further accentuated [48] Compared with $MAPbI_3$, $FAPbI_3$ exhibits superior thermal stability, which is mainly attributed to the higher intrinsic stability and lower volatility of FA^+ cations. Nevertheless, upon exposure to high temperatures, $FAPbI_3$ undergoes analogous decomposition pathways, demonstrating the relatively universal detrimental effect of heat in triggering direct material decomposition for organic cation-based perovskites.

As for the multi-cation perovskite materials, the thermal degradation is even more complex. The work by Wang et al. indicated that in $FA_{0.9}Cs_{0.1}PbI_3$, the degradation behavior exhibits a distinct transition at approximately 106°C. Detailly, in the low-temperature region (77°C–106°C), the dominant mechanism is the segregation of A-site cations (phase separation) with an activation energy of about 0.96 eV, whereas in the high-temperature region (>106°C), the degradation shifts to perovskite decomposition (phase transition), and the activation energy rises significantly to about 3.01 eV. This finding suggests that the thermal degradation of perovskites possesses a temperature-dependent threshold feature [49].

For more compositionally complex mixed-cation lead mixed-halide perovskites (e.g. $Cs_xFA_{1-x}PbI_\gamma Br_{3-\gamma}$), the thermal degradation process displays an even more refined staging. In the first stage (80°C–160°C), degradation is characterized by the cooperative release of FA^+ and Br^-, which escape predominantly as FABr in an approximate 1:1 ratio. The lattice framework remains intact at this stage, but the loss of Br^- leads to lattice expansion and a slight reduction in the bandgap, while generating a high density of cation and anion vacancies. These defects not only aggravate ion migration and hysteresis effects but also pave the way for subsequent decomposition. In the second stage (160°C-220°C), I^- begins to be lost, and signals of Pb^0 as well as hexagonal-phase PbI_2 impurities appear, resulting in a heavy decomposition. The third stage (220°C-320°C) sees complete depletion of FA^+, with the final products being yellow $CsPbI_{3-z}Br_z$ ($z << 1$) and PbI_2, while no $PbBr_2$ is formed, confirming that Br^- is preferentially lost at an early stage.

The anomalous cooperative release of FA^+ and Br^- originates from the higher electronegativity of Br^-, which strengthens the FA-Br bonding compared to FA-I bonding, thereby making the FABr unit more prone to volatilize as a whole and initiating degradation at relatively low temperatures. In contrast, the bromide-free $Cs_{0.17}FA_{0.83}PbI_3$ shows no significant weight loss below 200 °C, demonstrating superior thermal stability. This directly proves that the incorporation of Br, through its strong coupling with FA^+, becomes a weak link in the stability of this system [50].

In tin halide perovskite, thermal effects have a significant influence on Sn^{2+}. Unlike Pb^{2+}, Sn^{2+} is intrinsically unstable and prone to oxidation to Sn^{4+}. According to the Arrhenius law, a temperature rise drastically lowers the activation energy required for the oxidation of Sn^{2+}, sharply increasing the reaction rate, which can be described as follows:

$$2ASnI_3 + O_2 \xrightarrow{\Delta} SnI_4 + SnO_2 + 2AI \quad (3)$$

$$ASnI_3 + O_2 \xrightarrow{\Delta} I_2 + SnO_2 + AI \quad (4)$$

The Sn^{4+} cannot occupy the B-site in the ABX_3 perovskite crystal structure. The incorporation of Sn^{4+} at the B-site sets up a strong local positive electric field, pulling surrounding I^- ions closer

16136829, 0, Downloaded from https://onlinelibrary.wiley.com/doi/10.1002/smll.202514991 by Meicheng Li - North China Electric Power University Beijing , Wiley Online Library on [25/05/2026]. See the Terms and Conditions (https://onlinelibrary.wiley.com/terms-and-conditions) on Wiley Online Library for rules of use; OA articles are governed by the applicable Creative Commons License

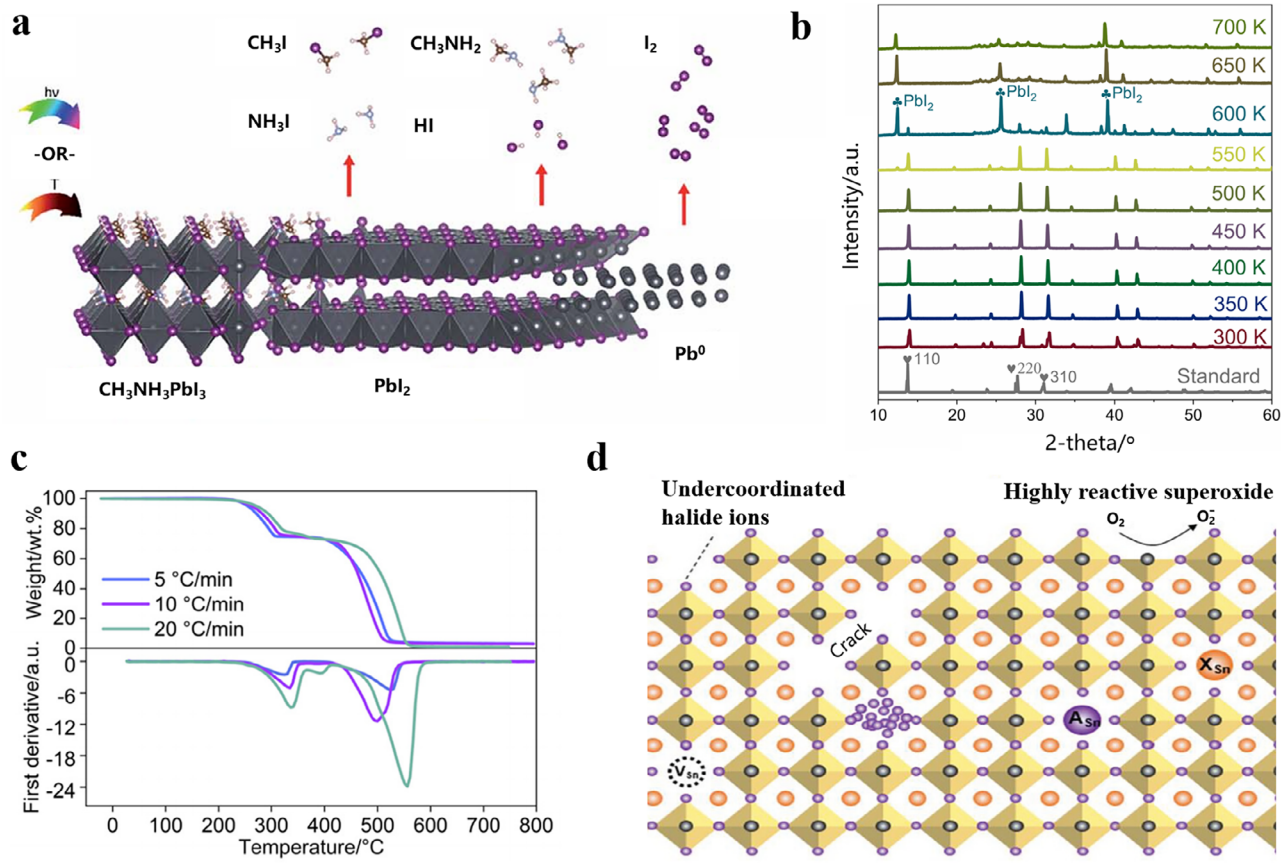


FIGURE 5 | (a) Schematic diagram of $MAPbI_3$ thermal degradation processes. Reproduced under the terms of the CC-BY 3.0 license [46]. Copyright 2018, Juarez-Perez et al. (b) In situ XRD patterns of $MAPbI_3$ at different temperatures [47] (c) Thermogravimetric analysis and the first derivative of analysis curves of heating $MAPbI_3$ with different heating paces. Reproduced with permission [47]. Copyright 2024, Royal Society of Chemistry. (d) Sn vacancies, atomic clusters, and other defects caused by the oxidation of Sn^{2+}. Reproduced with permission [51]. Copyright 2023, John Wiley and Sons.

and distorting the octahedral framework. This oxidation of Sn^{2+} can further generate defects of tin vacancies (V_{Sn}) and iodine interstitials (I_i) to maintain charge balance (Figure 5d). Both this lattice distortion and the presence of defects inevitably accelerate the degradation of the perovskite [51].

3.3 | Thermal Induced Stress

In real-world terrestrial applications, the thermal cycling induced by diurnal temperature fluctuations poses a significant challenge to the long-term durability of PSCs. A fundamental perspective for analyzing the evolution of thermally induced mechanical strain can be divided into interlayer strain and internal strain.

Interlayer strain primarily originates from the significant mismatch in coefficients of thermal expansion (CTE) (Figure 6a) among the constituent functional layers, as well as the relatively low fracture energy at the heterojunction interfaces [52]. During the heating and cooling protocols of device fabrication or operation, the layers undergo disparate degrees of expansion and contraction. Due to strong interfacial coupling, these layers constrain each other, thereby generating pronounced shear and tensile/compressive stresses. As visualized in the stress distribution profiles (Figure 6b,c), the alternation between high (85°C) and low (−40°C) temperature creates significant stress gradients within the perovskite bulk, leading to stress concentration near the interfaces [53]. When the interfacial adhesion is insufficient to withstand the accumulated shear stress, delamination and debonding occur between the layers (Figure 6d–f).

Internal strain also exists within the bulk perovskite. Factors such as the non-uniformity of spin-coating or blade-coating processes, along with suboptimal control over crystallization quality, often lead to microstructural heterogeneities, including non-uniform thickness distributions and localized aggregation. During temperature fluctuations, these structural inhomogeneities induce localized disparities in thermal stress, thereby generating a corresponding internal stress field within the thin film. Once the stress exceeds the elastic limit of the material, irreversible lattice distortions, such as dislocations, slips, and twinning, are triggered. The pronounced hysteresis observed in the stress-temperature hysteresis loop (Figure 6g) precisely originates from the energy dissipation associated with these irreversible processes [54].

During thermal cycling, alternating tensile and compressive stresses continuously act upon the perovskite lattice [55], leading to cumulative and irreversible structural distortions (Figure 6h). When these distortions reach a threshold that disrupts the

16136829, 0, Downloaded from https://onlinelibrary.wiley.com/doi/10.1002/smll.202514991 by Meicheng Li - North China Electric Power University Beijing , Wiley Online Library on [25/05/2026]. See the Terms and Conditions (https://onlinelibrary.wiley.com/terms-and-conditions) on Wiley Online Library for rules of use; OA articles are governed by the applicable Creative Commons License

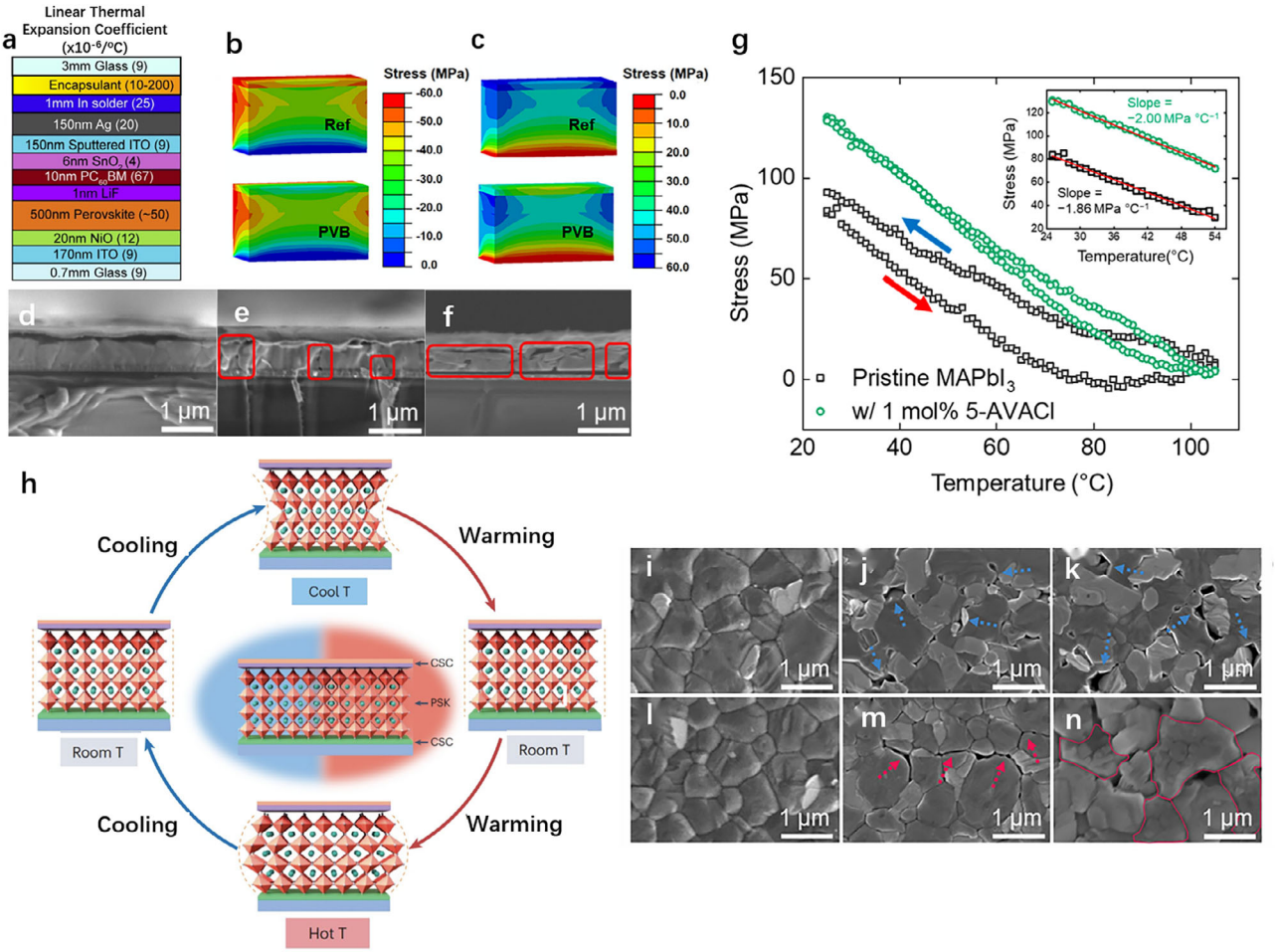


FIGURE 6 | (a) Reported linear thermal expansion coefficients for each layer. Reproduced with permission [52]. Copyright 2018, RCS Publishing. Cross-sectional stress distribution in the perovskite layer at (b) 85°C and (c) −40°C [53] Cross-sectional SEM morphology of the perovskite device under different conditions: (d) as-prepared, (e) after 1000 h at 85°C and (f) after 200 thermal cycles [51] (g) Stress-temperature response curves of $MAPbI_3$ thin films during thermal cycling. The figure shows the evolution of biaxial stress in the film during thermal cycles between 25°C and 105°C. Reproduced with permission [54]. Copyright 2024, American Chemical Society. (h) Schematic of perovskite lattice response to thermal cycling in devices. Periodic heating/cooling generates stress, causing lattice expansion and stretching. Reproduced with permission [55]. Copyright 2025, Nature Research. SEM images of films after thermal aging test at 85°C for (i) 0 h, (j) 500 h and (k) 1000h. SEM morphology after thermal cycling test for (l) 0 cycle, (m) 100 cycles and (n) 200 cycles. Reproduced under the terms of the CC-BY 3.0 license [53]. Copyright 2024, S. Ma et al.

long-range order of the $[BX_6]4^-$ octahedral frameworks, phase transitions are induced, such as the transformation from the photoactive cubic phase to the photo-physically inferior tetragonal or orthorhombic phases. Simultaneously, persistent stress directly triggers the formation of high-density defects and promotes the evolution of inherent weak regions, such as grain boundaries and voids, into pinholes and microcracks. As illustrated in Figure 6i–k, during isothermal aging at 85°C, both the density and dimensions of pinholes increase progressively with aging time. Conversely, Figure 6l,m demonstrate the formation of observable microcracks after 100 thermal cycles [51]. These cracks continuously propagate and interconnect until they penetrate the entire film. Such structural degradation not only impedes charge carrier transport and compromises device performance but, more critically, creates direct pathways for the ingress of moisture and oxygen, thereby drastically accelerating the chemical decomposition of the perovskite material.

3.4 | Interfacial Degradation

The impact of thermal stress on perovskite stability extends beyond the direct weakening of internal chemical bonds, more critically, it significantly lowers the activation energy for interfacial reactions, leading to the interfacial degradation. This acceleration of chemical interactions between the perovskite layer and adjacent functional layers, such as charge transport layers, poses a severe threat to the overall device stability. Its fundamental role is to act as an external perturbation that accelerates both the chemical and structural degradation of the perovskite film [56]. The following sections will analyze the interfacial degradation from perspective of interfacial reaction and HTL desorption-induced interface degradation.

The thermal input can effectively activate and accelerate the interface reaction, thus inducing the interface degradation. The most concerned interfacial reaction in the current field of PSCs

16136829, 0, Downloaded from https://onlinelibrary.wiley.com/doi/10.1002/smll.202514991 by Meicheng Li - North China Electric Power University Beijing , Wiley Online Library on [25/05/2026]. See the Terms and Conditions (https://onlinelibrary.wiley.com/terms-and-conditions) on Wiley Online Library for rules of use; OA articles are governed by the applicable Creative Commons License

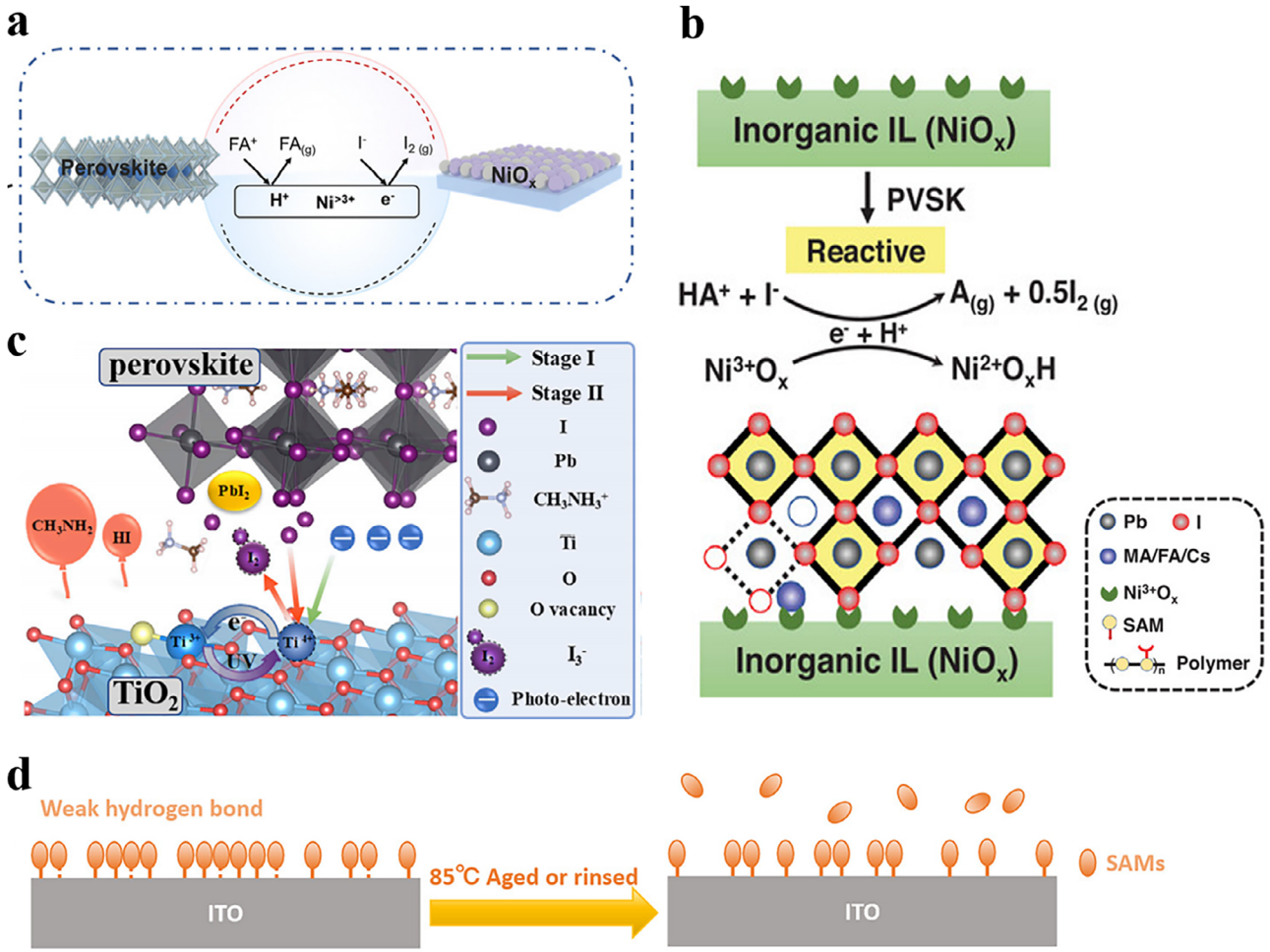


FIGURE 7 | (a) Diagram and equations of interfacial redox reactions. Reproduced with permission [56]. Copyright 2025, RSC Publishing. (b) Schematic illustration of hybrid interfacial layer simultaneously optimizing the bilateral surfaces of charge-selective metal oxide and perovskite. Reproduced with permission [58]. Copyright 2025, John Wiley and Sons. (c) The mechanism of PSCs degradation under continuous UV irradiation. Reproduced under the terms of the CC-BY-NC-ND 4.0 license [59]. Copyright 2020, J. Ji et al. (d) SAM desorption from the substrate and the reinforcing mechanism through ITO nanoparticle insertion. Reproduced with permission [62]. Copyright 2025, John Wiley and Sons.

is the reaction between perovskite and nickel oxide (NiO_x), normally as the HTL in the inverted PSCs, which is attributed to the strong oxidizing property of high-valence nickel species ($Ni^{>3+}$). Under thermal stress, the high-valence nickel species and abundant hydroxyl groups can trigger a series of destructive interfacial reactions [57]. The strongly oxidizing $Ni^{>3+}$ can oxidize halide ions in the perovskite lattice, while surface hydroxyls attack the organic cations or inorganic framework through protonation (Figure 7a,b) [57, 58]. Similarly, the Ti^{4+} states in TiO_2 can also oxidize halide ions in the perovskite lattice, triggering interfacial decomposition reactions (Figure 7c) [59]. These diverse reactions jointly induce perovskite decomposition at the interface, forming insulating lead halides and metallic lead defects.

In regular PSCs, after being doped by lithium salts (e.g., LiTFSI) and 4-tert-butylpyridine (tBP), the 2,2',7,7'-tetrakis[N,N-di(4-methoxyphenyl)amino]-9,9'-spirobifluorene (Spiro-OMeTAD) normally serves as HTL. Under thermal stress, these additives, particularly LiTFSI, undergo a series of physicochemical transformations that lead directly to interfacial reaction and degradation. In thermal environments, the pronounced hygroscopicity of LiTFSI renders it highly sensitive to moisture. Upon exposure, LiTFSI undergoes hydrolysis to produce HTFSI [60]. The generated HTFSI is prone to further decompose into highly corrosive gases, such as HF and SO_2F_2. As a strong electron acceptor, SO_2F_2 abstracts electrons from Pb^{2+}, thereby weakening the Pb—I bonds. Meanwhile, HF reacts with Pb^{2+} to form PbF_2. This reaction exacerbates lead vacancy defects, while the resulting PbF_2, acting as an insulator, obstructs hole transport at the interface. The subsequent accumulation of holes creates a localized high electric field, which acts as a potent driver for accelerated ion migration and localized phase instability within the perovskite lattice. Rather than mere interfacial resistance, these chemically induced lead vacancies and the formation of insulating PbF_2 serve as degradation nuclei, triggering the deep-level structural decomposition of the perovskite film from the surface into the bulk phase.

As for the HTL desorption-induced interfacial degradation, it generally refers to the interfacial degradation induced by the desorption of self-assembled monolayers (SAMs). As an excellent ultrathin hole-selective contact material, SAM have witnessed the significantly efficiency advancement of inverted PSCs. However,

16136829, 0, Downloaded from https://onlinelibrary.wiley.com/doi/10.1002/smll.202514991 by Meicheng Li - North China Electric Power University Beijing , Wiley Online Library on [25/05/2026]. See the Terms and Conditions (https://onlinelibrary.wiley.com/terms-and-conditions) on Wiley Online Library for rules of use; OA articles are governed by the applicable Creative Commons License

the inherent thermal instability of SAMs remains a key challenge limiting the long-term reliability of devices. The thermal desorption of SAM molecules leads to the loss of interfacial anchoring, resulting in a high density of uncoordinated lead sites at the buried interface. These interfacial defects do not merely act as recombination centers but serve as initial sites for perovskite lattice decomposition. Furthermore, the resulting charge accumulation and electric field concentration at the mismatched interface provide a strong driving force for ion migration within the perovskite bulk, eventually triggering an irreversible phase transition and the collapse of the crystalline framework from the interface upward.

Analyzing from the molecular scale, the chemical structure of SAMs endow their feasible self-assembled ability, but it also represents the primary origin of their thermal degradation. An ideal SAM molecule typically consists of an anchoring group, a conjugated spacer group and a functional terminal group [61]. However, the chemical bonds between the anchoring group and the metallic oxide substrate may break under thermal stress, resulting in molecular desorption from the interface (Figure 7d) [62]. The molecular structure, especially the spacer group, is also susceptible to thermal degradation or irreversible chemical alteration, which compromises its passivation function. Furthermore, elevated temperatures can induce conformational changes in molecular stacking, exacerbating interfacial stress imbalance and leading to the failure of the interfacial structure. In traditional planar SAMs, while strong π-π interactions between molecules are beneficial for charge transport [61, 63], they often cause aggregation during solution processing and result in non-uniform film formation. More critically, such highly ordered packing lacks the robustness to withstand sustained thermal or mechanical stress.

In addition to the chemical reactions above, heat drives structural failure of the perovskite film through the coupled effects of defect generation and charge accumulation at its boundaries. Elevated temperatures cause differential shifts in the work functions of adjacent layers relative to the perovskite, leading to a localized electronic imbalance. This imbalance creates a strong interfacial electric field that acts as a potent driving force for the internal migration of ions, particularly halide anions and organic cations [64]. This field accelerates the migration of ions, particularly halide anions and organic cations, along grain boundaries toward the interface. The accumulated ions not only create structural defects but also become nucleation sites for chemical decomposition. Grain boundaries are especially vulnerable, as charges preferentially accumulate there and degradation initiates from these sites [65]. Meanwhile, trapped charges directly participate in detrimental reactions. Holes convert shallow iodide interstitials ($I_{i\cdot}$) into deep-level neutral iodine interstitials (I_{i0}), leading to irreversible I_2 formation and perovskite breakdown [65].

3.5 | Thermal-Induced Passivation Failure

Defects within perovskite materials introduce trap states that facilitate non-radiative recombination, thereby compromising device efficiency. The introduction of passivators can effectively mitigate defect density by neutralizing charged species, anchoring surface atoms, filling vacancies, and inhibiting ion oxidation, leading to the improvement in photovoltaic performance of PSCs.

However, the practical application of these passivators is significantly constrained by their potential failure under high-temperature stress. Phenethylammonium iodide (PEAI) is a widely adopted passivator [66], yet physical desorption has been identified as a primary failure mechanism at elevated temperatures. Hu et al. observed that heating to approximately 100°C triggers the sublimation of iodide ions from PEAI molecules [67]. Similarly, Pei et al. demonstrated that at 120°C, PEA^+ cations undergo a desorption process that propagates from the surface inward, leading to reduced passivation coverage and the re-exposure of surface defects (Figure 8a) [68]. DFT simulations further reveal that the energy required for PEA^+ to desorb from its adsorption sites is extremely low, whereas the initial energy barrier for its chemical decomposition (such as deprotonation) is several times higher. This substantial energy disparity renders physical desorption thermodynamically and kinetically more favorable than chemical reactions, establishing it as the dominant pathway for passivation failure. To address this, Pei et al. synthesized a novel passivator, 4-(2-Aminoethyl) benzenesulfonyl fluoride (TAR3), by introducing a sulfonyl fluoride group ($-SO_2F$) at the para-position of the PEAI benzene ring, which maintain strong adsorption under photothermal stress (Figure 8a).

Nevertheless, thermal degradation initiated by deprotonation remains a non-negligible factor. Under intense thermal stress, PEA^+ cations within the perovskite structure lose a proton (H^+) to transform into neutral, highly reactive PEA^0 molecules [69] This transformation enhances the nucleophilicity of PEA^0, enabling it to attack the carbon atom of the C═N bond in the FA^+ cation via an S_n2 nucleophilic substitution mechanism. This reaction yields a new cation, $PEAMA^+$, accompanied by the release of ammonia gas (NH_3). The escape of NH_3 disrupts the perovskite lattice, accelerating material decomposition and overall thermal degradation (Figure 8b) [69]. X-ray diffraction (XRD) analysis confirms the chemical reaction between PEA^+ and FA^+ under thermal stress, evidenced by the emergence of a new diffraction peak at 7.1° corresponding to a $PEAMA^+$-based low-dimensional phase, accompanied by the consumption of the 3D perovskite phase (Figure 8c). Concurrently, cross-sectional scanning electron microscopy (SEM) reveals that in PEA^+-passivated samples under thermal stress, voids progressively form along grain boundaries (Figure 8d).

In short, bulk passivators such as PEAI are susceptible to both physical desorption and chemical decomposition under thermal condition, directly compromising the integrity of the perovskite film. These degradation mechanisms highlight the critical need to develop thermally robust passivators with stronger surface anchoring and higher resistance to deprotonation for enhancing the intrinsic thermal stability of perovskite.

3.6 | Thermally Coupled Degradation Scenarios

In practical operational conditions, PSCs are inevitably subjected to multiple environmental stressors including light irradiation, heat, oxygen and moisture. As a pivotal coupling factor, heat not only directly triggers ion migration, phase transition and

16136829, 0, Downloaded from https://onlinelibrary.wiley.com/doi/10.1002/smll.202514991 by Meicheng Li - North China Electric Power University Beijing , Wiley Online Library on [25/05/2026]. See the Terms and Conditions (https://onlinelibrary.wiley.com/terms-and-conditions) on Wiley Online Library for rules of use; OA articles are governed by the applicable Creative Commons License

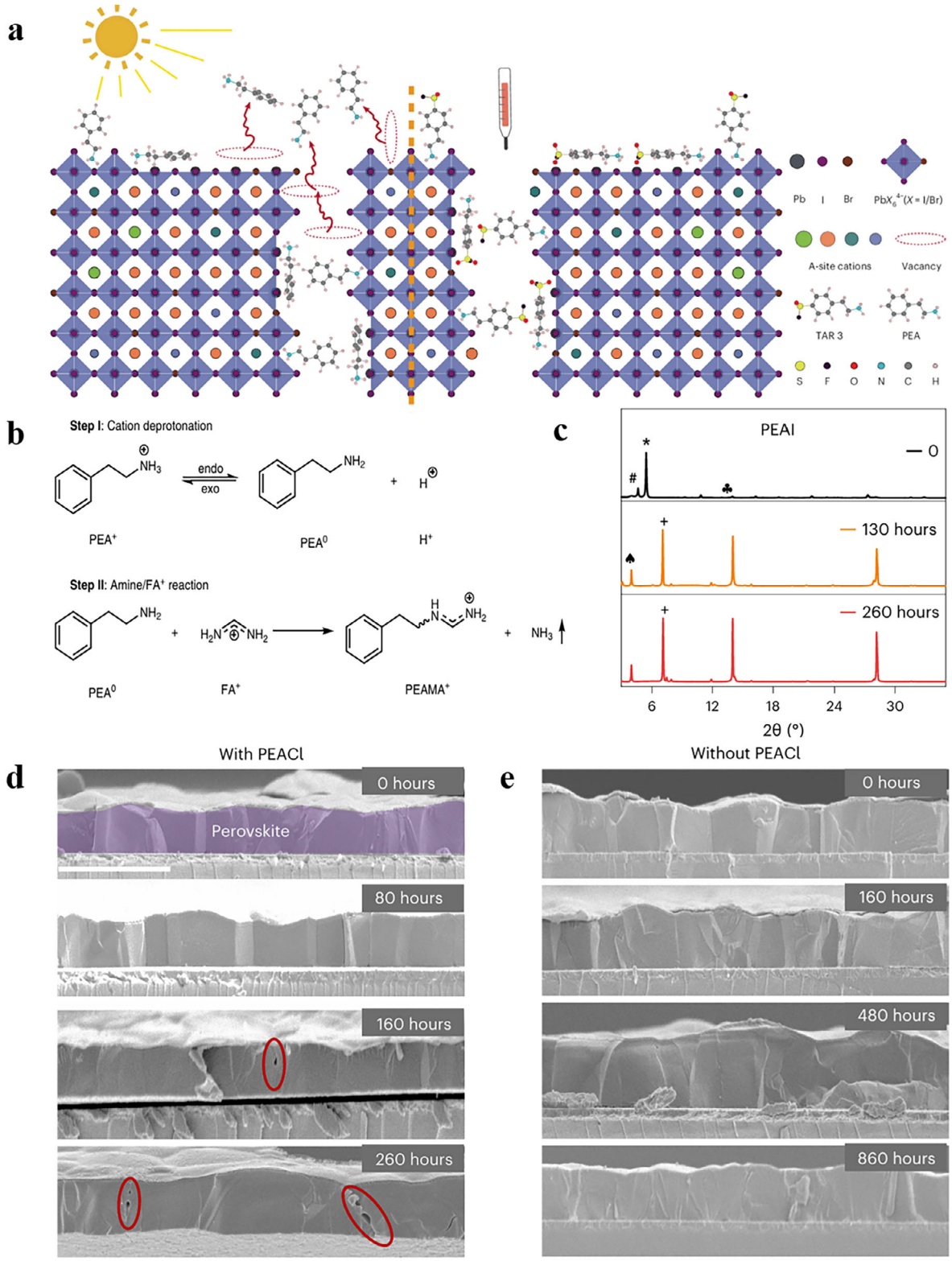


FIGURE 8 | (a) Schematic showing the desorption of PEA^+(indicated by red arrows) from the WBG perovskite lattice under photothermal stress, while TAR3 maintains strong adsorption. An orange dashed line separates the left (PEA^+-passivated) and right (TAR3-passivated) grain regions. Reproduced with permission [68]. Copyright 2025, Springer Nature. (b) Reaction scheme of PEA^+ with FA^+ [69] (c)XRD of $FA_{0.9}Cs_{0.1}PbI_3$ perovskite films with PEAI surface treatment [69] Cross-sectional SEM images of (d) PSCs prepared with PEACl and (e) with PEACl after stability measurement under 1 sun illumination at 85°C and open circuit condition for 0, 80, 160 and 250 h, respectively. Red circles indicate voids formed along grain boundaries. Reproduced with permission [69]. Copyright 2016, Nature Research.

16136829, 0, Downloaded from https://onlinelibrary.wiley.com/doi/10.1002/smll.202514991 by Meicheng Li - North China Electric Power University Beijing , Wiley Online Library on [25/05/2026]. See the Terms and Conditions (https://onlinelibrary.wiley.com/terms-and-conditions) on Wiley Online Library for rules of use; OA articles are governed by the applicable Creative Commons License

lattice distortion within perovskite materials, but also drastically accelerates the degradation processes induced by light, oxygen and moisture [70, 71] When these environmental factors act synergistically, their combined degradation effect is not merely a simple additive superposition; instead, the device performance decay rate can be remarkably amplified due to the synergistic coupling interactions among multiple stimuli. To gain an in-depth understanding of the practical stability of PSCs and clarify the core mechanism of device failure, an urgent and thorough investigation into the synergistic coupling effects between heat and other environmental factors (e.g., light, oxygen and moisture) is highly warranted [72–74].

3.6.1 | Thermal-Oxygen Coupling

The degradation of perovskites under combined heat and oxygen is a multi-step process that exhibits strong acceleration. Rising temperature increases both the diffusion and reactivity of oxygen molecules within the material. More importantly, it promotes the formation and migration of defects such as halide vacancies in the perovskite lattice. These defects act as efficient electron traps and can significantly raise the probability of capturing photogenerated electrons. This process greatly enhances the chance for oxygen molecules to capture electrons and form superoxide anions as the following equation ($\cdot O_2^-$) (Figure 9a) [75–77].

$$O_2 + e^- \xrightarrow{\Delta} \cdot O_2^- \tag{5}$$

As a strong Brønsted base, the destructive effect of the superoxide anion is further intensified by heat. Higher temperature vastly lowers the activation energy for bond breaking and reformation. As a consequence, it is easier for$\cdot O_2^-$ to attack on the Pb-X bonds, forming more stable Pb—O bonds, leading to massive halide loss [78] (Figure 9b–e) illustrate this pathway via DFT calculations. Heating also brings about the deprotonation reaction between acidic organic cations in the perovskite, especially those with NH_3^+ groups and$\cdot O_2^-$. For instance, MA^+ can be converted into methylamine (CH_3NH_2) under the function of $\cdot O_2^-$.

$$O_2^- + CH_3NH_3^+ \xrightarrow{\Delta} HO_2 + CH_3NH_2 \tag{6}$$

The deprotonation of A-site cations would inevitably cause perovskite lattice's disorder and even collapse, which is the beginning of chemical degradation. Besides, the hydroperoxyl radical ($HO_2\cdot$), a strongly oxidizing agent [79]. is also generated, which can further oxidize iodide ions to iodine radicals (I·), initializing further reactions to form molecular iodine (I_2) [80].

3.6.2 | Thermal-Light Coupling

The core of thermal-light coupling lies in the combined effect of accelerating the defect-assisted ion migration and chemical reaction. As is illustrated in Figure 10a [81], PSCs under illumination are most severely compromised at open-circuit conditions (highest charge density) and elevated temperature (60°C).

This coupling effect manifests first through defect-assisted ion migration. Elevated temperature enhances atomic vibrations and ion migration. The intensified lattice vibrations facilitate halide ion escape, thereby generating numerous vacancy defects. At the same time, the excess electron-hole pairs introduced by light illumination can neutralize charged defects. Once neutralized, the defects are no longer electrostatically pinned by surrounding ions, and their migration barrier drops significantly [81]. Consequently, these defects migrate from surfaces and grain boundaries into the bulk, forming a high density of deep-level trap states and leading to a significant decrease in carrier recombination lifetime (Figure 10b,c).

When it comes to more extreme conditions of high temperature and intense light, perovskite materials can follow new degradation pathways. Elevated temperature inherently weakens chemical bonds, while a high density of energetic charge carriers further destabilizes them. Abdelmageed et al. observed that under strong illumination at 75°C, decomposition products (PbI_2) and metallic lead (Pb^0) were formed (Figure 10d), which indicates perovskite's deep breakdown. Further investigation reveals that Pb-I bonds rupture under intense light [82]. The resulting PbI_2 decomposes, releasing Pb^{2+} ions, which are then reduced to lead by high-energy photogenerated electrons in the material. The formation of metallic lead inflicts deeper damage on the device. particles are highly effective non-radiative recombination centers, promoting electron-hole recombination. Moreover, as conductive impurities, Pb° can create current-leakage pathways within the perovskite layer, resulting in a sharp drop in output voltage and efficiency.

3.6.3 | Thermal-Moisture Coupling

One major concern about perovskite's instability is its huge susceptibility to moisture [83]. The moisture-driven perovskite degradation starts with the entry of water molecules into grain boundaries and surface defects. As illustrated in Figure 10e, water molecules insert themselves between the $[PbI_6]4^-$ octahedral units, weakening the original 3D network and triggering a dimensional reduction of the structure [84]. Concurrently, water reacts with organic cations (e.g. MA^+), producing yellow PbI_2 along with volatile products such as CH_3NH_2 and HI. This process is typically accompanied by a visible color change of the film from dark to yellow [85, 86].

When combined with elevated temperature, the degradation kinetics are markedly accelerated. On one hand, higher thermal energy provides greater activation for hydration reactions and ion migration, promoting the diffusion of water within the lattice and the formation of hydrated phases. On the other hand, these hydrated phases can reversibly form and decompose upon temperature cycling, causing repeated lattice expansion and contraction. This builds up mechanical stress inside the material can initiate micro-cracks, extend lattice defects, and eventually drive irreversible phase separation, thereby decomposing the perovskite.

16136829, 0, Downloaded from https://onlinelibrary.wiley.com/doi/10.1002/smll.202514991 by Meicheng Li - North China Electric Power University Beijing , Wiley Online Library on [25/05/2026]. See the Terms and Conditions (https://onlinelibrary.wiley.com/terms-and-conditions) on Wiley Online Library for rules of use; OA articles are governed by the applicable Creative Commons License

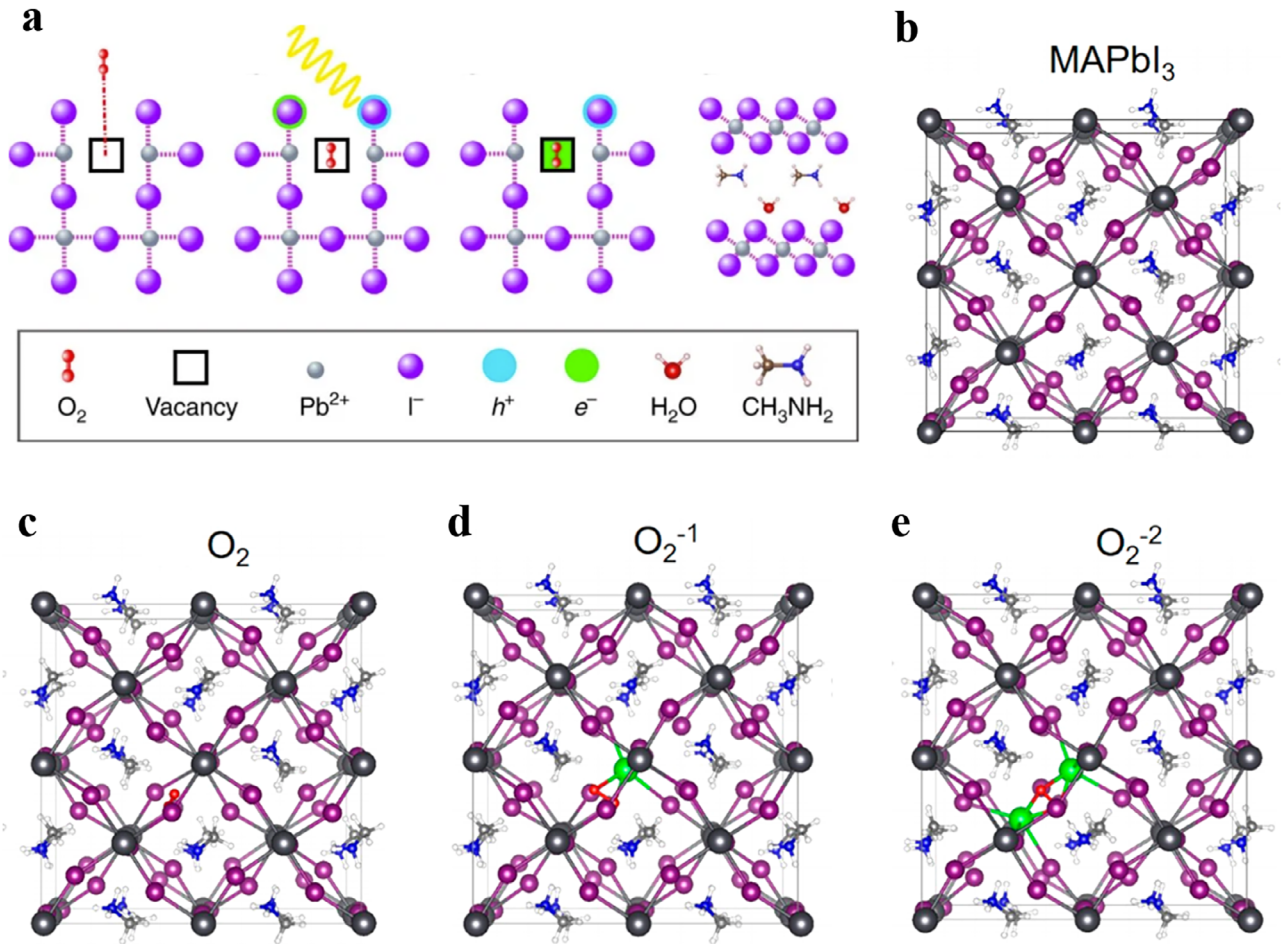


FIGURE 9 | (a) Mechanism of oxygen-triggered photodegradation in $MAPbI_3$ perovskite. Reproduced under the terms of the CC-BY 4.0 license [75]. Copyright 2017, N. Aristidou et al. Comparative DFT-optimized structures of $MAPbI_3$ interacting with oxygen species b) pristine $MAPbI_3$, (c) O_2 (weak interaction), (d)·O_2^-(breaks 1×Pb-I and forms 2×O-Pb) and e) O_2^{-2} (breaks 2×Pb-I and forms 4×O-Pb). Interstitial O (red) and bonded Pb (green) are highlighted. Reproduced with permission [78]. Copyright 2020, American Chemical Society.

Coupled heat and moisture also shows a synergy effect on aggravating ion migration. Moisture creates conduction pathways along grain boundaries and defects, while heat significantly lowers the migration barrier for ions. This synergetic effect on accelerating the ion migration enable rapid ion accumulation at the interfacial regions, leading to severe band bending and interfacial degradation. Further, the massive loss of ion from the lattice also induce the lattice distortion, inducing the phase transition and even perovskite decomposition.

Furthermore, during damp-heat aging, moisture and oxygen jointly penetrate along the grain boundaries. This promotes preferential decomposition at the boundary regions, resulting in blurred grain morphology and the precipitation of PbI_2 particles. The small grains gradually coalesce, forming large, disordered grains with poor optoelectronic properties (Figure 10f) [87]. As the crystalline integrity deteriorates, a high density of defect states emerges within the film. These defects act as non-radiative recombination centers for charge carriers, severely reducing carrier lifetime and device performance. Ultimately, this cascade leads to accelerated failure of the PSCs.

3.6.4 | Thermal Coupling With Decomposition Products

The thermal decomposition products discussed in Section 3.2 including organic volatiles, PbI_2 and HI, are not merely inert endpoints. Under sustained thermal stress, they actively participate in secondary destructive reactions that accelerate device failure. Among these, organic cation decomposition generates volatile species that drive further degradation. For pure MAI, heating to 140°C produces NH_3 along with CH_3I or CH_3Br. For pure FAI, decomposition at elevated temperatures yields HCN, NH_3, and HI (Figure 11a–c) [88]. However, when MA and FA coexist, as in most high-efficiency perovskites, these primary products undergo irreversible secondary reactions even at moderate temperatures (~85°C). CH_3NH_2 reacts with HI to form additional CH_3I and NH_3. At higher temperatures (~350°C), HCN further reacts with CH_3X to form CH_3CN. These findings confirm that MA/FA mixing creates new decomposition pathways that are thermally driven and irreversible, generating reactive gases at temperatures relevant to device operation.

These gaseous products will actively interact with residual PbI_2 to accelerate degradation. On one hand, PbI_2-rich domains act

16136829, 0, Downloaded from https://onlinelibrary.wiley.com/doi/10.1002/smll.202514991 by Meicheng Li - North China Electric Power University Beijing , Wiley Online Library on [25/05/2026]. See the Terms and Conditions (https://onlinelibrary.wiley.com/terms-and-conditions) on Wiley Online Library for rules of use; OA articles are governed by the applicable Creative Commons License

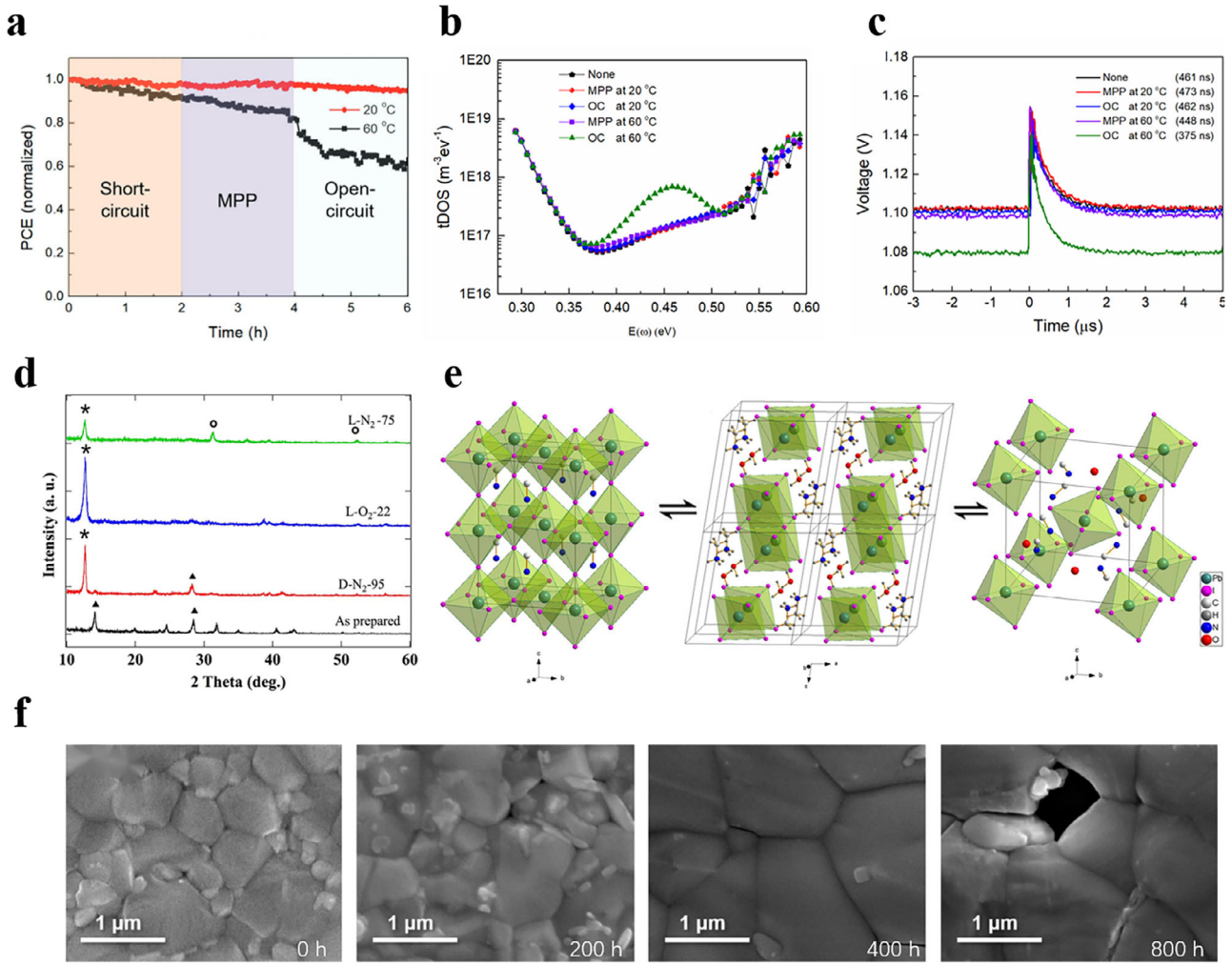


FIGURE 10 | (a) PCE decay of encapsulated device at short-circuit, maximum power point (MPP), and open circuit condition with device temperature of 60 and 20°C, respectively [81] (b) The tDOS profiles of $MAPbI_3$ solar cells measured by thermal admittance spectroscopy after 2 h of illumination under MPP at 20°C, open circuit (OC) at 20°C, MPP at 60°C, and OC at 60°C [81] (c) The drastic reduction in carrier recombination lifetime, as measured by TPV, directly correlates with (b). Reproduced with permission [81]. Copyright 2019, John Wiley and Sons. (d) X-ray diffraction (XRD) spectra of $MAPbI_3$ perovskite films in different conditions: as prepared (black), aged in dark at 95°C (red), aged under light in dry air at room temperature ~30°C (blue), and aged under light in N_2-filled environment at ~75°C (green). Reproduced with permission [82]. Copyright 2018, Elsevier. (e) Chemical pathways of moisture-perovskite interactions. Reproduced under the terms of the CC-BY 3.0 license [84]. Copyright 2024, B. P. Kore et al. (f) SEM images of uncoated perovskite films showing their morphological evolution (grain coalescence and enlargement) after storage at 65°C/65% RH for 0, 200, 400, and 800 h. Reproduced with permission [87]. Copyright 2026, Elsevier.

as catalytic centers that promote the formation of the inactive δ-$FAPbI_3$ phase. As demonstrated by Fu et al., δ-$FAPbI_3$ appears during heat-light soaking of complete devices due to the reaction of PbI_2 with gaseous species such as FAI and I_2 released from perovskite decomposition. In bare films, these gases escape and no δ-phase is detected, while in full devices, the contact layers hinder gas release, favoring their interaction with PbI_2 to form δ-$FAPbI_3$ (Figure 11d) [89]. This gas-retention effect accelerates degradation by continuously converting the photoactive α-phase into the inert δ-phase.

On the other hand, under combined thermal and light stress, PbI_2 itself decomposes further into Pb^0 and I_2. The resulting I_2 is a highly reactive oxidant that drives multiple degradation pathways. It diffuses into the perovskite lattice to form deep-level defects such as I_3^- complexes [65]. and also migrates to the hole transport layer where it degrades spiro-OMeTAD conductivity via redox reactions [90], and can further reacts with Ag electrodes to form insulating AgI. The migration of iodine species to the HTL has been directly visualized by time-of-flight secondary ion mass spectrometry (ToF-SIMS) (Figure 11e,f) [91], where a strong I^- signal appears within the spiro-OMeTAD layer after thermal aging.

Collectively, these findings outline an autocatalytic degradation loop driven by self-generated species, as schematically summarized in Figure 11g,h. Thermal decomposition products-PbI_2, I_2, HI, and CH_3NH_2-function as active agents that propagate localized degradation into global device failure. Effective thermal stabilization must therefore intercept these self-generated species before they engage in this destructive feedback loop.

16136829, 0, Downloaded from https://onlinelibrary.wiley.com/doi/10.1002/smll.202514991 by Meicheng Li - North China Electric Power University Beijing , Wiley Online Library on [25/05/2026]. See the Terms and Conditions (https://onlinelibrary.wiley.com/terms-and-conditions) on Wiley Online Library for rules of use; OA articles are governed by the applicable Creative Commons License

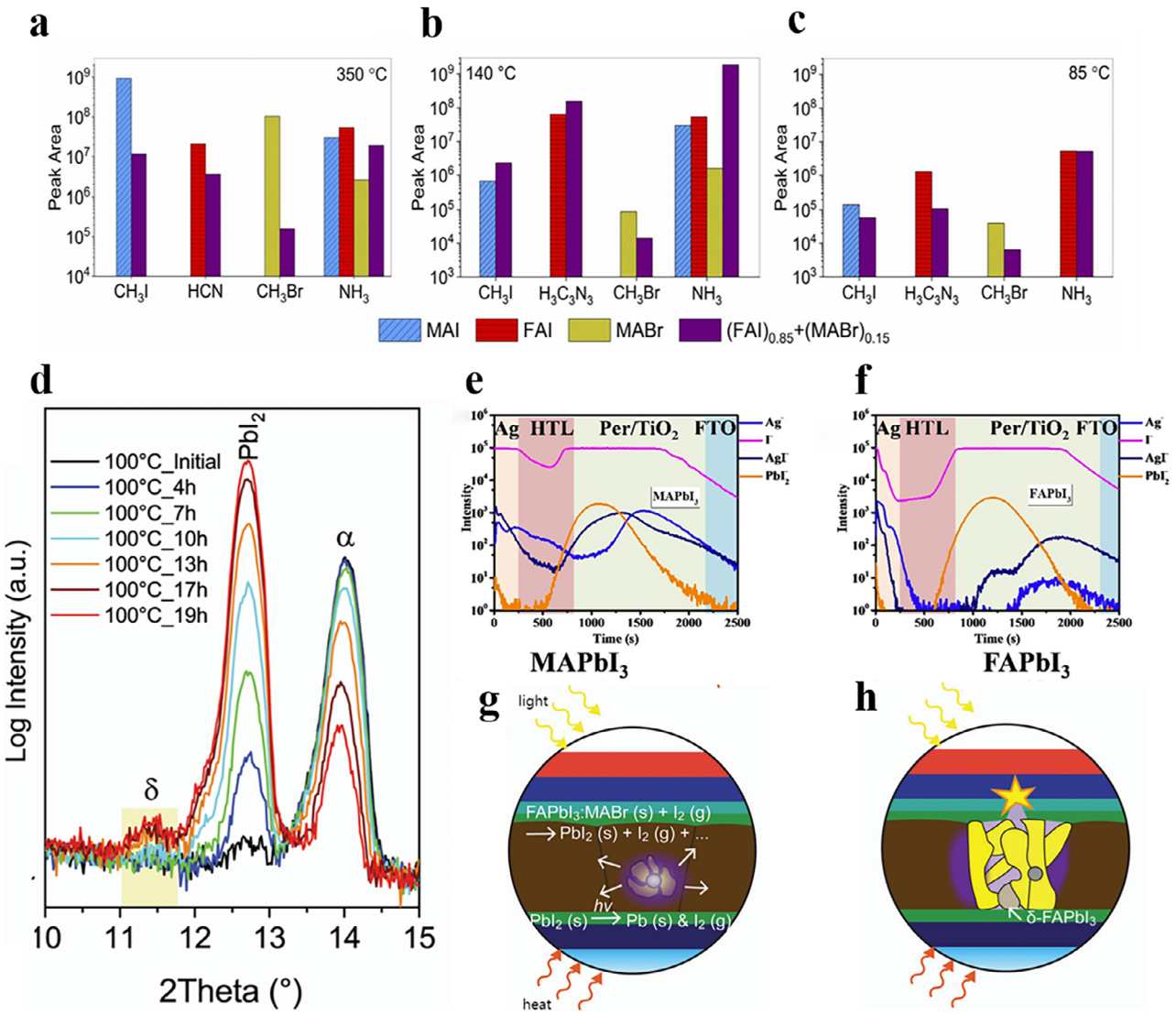


FIGURE 11 | Decomposition products of dry perovskite precursor powders. GC-MS peaks of products after annealing at (a) 350°C for 15 min, (b) 140°C for 10 h and (c) 85°C for 100 h. Reproduced with permission [88]. Copyright 2020, The American Association for the Advancement of Science. (d) In situ XRD of $FAPbI_3$:MABr (10 mg·ml^{-1}) NIR-transparent perovskite solar cells measured at 100°C. The sample was flushed with N_2 at a flow rate of 50 sccm [89] TOF-SIMS spectrum for degraded devices of (e) $MAPbI_3$ and (f) $FAPbI_3$ kept with in the dry box for a month. Reproduced with permission [91]. Copyright 2017, Royal Society of Chemistry. (g,h) Schematic illustration of the I_2 vapor-assisted degradation mechanism. Reproduced under the terms of the CC-BY-NC 3.0 license [89]. Copyright 2019, F. Fu et al.

In this section, we have systematically reviewed the degradation mechanisms of perovskite from the perspectives including phase transition, decomposition, thermal stress, interfacial degradation, passivation failure, and coupled degradation scenarios. Among these mechanisms, we think that thermal-induced passivation failure and thermally coupled degradation are currently the areas that needs more attention. Of these two aspects, thermal-induced passivation failure is a relatively small point which is often overlooked in previous researches, but it has a significant impact on the thermal stability of perovskites. Targeted research focusing on this detail might yield promising results. In contrast, thermally coupled degradation is more closely related to the operating conditions of the device. This characteristic, which aligns with real-world conditions, is precisely what is needed for commercialization; therefore, research based on this mechanism can be considered a key direction for future research.

4 | Strategies for Enhancing Thermal Stability

The PSCs' performance failure under thermal conditions normally results from a synergistic consequence of multiple factors including bulk thermodynamic instability, interfacial chemical reactions, accelerated ion migration and the accumulation of thermo-mechanical coupling stress. Correspondingly, the treatments for enhancing thermal stability have gradually evolved into multi-scale and multi-dimensional regulation strategies from diverse perspectives. These strategies, although diverse in form,

16136829, 0, Downloaded from https://onlinelibrary.wiley.com/doi/10.1002/smll.202514991 by Meicheng Li - North China Electric Power University Beijing , Wiley Online Library on [25/05/2026]. See the Terms and Conditions (https://onlinelibrary.wiley.com/terms-and-conditions) on Wiley Online Library for rules of use; OA articles are governed by the applicable Creative Commons License

can be fundamentally linked to specific degradation pathways discussed above. For instance, composition engineering primarily addresses phase instability and decomposition, while facet and dimensional engineering mitigates thermal stress and thermal induced ion migration. Similarly, stress engineering targets mechanical degradation, and interfacial optimization mitigates chemical reactions and passivation failure. These potential correlations have been validated in experimental studies over the past decade. Notably, Current research has demonstrated that devices retain 90% of their initial efficiency after 5000 h of MPP tracking tests in air at 85°C [92], demonstrating the impressive thermal stability advancement through the effective enhancement strategies. In this section, we systematically review the strategies for enhancing thermal stability, focusing on cation composition engineering, facet engineering, dimensional engineering, stress engineering, ion migration inhibition, as well as other relevant auxiliary strategies. Besides, a systematic summary table, which directly links the thermal degradation mechanisms, the strategies, and the representative thermal stability achievements has been summarized (Table 2).

4.1 | A-Site Cation Composition Engineering

Composition engineering of the perovskite system primarily targets thermally induced phase instability and decomposition by improving lattice thermodynamics. The improvement of lattice robustness can be achieved by tailoring the stoichiometric ratio or elements of ions at the A, B and X sites, respectively. Among them, the A-site cations locate in the interstitial voids of the 3D $[PbI_6]4^-$ octahedral framework, which provide structural support for the entire crystal framework and exert a decisive effect on the lattice tolerance factor. As mentioned in Section 3.1 above, adjusting the A-site cation is a major and effective strategy for dealing with thermal phase transitions. Currently, the A-sites in high-efficiency PSCs are normally organic cations (e.g., FA^+, MA^+, GUA^+, EA^+), and the thermal stability issues associated with these cations become the main limitation of perovskite stability, which has attracted extensive attention. Consequently, the regulation strategies based on A-site cations have become effective approaches to enhance the thermal stability of perovskite and corresponding PSCs.

In the early stage of PSCs research, $MAPbI_3$ was the most widely used perovskite material, benefiting from its suitable lattice tolerance factor, excellent processability for high-quality film crystallization (Figure 12a). Nevertheless, MA^+ suffers from inferior thermal stability, which tends to decompose and volatilize upon heating. Then, the FA^+ was gradually utilized as the cation in perovskite. The ionic radius of FA^+ is approximately 2.53 Å, which is larger than that of MA^+ (≈2.17 Å). Owing to the higher intrinsic stability and lower volatility of FA^+, $FAPbI_3$ exhibits remarkably superior thermal stability to $MAPbI_3$ (Figure 12b) [93]. In addition, $FAPbI_3$ features an optical band gap of around 1.48 eV, endowing it with a more pronounced advantage in optical absorption (Figure 12c) [94]. Currently, $FAPbI_3$ has become the core component of high-efficiency PSCs. However, the relatively large ionic radius of FA^+ results in an excessively high lattice tolerance factor of $FAPbI_3$, which impairs its phase stability from a thermodynamic perspective. This drawback further kinetically manifests as the difficulty in fabricating high-quality films with the photoactive α-phase, posing a significant challenge to the preparation of high-performance $FAPbI_3$ PSCs.

To address the drawbacks of single-cation perovskite systems, researchers attempt to co-employ various cations by taking advantage of their respective intrinsic merits. In response to the characteristics of α-$FAPbI_3$ perovskites with excellent thermodynamic stability yet poor crystallizability, researchers regulate the crystallization behavior of $FAPbI_3$ by introducing MA^+ cations, leveraging the superior crystallizability of MA-based perovskites. Methylammonium chloride (MACl) has been developed as an additive to modulate the crystallization of α-$FAPbI_3$. Relevant studies have demonstrated that MACl can induce an intermediate α-$FAPbI_3$ phase without annealing, thereby stabilizing the crystal structure effectively. Moreover, the introduced MACl is prone to volatilization during the annealing process, which avoids excessive residual MA^+ and thus contributes to the enhancement of the thermal stability of α-$FAPbI_3$. Currently, the introduction of MACl as a crystallization regulator for α-$FAPbI_3$ has become a well-established technology and has been widely adopted in the fabrication of various high-efficiency PSCs. Nevertheless, despite the high volatility of MACl during annealing, trace residual MA^+ in α-$FAPbI_3$ is inevitable, which impacts the thermal stability of α-$FAPbI_3$ films and the corresponding PSCs. To eliminate the employment of MA^+, Zhang et al. proposed a kinetic modulation strategy to fabricate high-quality and stable α-$FAPbI_3$ films, assisted by cogenetic volatile iodine intercalation and dealation (Figure 12d) [95]. Eventually, the α-$FAPbI_3$-based PSCs achieved a PCE exceeding 24%, and retained 99% of their initial PCE after continuous operation for over 1100 h under illumination at 85°C±5°C (Figure 12e). In addition to using MA^+, researchers have also attempted to stabilize the α-$FAPbI_3$ lattice by doping with Cs^+. This approach works by increasing the configurational entropy of the perovskite system and regulating the lattice tolerance factor [96]. It was revealed that even a small amount of Cs^+ doping can effectively suppress the phase transition from the α-$FAPbI_3$ to the δ-$FAPbI_3$ [97]. Although the fabrication of high-quality α-$FA_xCs_{1-x}PbI_3$ films remains challenging, the $FA_xCs_{1-x}PbI_3$ system has emerged as a promising candidate for achieving efficient and stable PSCs. Li et al. demonstrated that a surface-coordinated acetate intermediate-assisted crystallization pathway enabled the fabrication of high-quality α-$FA_xCs_{1-x}PbI_3$ films without any MA-based additives (Figure 12f) [98]. The corresponding PSCs delivered a stabilized power output (SPO) efficiency of 25.94%, and retained over 95% of their initial PCE after continuous operation for more than 2000 h under 1 sun illumination at 85°C (Figure 12g). Besides, other organic cations (e.g., EA^+ and GUA^+) have also been attempted in perovskite systems to further optimize the thermal stability of PSCs [99, 100]. The superior performance of dual-cation perovskites over single-cation counterparts verified in numerous studies has confirmed the rationality of A-site component regulation strategies, which have gradually become one of the mainstream approaches to simultaneously improve the PSCs' photovoltaic performance and stability.

Researchers further attempted to design multi-cation perovskites by building on the dual-cation systems. To tackle the instability issue that the FA/MA mixed perovskite systems tend to transform from the desirable α-$FAPbI_3$ to the photo-inert δ-$FAPbI_3$, Saliba

16136829, 0, Downloaded from https://onlinelibrary.wiley.com/doi/10.1002/smll.202514991 by Meicheng Li - North China Electric Power University Beijing , Wiley Online Library on [25/05/2026]. See the Terms and Conditions (https://onlinelibrary.wiley.com/terms-and-conditions) on Wiley Online Library for rules of use; OA articles are governed by the applicable Creative Commons License

TABLE 2 | Summarization of strategies for enhancing thermal stability.

Device structure	Degradation mechanism	Condition	Time	Initial PCE	Retention rate/%	Strategies	Refs.
ITO/PTAA/MoS_2/$FAPbI_3$/MoS_2/C_{60}/SnO_2/ITO/Ag	Interfacial degradation	85°C/air/Encapsulation	1200h	26%	96+	Ion migration inhibition	[20]
glass/ITO/2PACz/perovskite/PCBM/BCP/Cu	Thermal stress	90°C/−/Encapsulation	3670h	>25%	97+	Stress engineering	[21]
FTO/NiO_x/n-HfOx/Me4PACz/perovskite/3F-PEAI/p-HfO_x/C_{60}/BCP/Cu	Interfacial degradation	85°C/50%RH/Encapsulation	5000h	26.60%	90+	Ion migration inhibition	[92]
ITO/SnO_2/α-$FAPbI_3$/PTAA/Au	Phase transition	85±5°C/N_2/−	1100h	>24%	99+	A-site engineering	[95]
ITO/SnO_2/$FA_{0.94}Cs_{0.06}PbI_3$/Spiro-OMeTAD/Au	Thermal decomposition	85°C/60±10%RH/Encapsulation	2000h	25.94%	95+	A-site engineering	[98]
FTO/c-TiO_2/Perovskite/MeO-PEAI/Spiro-OMeTAD/Au	Ion migration	85°C/25%RH/−	720h	25.40%	91	Crystal facet engineering	[111]
ITO/NiO_x/SAM/$Cs_{0.03}FA_{0.97}PbI_3$/GABr/PCBM/BCP/Cu	Thermal decomposition	85°C/N_2/−	1088h	25.12%	92	Crystal facet engineering	[116]
ITO/PTAA/$(MA)_{n-1}PbnI_{3n+1}$/C_{60}/BCP/Ag	Coupled degradation	85°C/N_2/−	3000h	19.11%	≈100	Dimensional engineering	[124]
ITO/SnO_2/3D PVK/(S-2)2$(MA)_{n-1}PbnI3_{n+1}$/C_{60}/BCP/Ag	Defect disturbance	55°C/N_2/−	1000h	25.41%	85+	Dimensional engineering	[125]
ITO/SnO_2/$FAPbI_3$/2D PVK(PEA-based)/Spiro-OMeTAD/Au	Defect disturbance	85°C/N_2/−	1074h	25.90%	91	Dimensional engineering	[127]
ITO/2PACz/$FA_{0.72}MA_{0.18}Cs_{0.1}PbI_3$/HUBLA/$C_{60}$/BCP/Au	Passivation failure	85°C/30%RH/Encapsulation	1000h	25.10%	88	Ion migration inhibition	[153]
ITO/2PACz/$FA_{0.72}MA_{0.18}Cs_{0.1}PbI_3$/HUBLA/$C_{60}$/BCP/Au	Passivation failure	85°C/N_2/Encapsulation	1500h	25.10%	94	Ion migration inhibition	[153]

16136829, 0, Downloaded from https://onlinelibrary.wiley.com/doi/10.1002/smll.202514991 by Meicheng Li - North China Electric Power University Beijing , Wiley Online Library on [25/05/2026]. See the Terms and Conditions (https://onlinelibrary.wiley.com/terms-and-conditions) on Wiley Online Library for rules of use; OA articles are governed by the applicable Creative Commons License

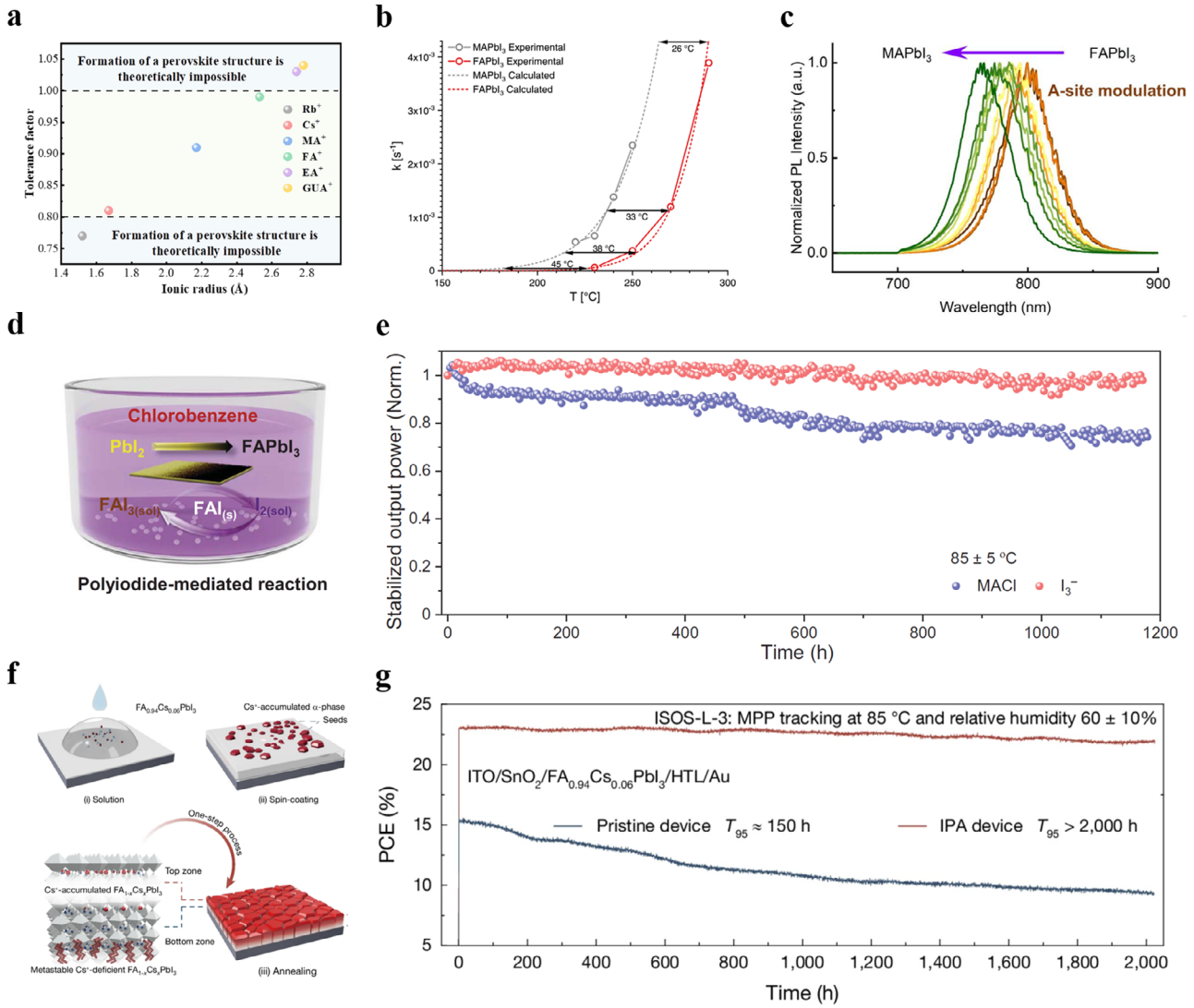


FIGURE 12 | (a) The tolerance factor of perovskite lattice with different cations. (b) Comparison of how the rate constant of the thermal decomposition k depends on the temperature for $MAPbI_3$ and $FAPbI_3$. Reproduced with permission [93]. Copyright 2022, American Physical Society. (c) the bandgap of perovskite with different molar ratio of MA^+ and FA^+. Reproduced under the terms of the CC-BY 4.0 license [94]. Copyright 2025, C. Zhu et al. (d) Schematics of α-$FAPbI_3$ converted from PbI_2 films immersed in chlorobenzene with soluble iodine and FAI solids [95]. (e) Evolution of the normalized power output of unencapsulated I_3^- and MACl device under continuous light irradiation at 85° ±5°C in a nitrogen glovebox. Reproduced with permission [95]. Copyright 2025, The American Association for the Advancement of Science. (f) Schematic of the typical crystallization process of α-$FA_{1-x}Cs_xPbI_3$ (x = 0.06) perovskite films [98] (g) Long-term stability for the encapsulated α- $FA_{1-x}Cs_xPbI_3$ (x = 0.06) devices. The encapsulated device was measured under tracking at MPP at approximately 85°C and an ambient humidity of 60 ± 10%. Reproduced with permission [98]. Copyright 2024, Springer Nature.

et al. incorporated Cs^+ into the FA^+/MA^+ mixed cation perovskite to reduce the effective ionic radius of A-site cations, thus finely tuning the lattice tolerance factor and stabilizing the lattice structure [101]. Moreover, the embedding of Cs^+ into the perovskite lattice increases the configurational entropy of the system, which thermodynamically facilitates the transition of α-$FAPbI_3$ from an intermediate phase, suppresses the formation of the yellow δ-phase. Rb^+ has also been attempted to be incorporated into FA/MA-perovskite and Cs/FA-perovskite, where Rb^+ occupies partial A-site lattice sites to form novel ternary cation perovskite systems. Although Rb^+ and Cs^+ both belong to Group IA of the periodic table, the excessively small ionic radius of Rb^+ deviates from the optimal range for forming ideal perovskite structures, making it difficult for a large amount of Rb^+ incorporation in perovskite lattice. Instead, only a small fraction of Rb^+ can occupy the A-site vacancies to provide structural support, with most Rb^+ species segregating at the grain boundaries and film surfaces. Due to the entropy increment effect and surface passivation, Rb^+ doping can effectively improve the thermal stability and efficiency of the resultant PSCs. Furthermore, researchers attempted to fabricate quaternary cation perovskite systems by simultaneously incorporating FA^+, MA^+, Cs^+ and Rb^+ to deposit perovskite film. The further diversification of cation components with different ionic radii at the A-sites enables more precise modulation of the band gap, but also endows the perovskite crystals with a higher configurational entropy and mitigated lattice distortion, potentially delivering a highly stable perovskite film [102–104].

16136829, 0, Downloaded from https://onlinelibrary.wiley.com/doi/10.1002/smll.202514991 by Meicheng Li - North China Electric Power University Beijing , Wiley Online Library on [25/05/2026]. See the Terms and Conditions (https://onlinelibrary.wiley.com/terms-and-conditions) on Wiley Online Library for rules of use; OA articles are governed by the applicable Creative Commons License

4.2 | Crystal Facet Engineering

Component engineering can remarkably enhance the thermodynamic stability of the perovskite film mainly through regulating the thermal disperse, mitigating thermal induced stress and ion migration. However, perovskite films usually exhibit a distinct orientational tendency during practical fabrication processes, and the type and distribution of their exposed crystal facets also exert a crucial impact on thermally induced defect formation, ion migration and surface reaction behaviors [105, 106] Therefore, based on the optimized component, further integration with crystal facet engineering enables more efficient optimization of the thermal stability of perovskite film.

In current works, some low Miller index crystal facets, likely (100), (110) and (111), become the dominant facets of perovskite films owing to their relatively low surface free energy. Except for a few studies where the (110) facet exhibits superior optoelectronic performance after elaborate artificial treatments, the (100) and (111) facets are generally recognized as the more favorable choices in efficient PSCs [107, 108] In contrast, the (110) facet is intentionally suppressed in most crystal facet engineering strategies, primarily due to its higher surface energy accompanied by more active defect evolution and accelerated ion migration. In comparison between these two favorable facets of (100) and (111), the (100) facet features loose and simple atomic arrangement with a relatively low coordination number. Perovskite films dominated by the (100) facet expose more surface atoms, rendering them more susceptible to external stimuli (such as thermal stress, moisture invasion) and thus prone to forming abundant defect sites. By contrast, the (111) facet has a triangular close-packed structure with high symmetry, dense atomic arrangement and a higher coordination number. This structural feature enables the surface layer to effectively block the infiltration of external moisture and oxygen molecules as well as the outward migration of internal ions [109, 110] Correspondingly, perovskite films dominated by the (111) facet exhibit a higher ion migration energy barrier, a lower surface defect density, and enhanced stability under thermal and moisture conditions. Qu et al. observe facet-related ion migration and reveal that the (100) facet is substantially more vulnerable to cationic migration than the (111) facet (Figure 13a,b) [111] The PSCs based on the (111)-dominated perovskite film can maintain 91% of its initial PCE after storage at 25% RH and 85°C for 720 h, superior to PSCs based on (100)-dominated perovskite film.

Although the (111) facet, as a close-packed plane, is susceptible to the formation of nanotwins, which not only hinders the vertical transport of carriers but also induces non-radiative recombination, such adverse effects can be mitigated via additional modulation strategies. A typical example is the work by Liu et al., who explored the growth kinetics of (111)-oriented perovskites and introduced organic ammonium salt (OAS) into the PbI_2 precursor solution to suppress the growth of the (100) facet, thereby enabling the (111) facet to become the dominant crystalline orientation [112] Meanwhile, the incorporated OAS also reduces the defect density of perovskite film. Such regulatory strategies targeting the crystal regulation of (111) for enhancing thermal stability can effectively alleviate the defect-related issues [113, 114] Furthermore, integrating the intrinsic characteristics of different crystal facets can synergistically elevate the limits of both device performance and stability (Figure 13c). Gao et al. attempted to construct a facet heterojunction, in which a thin layer of (111)-oriented perovskite was inserted beneath the deposited (001)-oriented perovskite film to form a crystalline facet heterojunction (Figure 13d) [115] This design successfully combines the excellent photovoltaic performance of the (001) facet with the superior stability of the (111) facet. Consequently, the modified devices realize enhancements in long-term operational stability alongside improved efficiency.

Different crystal facets of perovskites also exhibit distinct thermal transport properties due to the differences in atomic arrangement and lattice vibration. Theoretical calculations demonstrated that when perovskites are irradiated with light, the (100) facet can exhibit quasi-metallic characteristics, leading to a substantial enhancement in electronic thermal conductivity [116] In addition, this facet possesses fewer lattice defects and grain boundaries, and the phonon scattering effect is significantly suppressed, which further facilitates thermal diffusion. In contrast, the (110) and (111) facets show markedly lower thermal transport efficiency, arising from their stronger electron-phonon coupling interactions and faster relaxation of hot carriers (Figure 13e). Taking advantage of the superior thermal conductivity of the (100) facet, MACl was adopted as an additive to realize the directional growth regulation of the (100) facet via a dual function involving buried interface modification and perovskite precursor doping. This regulation not only optimized the crystal facet orientation but also reduced the film defect density, thus providing efficient channels for thermal transport. Perovskite films dominated by the (100) facet can accelerate the diffusion of heat from the bulk to the external environment and avoid the formation of local hotspots, thereby suppressing the thermal-induced degradation processes including ion migration, lattice expansion and phase transition, which fundamentally enhances the thermal stability of the devices. Compared with the control device, the modified device exhibited a lower average temperature during operation under standard solar illumination, with reduced efficiency fluctuation as the temperature increased. The device retained over 90% of their initial efficiency after storage at 85 °C for 1100 h.

In addition to the cation component engineering, which improves the thermal stability of perovskites from the perspective of bulk thermodynamics, crystal facet engineering directly modulates the surface energy and defect formation energy by regulating the crystalline facets. By increasing the proportion of crystal facets with superior thermodynamic and kinetic stability, the intrinsic origins of thermally induced defects and ion migration are effectively suppressed, thereby significantly inhibiting the surface decomposition and phase transition of perovskites. These two strategies exhibit excellent mechanistic complementarity in the synergetic optimization design for enhancing the thermal stability of perovskites.

4.3 | Dimensional Engineering

Dimensional engineering enhances thermal stability mianly by increasing ion migration barriers and suppressing phase transition. Conventional 3D perovskites conform to the general formula

16136829, 0, Downloaded from https://onlinelibrary.wiley.com/doi/10.1002/smll.202514991 by Meicheng Li - North China Electric Power University Beijing , Wiley Online Library on [25/05/2026]. See the Terms and Conditions (https://onlinelibrary.wiley.com/terms-and-conditions) on Wiley Online Library for rules of use; OA articles are governed by the applicable Creative Commons License

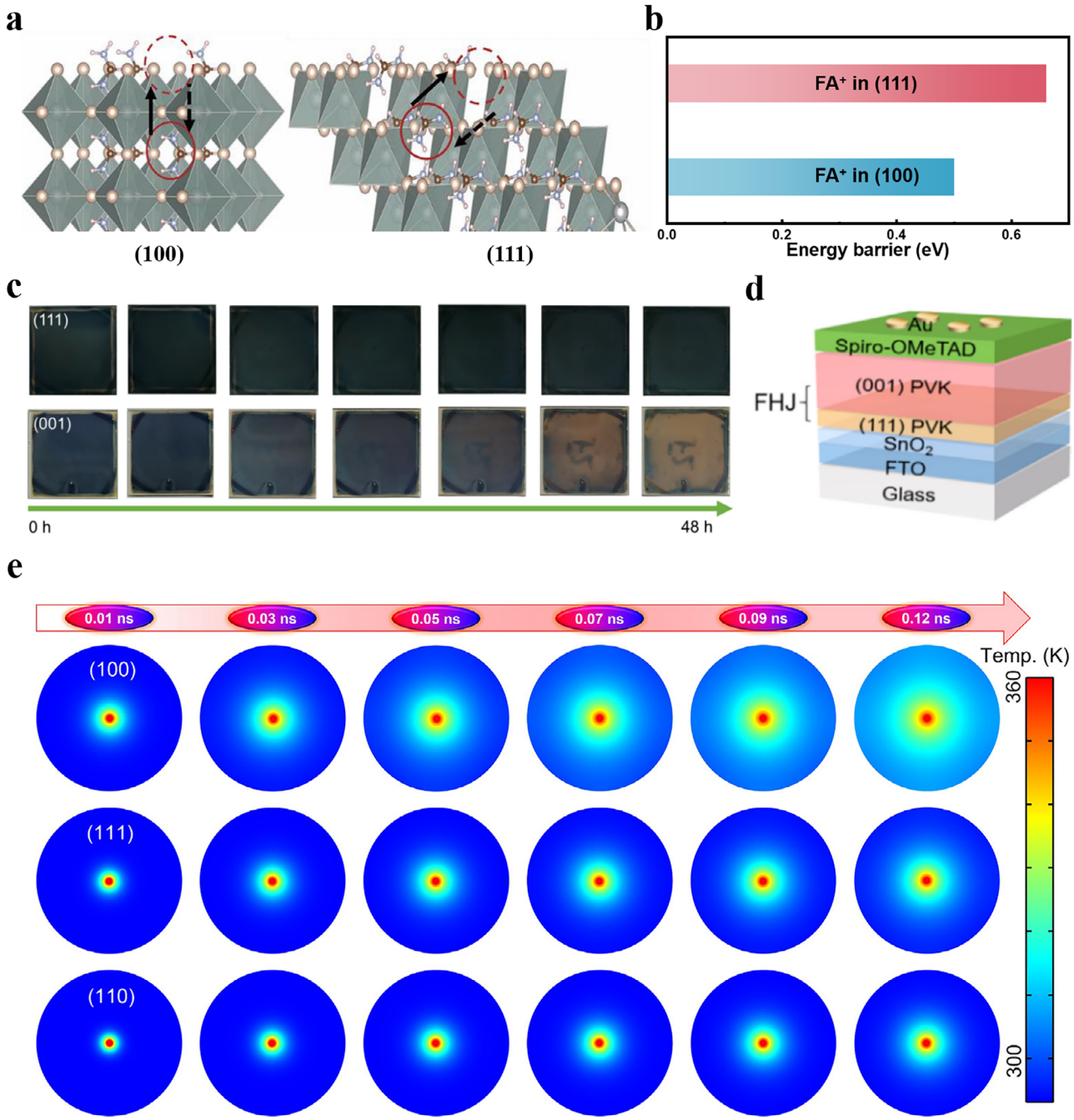


FIGURE 13 | (a) Schematic diagram of the cationic migration route in the (100) and (111) facets [111] (b) Active migration energy of cationic migration in the (100) and (111) facets. Reproduced with permission [111]. Copyright 2024, John Wiley and Sons. (c) the stability difference of (100) and (100) films [115] (d) Schematic diagram of PSCs with facet heterojunction. Reproduced with permission [115]. Copyright 2025, Elsevier. (e) Simulations of heat transfer dynamics of various facets, from COMSOL simulations based on the finite element method. Reproduced under the terms of the CC-BY 4.0 license [116]. Copyright 2025, J. Li et al.

of ABX_3 and feature a 3D interconnected octahedral framework. This crystalline structure endows PSCs with excellent photovoltaic performance, yet renders them susceptible to degradation induced by environmental stimuli including heat, light, oxygen and moisture. A typical example is that FA-based perovskites tend to transform from the desirable photoactive α-$FAPbI_3$ to the δ-$FAPbI_3$ under thermal input. In contrast, low-dimensional perovskites exhibit distinctive advantages in physical properties via molecular-level engineering, including superior thermal stability. Thus, dimensional engineering offers an effective approach to tackle the thermal instability of perovskites by constructing low-dimensional architectures. Currently, low-dimensional perovskites are mainly categorized into 0D, 1D and 2D structures. Considering the regulation of carrier transport behavior, the 2D perovskite structures have attracted the most intensive research attention among the three types (Figure 14a) [117, 118].

16136829, 0, Downloaded from https://onlinelibrary.wiley.com/doi/10.1002/smll.202514991 by Metcheng Li - North China Electric Power University Beijing , Wiley Online Library on [25/05/2026]. See the Terms and Conditions (https://onlinelibrary.wiley.com/terms-and-conditions) on Wiley Online Library for rules of use; OA articles are governed by the applicable Creative Commons License

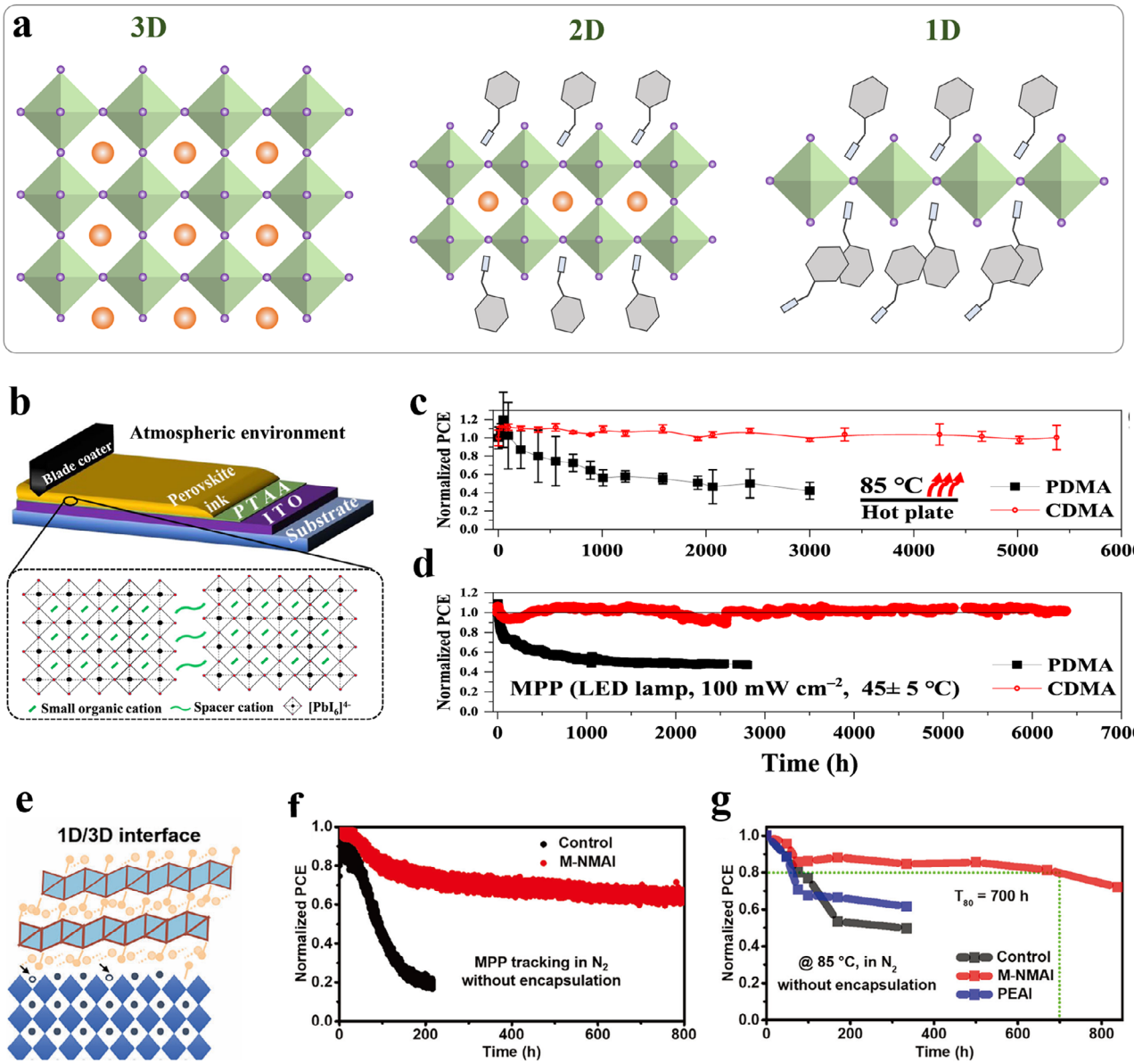


FIGURE 14 | (a) Schematic diagram of 3D perovskite, 2D perovskite, 1D perovskite and 0D perovskite. (b) Schematic illustration of the device configuration. A schematic diagram of the $n = 5$ DJ perovskite structure is shown in the dashed box [124] (c) Thermal stability of solar cells treating at an 85°C hotplate in N_2 atmosphere [124] (d) MPP tracking measured for the PSCs at ~45°C in N_2 atmosphere.Reproduced with permission [124]. Copyright 2024, Nature Publishing Group. (e) Schematic diagram of 1D/3D structure [131] (f) Stability test of unencapsulated devices under tracking at maximum power point under AM 1.5G illumination [131] (g)Thermal stability of devices without encapsulation at 85°C in N_2 atmosphere.Reproduced with permission [131]. Copyright 2025, John Wiley and Sons.

2D perovskites possess a layered structure in which inorganic octahedra are confined into 2D or quasi-2D configurations by large-sized organic cations serving as spacing layers. This unique structure retains a conductive inorganic network like that of conventional 3D perovskites in the in-plane direction for efficient carrier transport, whereas the vertical charge transport is impeded by the relatively large band gap of the organic interlayers. In practical high-temperature aging tests, this heterostructure configuration enables the low-dimensional perovskite phase to function as a mechanical buffer layer. By accommodating the thermal expansion mismatch between the 3D perovskite crystals and the underlying substrate or charge transport layers, it effectively alleviates interfacial tensile strain and suppresses lattice distortion during thermal stress. Consequently, the structural integrity of the photoactive 3D framework is preserved through enhanced lattice rigidity and surface anchoring, which serves as the primary mechanism for the improved thermal stability [119–122]. Taking advantage of the superior thermal stability of 2D perovskites, researchers attempted to introduce a 2D perovskite phase into 3D perovskite films to enhance their thermal stability. Based on the spatial configuration of 3D and 2D perovskite components, such research can be broadly classified into two categories: 2D/3D mixed-phase perovskites (quasi-2D perovskites) and 2D/3D heterojunction perovskites. The 2D/3D mixed-phase perovskites refer to a mixed-dimensional structure where 2D perovskites with different n values (the number of inorganic layers

16136829, 0, Downloaded from https://onlinelibrary.wiley.com/doi/10.1002/smll.202514991 by Meicheng Li - North China Electric Power University Beijing , Wiley Online Library on [25/05/2026]. See the Terms and Conditions (https://onlinelibrary.wiley.com/terms-and-conditions) on Wiley Online Library for rules of use; OA articles are governed by the applicable Creative Commons License

between two organic cation layers) and 3D perovskites coexist within a single film. This internal multi-phase heterostructure creates a series of coordinated phase-domain interfaces that effectively facilitate interfacial strain relaxation. The coherent growth between different n-phase domains helps to accommodate the lattice mismatch, thereby suppressing the formation of structural defects and thermal decomposition centers. Furthermore, the high formation energy and intrinsic chemical stability of the low-dimensional layers provide a robust scaffold that reinforces the crystalline framework of the 3D perovskite. This structural reinforcement not only enhances the film's resistance to thermal-induced phase degradation but also ensures a more durable and high-quality photoactive layer, which is fundamental to the sustained performance of the resulting devices [123]. In the work reported by Zhang et al., a structural design strategy of quasi-2D perovskites with slight interlayer dislocation was proposed and verified, in which 1,4-cyclohexanedimethylammonium (CDMA) was employed as a bifunctional organic spacer cation (Figure 14b) [124]. This special quasi-2D structure provides interlayer slip freedom to enhance the ability of the film to buffer internal strain, and can strengthen the interlayer electronic coupling due to relatively small interlayer spacing. Moreover, the researchers found that this slight dislocation structure can weaken the adsorption of water molecules. Given the consensus that moisture-thermal coupling effects tend to degrade the stability of perovskites, this characteristic is also beneficial to the thermal stability of the devices. Ultimately, the modified devices retained nearly their initial efficiency after thermal aging at 85°C for more than 5000 h and tracking at MPP under continuous illumination for 6000 h (Figure 14c,d).

In contrast, the 2D/3D heterojunction perovskites typically involve constructing a thin 2D perovskite capping layer on the surface/interfaces of 3D perovskites to form an interfacial passivation layer or encapsulation layer, where the 2D and 3D phases form a heterojunction structure. This relatively well-defined architecture can preserve the superior carrier transport properties of the 3D perovskites. With precise control over the uniformity and thickness of the capping layer, the carrier blocking effect induced by the 2D layer is milder than that of the mixed-dimensional quasi-2D counterparts, making it a preferable strategy for synergistically balancing photovoltaic efficiency and device stability [125, 126]. Tan et al. regulated the crystallinity and phase purity of 2D perovskite via a mixed-solvent strategy to form a robust 2D layer on the surface of 3D perovskite films [127]. The resultant device with 2D/3D heterojunction achieved a PCE of 25.9%, and retained 91% of their initial efficiency after continuous tracking at MPP for 1074 h at 85°C, demonstrating exceptional long-term durability. Based on the basic 2D/3D heterojunction structure, Liu et al. designed a cross-linked polymer interlayer (PIL) synthesized via free-radical polymerization of pentaerythritol tetraacrylate (PETTA) and N-vinylcarbazole (NVCZ), thus constructing a 3D/PIL/2D perovskite heterojunction [128]. This structure passivates the surface defects of 3D perovskites and alleviates tensile strain, while acting as a robust physical barrier to inhibit the migration of A-site cations between 2D and 3D perovskite under thermal stress, which consequently leads to a remarkable enhancement in the thermal stability of the devices.

In contrast to 2D low-dimensional perovskites, the physical properties of 1D perovskites exhibit distinct differences owing to the extreme quantum confinement effect and their unique crystal stacking modes [129, 130]. In 1D perovskites, inorganic octahedra are fully encapsulated by organic cations to form 1D long-chain structures, which present a more prominent isolation effect than 2D perovskites and possess higher rigidity, thus enabling more effective suppression of thermally induced phase transition. Liang et al. introduced N-methyl-1-(naphthalen-1-yl)methanaminium iodide (M-NMAI) to facilitate the stable formation of 1D perovskites, therefore forming a robust 1D/3D heterostructure via interfacial interactions with the 3D perovskite matrix (Figure 14e) [131]. Benefiting from the superior thermal stability of the 1D phase, the fabricated devices exhibited significantly better thermal stability than the pure 3D and 2D/3D heterojunction control devices during operation at 85°C, which verified the stronger thermal degradation resistance of 1D perovskite phases (Figure 14f).

In general, despite the sophisticated fabrication process of low-dimensional perovskites, their organic barrier layers can effectively inhibit internal ion migration and thermally induced phase transition in the crystal lattice. The integration of low-dimensional structural engineering with other stabilization strategies can not only preserve the merits of interfacial optimization, but also further strengthen the multi-level thermal stability of both the bulk phase and grain boundaries, which provides an important guidance for the construction of PSCs with ultrahigh thermal stability.

4.4 | Stress Engineering

Mechanical stress and thermal strain are also recognized as critical factors affecting the thermal stability of PSCs. Thermal instability of PSCs usually originates from the accumulation of internal and interlayer stress within the materials. During thermal cycling, the accumulated stress can induce interfacial microcracks, lattice distortion, phase segregation and accelerated ion migration, thus significantly accelerating the thermal degradation of the devices [132, 133]. Targeting the thermal induced stress and the following perovskite degradation, stress regulation strategies from different perspectives has been proposed.

In practical operation, the thermal stress in PSCs mainly arises from heat accumulation, thermal cycling and the mismatch in thermal expansion coefficients of functional layers. Heat accumulation is essentially attributed to a higher heat generation rate than heat dissipation rate during device operation, which may induce the formation of local hotspots. The film layers in these regions are prone to microcrack formation, and the local temperature gradient can cause inhomogeneous thermal expansion of the device, generating shear stress and further leading to interfacial delamination. In addition, prolonged local temperature elevation exerts a pronounced accelerating effect on the induction of ion migration, defect activation and local phase transition. To address these issues, feasible countermeasures include heat generation suppression [134], temperature homogenization and heat dissipation enhancement. Regarding temperature homogenization and heat dissipation enhancement, researchers attempted to construct thermal conduction pathways in PSCs to achieve improved thermal stability. Feng et al. reported their work on heat dissipation optimization to

16136829, 0, Downloaded from https://onlinelibrary.wiley.com/doi/10.1002/smll.202514991 by Meicheng Li - North China Electric Power University Beijing , Wiley Online Library on [25/05/2026]. See the Terms and Conditions (https://onlinelibrary.wiley.com/terms-and-conditions) on Wiley Online Library for rules of use; OA articles are governed by the applicable Creative Commons License

address the poor thermal transfer efficiency in PSCs, where graphitic carbon nitride (g-C_3N_4) nanosheets were introduced as thermal conduction channels between the perovskite layer and the electron transport layer (Figure 15a) [135]. This design significantly enhanced the thermal conduction efficiency without impeding carrier transport, and even facilitated carrier extraction, ultimately leading to a remarkable improvement in the thermal stability of the devices (Figure 15b,c). Similarly, Tan et al. incorporated ortho-carborane (o-CB) as an additive into perovskite films in all-perovskite tandem solar cells [136]. Due to its electron delocalization characteristics, the vertical thermal conductivity of the perovskite films was increased from 2.476 W $m^{-1}°C^{-1}$ to 2.697 W $m^{-1}°C^{-1}$, which effectively enhanced the film heat dissipation and maintained temperature uniformity. Verified by thermal aging tests at 85°C and X-ray diffraction (XRD) characterization, this treatment significantly improved the thermal stability of the perovskite films.

In practical operating conditions, PSCs are subjected to thermal expansion and contraction induced by prolonged temperature fluctuations. During this thermal cycling, the materials undergoes cyclic loading, generating the thermal stress, which gives rise to fatigue damage [137, 138]. In response to these issues, mechanisms such as elastic buffering and grain boundary adhesion enhancement can provide effective improvements. Li et al. introduced the ordered dipolar structure of β-poly(1,1-difluoroethylene) (β-PVDF) to regulate the crystallization kinetics and energy alignment of perovskite films, which addressed the issues of low efficiency and poor stability caused by thermal stress in conventional p-i-n structured devices (Figure 15d–f) [139]. The resultant devices retained 93.9% of their initial efficiency after 120 rapid thermal cycles between −60°C and +80°C. An innovative research work that integrated graphene with perovskite films was also reported to address the device thermal stability [21] Monolayer graphene was constructed at the internal interfaces of perovskite films via polymeric binders, which combined the ultrahigh mechanical rigidity of graphene with the excellent flexibility of polymers (Figure 15g). Graphene provides rigid mechanical confinement to restrict the amplitude of lattice strain in perovskites, thus preventing lattice plastic slip, fracture and mismatched thermal expansion of functional layers. Meanwhile, the polymer absorbs the accumulated thermal stress through elastic stretching and contraction during prolonged thermal cycling (Figure 15h). Ultimately, the modified devices retained more than 97% of their initial efficiency after continuous illumination under AM 1.5G solar light at 90°C for over 3670 h.

As for the cumulative stress fatigue damage in devices during long-term thermal cycling operation, dynamic self-healing regulation triggered by thermal stimuli offers an ideal solution to address these chronic degradation issues [140]. Tang et al. synthesized a framework material (HDSF) with a highly conjugated and ordered porous structure via dehydration condensation polymerization of 4-aminophenyl disulfide (APD) and tris(4-formylphenyl)amine [141]. The thermo-reversible temperature range for the cleavage and recombination of disulfide bonds in APD is precisely 60°C–80°C, which fully covers the operating temperature range of PSCs. At elevated temperatures, the chemical bonds break, and the material framework rearranges to repair defects and release accumulated stress. While at reduced temperatures, the disulfide bonds reform to stabilize the lattice structure and maintain efficient carrier transport. This thermally triggered dynamic self-healing behavior enables the devices to adapt to long-term temperature perturbations induced by thermal cycling.

In multilayer-stacked PSCs, the discrepant thermal expansion coefficients among different functional layers lead to inconsistent thermal expansion or contraction amplitudes of each layer during thermal cycling, which mainly results in thermally induced stress (Figure 15i) [142, 143]. In addition to impairing interfacial adhesion and inducing plastic deformation of functional layers, such thermal stress can also cause fracture of the perovskite films, as well as lattice distortion and even phase transition under localized stress [144]. To address such issues, regulating the intrinsic thermal expansion coefficient of the perovskite film can effectively mitigate thermal stress. For instance, Zhang et al. incorporated negative thermal expansion materials into perovskite films to suppress the thermal expansion coefficient mismatch between the perovskite layer and the substrate [145]. A similar stress compensation effect can also be achieved by regulating the adjacent functional layers of perovskites. As reported by Xue et al., they proposed a stress compensation strategy to enhance device thermal stability by introducing compressive stress via the HTL [143]. A HTL material with a high thermal expansion coefficient and strong interfacial bonding with perovskites (e.g., PDCBT) was deposited at elevated temperatures, which can exerts compressive stress on the perovskite layer upon cooling to room temperature, thus achieving a balance between tensile and compressive stress in the fabricated perovskite films. The introduction of an interfacial buffer layer can also effectively mitigate interfacial thermal stress. Gao et al. constructed a "pseudo-arch bridge" structure at the TiO_2/perovskite buried interface through 4-(5,6-difluoro-2-(pyridin-2-yl)-1Hbenzo[d]imidazol-1-yl)butan-1-ammonium iodide (abbreviated as FBI-PyAI), which significantly reduces the interfacial strain energy from 0.554 eV to 0.178 eV, thereby inhibiting defect formation and phase segregation (Figure 15j,k) [146]. The optimized devices retained 88% of their initial efficiency after 50 thermal cycles from −15°C to 65°C.

Besides the thermal stress arises during the long-term practical operation of PSCs, internal stress can also be generated during the fabrication process, including solvent evaporation, annealing treatment, and encapsulation procedures. For such initial residual stress in the as-fabricated PSCs, the regulatory strategies involving A-site cation component engineering [147] and crystal facet engineering, as well as the rational optimization of solvent systems, annealing protocols and encapsulation processes, can all reduce residual stress to a certain extent.

4.5 | Ion Migration Inhibition

Ion migration is closely correlated with the physical characteristics including defect property and crystal structure of perovskites, which is accompanied by the perovskite thermal degradation process [147–150]. Consequently, the aforementioned strategies including cation component engineering, crystal facet engineering, dimensional engineering and thermal stress regulation all exert a positive effect on mitigating ion migration. As alluded to in Section 4.3, dimension engineering not only reinforces the

16136829, 0, Downloaded from https://onlinelibrary.wiley.com/doi/10.1002/smll.202514991 by Meicheng Li - North China Electric Power University Beijing , Wiley Online Library on [25/05/2026]. See the Terms and Conditions (https://onlinelibrary.wiley.com/terms-and-conditions) on Wiley Online Library for rules of use; OA articles are governed by the applicable Creative Commons License

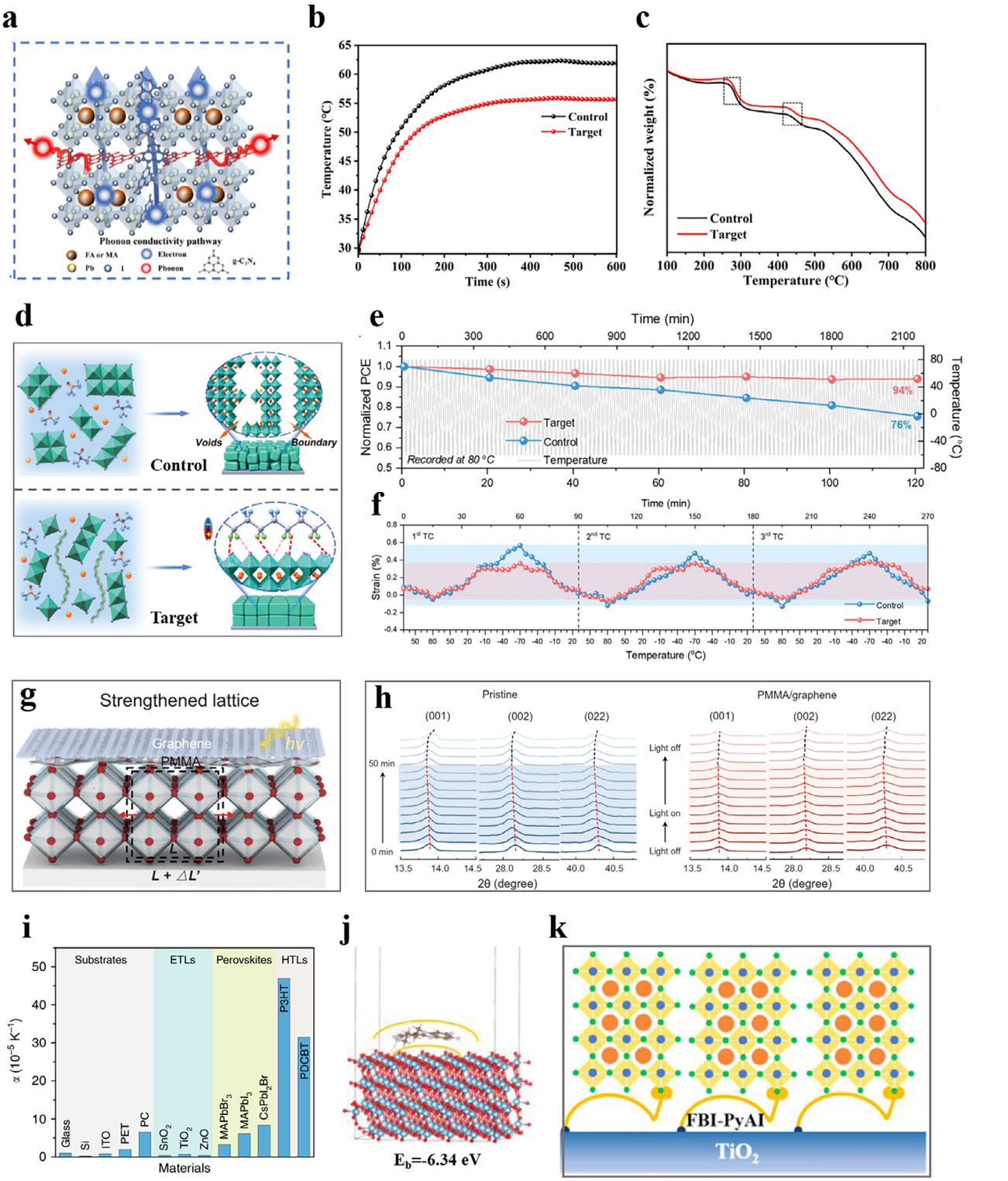


FIGURE 15 | (a) Heat dissipation illustration of the g-C_3N_4-treated perovskite film [135] (b) Real-time temperature tracking of different films under continuous one-sun illumination [135] (c) Thermogravimetric analysis curves for the different films. Reproduced with permission [135]. Copyright 2025, Royal Society of Chemistry. (d) Schematic of processing control and target perovskites, the target perovskite incorporating β-PVDF [139] (e) Device stability against thermal cycles between −60° and +80°C [139] (f) The temperature-resolved lattice strain for control and target perovskites. Reproduced with permission [139]. Copyright 2023, The American Association for the Advancement of Science. (g) Schematic diagram of PMMA/graphene integrated PSCs [21] (h) In situ XRD patterns of half-devices with various interface structures under white LED light irradiation for pristine device and PMMA/graphene device. Reproduced with permission [21]. Copyright 2025, The American Association for the Advancement of Science. (i) The thermal expansion coefficients among different functional layers. Reproduced under the terms of the CC-BY 4.0 license [143]. Copyright 2020, D.-J. Xue et al. (j) Proposed adsorption configuration of FBI-PyAI molecule on TiO_2 through DFT calculations [146] (k) Schematic diagram of the interaction between FBI-PyAI and perovskite. Reproduced with permission [146]. Copyright 2025, John Wiley and Sons.

16136829, 0, Downloaded from https://onlinelibrary.wiley.com/doi/10.1002/smll.202514991 by Meicheng Li - North China Electric Power University Beijing , Wiley Online Library on [25/05/2026]. See the Terms and Conditions (https://onlinelibrary.wiley.com/terms-and-conditions) on Wiley Online Library for rules of use; OA articles are governed by the applicable Creative Commons License

structural skeleton of the film but also imposes a significant energetic barrier for ion diffusion. In addition to these approaches, the strategies including defect passivation, ionic anchoring and ionic blocking can also significantly inhibit ion migration for enhanced thermal stability of perovskite through inhibiting phase transition and impeding perovskite decomposition.

Passivating defect via Lewis acid-base interactions or coordination bonding constitutes a widely adopted strategy to optimize PSCs, with the commonly used passivators including organic Lewis acids and Lewis bases [151]. As electron-pair donors, Lewis bases can effectively passivate the most prevalent and detrimental Pb^{2+}-related defects in perovskites, which can reduce the formation of non-radiative recombination centers, stabilize the octahedral framework of perovskites and improve their structural stability. Thus, Lewis bases have been extensively investigated in this field. By screening and comparing the binding interactions between various Lewis bases and undercoordinated Pb^{2+} via density functional theory (DFT) calculations, Li et al. found that phosphorus-containing molecules exhibit stronger binding strength than other sulfur-, nitrogen- and oxygen-based analogues, following a general order of P>N>S>O [152]. Further, a diphosphorus molecule, 1,3-bis(diphenylphosphino)propane (DPPP), was utilized to modify the PSCs through bridging the interfaces and grain boundaries of perovskite films (Figure 16a) [152]. Ultimately, the PSCs treated with DPPP retained approximately 90% of their initial efficiency after storage at 85°C for 1500 h. Thermally triggered dynamic interaction-based passivation strategies enable an ultra-specialized enhancement of the thermal stability of perovskites. Wang et al. designed and synthesized a Lewis acid-base material with hindered urea/thiocarbamate bonds (HUBLA), which can not only passivate pre-existing defects at room temperature, but also realize self-healing coordination reconstruction via two thermo-reversible dynamic covalent bonds (hindered urea (HUB) and thiocarbamate (TCB) bonds) upon heating to repair newly generated defects during thermal stress, thus endowing the devices with stable photovoltaic efficiency after prolonged thermal aging at 85°C (Figure 16b) [153].

Apart from defect passivation, additive molecules with strong interactions toward migrating ions can also be adopted to anchor ions, thereby suppressing ion migration. For the highly mobile halide ions and organic cations in perovskite films, additive molecules were incorporated to form hydrogen bonds, coordination bonds and other interactions with target ions via their molecular functional groups. This not only elevates the ion migration energy barrier but also synchronously passivates lattice defects, thus hindering halide ion migration and cation escape from the lattice. For iodide ions (I^-), anchoring or trapping I^- to suppress its migration is typically achieved by forming directional hydrogen bonds between I^- and amino, hydroxyl and other polar groups in additive molecules, or by forming halogen bonds between I^- and halogen atoms in additive molecules. Guo et al. reported a supramolecular calix[4]pyrrole (C[4]P) with surface anionic complexation capability, which anchors halides on the surface of perovskite films to stabilize the perovskite lattice structure and increase the activation energy for halide migration (Figure 16c,d) [154]. Cai et al. designed polyfluoro-substituted amide molecules to stabilize the perovskite framework and trap I^- via halogen bonding for ion migration suppression, leading to a remarkable enhancement in the thermal stability of the resultant PSCs [155].

For organic cations, research focused on additive molecules containing multidentate functional groups (e.g., guanidyl and amino groups), which form multiple hydrogen bonds or coordination bonds with FA^+ cations. This interaction significantly elevates the energy barrier for FA^+ deintercalation from the lattice. Meanwhile, such additives normally can participate in the crystallization process of perovskites to regulate grain growth kinetics, alleviate lattice distortion caused by the disordered arrangement of FA^+ cations, and inhibit the escape of FA^+ during phase transition. Du et al. adopted polyhexamethyleneguanidine hydrochloride (PHMG) as a molecular creeper on perovskite to inhibit its thermal-induced decomposition [156]. The PHMG possesses a long-line molecular structure where the guanidinium group can serve as suckers that strongly anchor FA^+ through multiple hydrogen bonds with an absorption energy of −3.47 eV, which is enough to immobilize the FA^+ (Figure 16e).

This ionic anchoring strategy can be further extended to a dual-ion synergistic anchoring system, where different functional groups of a single additive molecule bind to I^- and FA^+ respectively, enabling the simultaneous suppression of both ions. He et al. proposed a hydrophobic calixarene supramolecular strategy, utilizing the rigid cavity (1.2 nm in diameter) and eight phenolic hydroxyl multi-sites of 4-tert-butylcalix[8]arene (C8A) [157]. Through host-guest interactions, C8A synchronously anchors I^-, FA^+ and other mobile ions, which significantly enhances the moisture and thermal stability of PSCs.

Constructing ion-blocking layers represents another effective strategy for suppressing ion migration in perovskites. Detailly, A functional layer with integrated physical barrier and chemical anchoring properties is constructed between the perovskite layer and charge transport layers, which blocks ion migration via the synergistic effect of physical confinement and chemical bonding. Such ion-blocking layers are generally required to form a dense and continuous physical structure, thus constructing a spatial barrier against ion diffusion and impeding the migration and diffusion of mobile ions (e.g., I^- and FA^+) toward the interfaces or other functional layers. Meanwhile, the ion-blocking layer materials may form chemical interactions with perovskite via dedicated functional groups or chemical bonds, thus passivating interfacial defects. Yang et al. introduced sulfate or phosphate anions onto the perovskite surface to convert the surface of lead halide perovskites into water-insoluble wide-bandgap lead oxysalts. This surface modification effectively stabilized the perovskite, enabling the resulting PSCs to retain 96.8% of their initial efficiency after 1200 h of operation at 65°C [158]. Zai et al. integrated wafer-scale continuous monolayer molybdenum disulfide (MoS_2) buffer layers on both the top and bottom surfaces of the perovskite layer via a transfer process (Figure 16f). These ultrathin films not only physically block the migration of ions from the perovskite layer to the charge transport layers, but also chemically stabilize perovskite via strong coordination interactions. The resultant devices demonstrated excellent high-temperature operational stability, with an efficiency decay of less than 4% after continuous operation at 85°C for 1200 h (Figure 16g).

16136829, 0, Downloaded from https://onlinelibrary.wiley.com/doi/10.1002/smll.202514991 by Meicheng Li - North China Electric Power University Beijing , Wiley Online Library on [25/05/2026]. See the Terms and Conditions (https://onlinelibrary.wiley.com/terms-and-conditions) on Wiley Online Library for rules of use; OA articles are governed by the applicable Creative Commons License

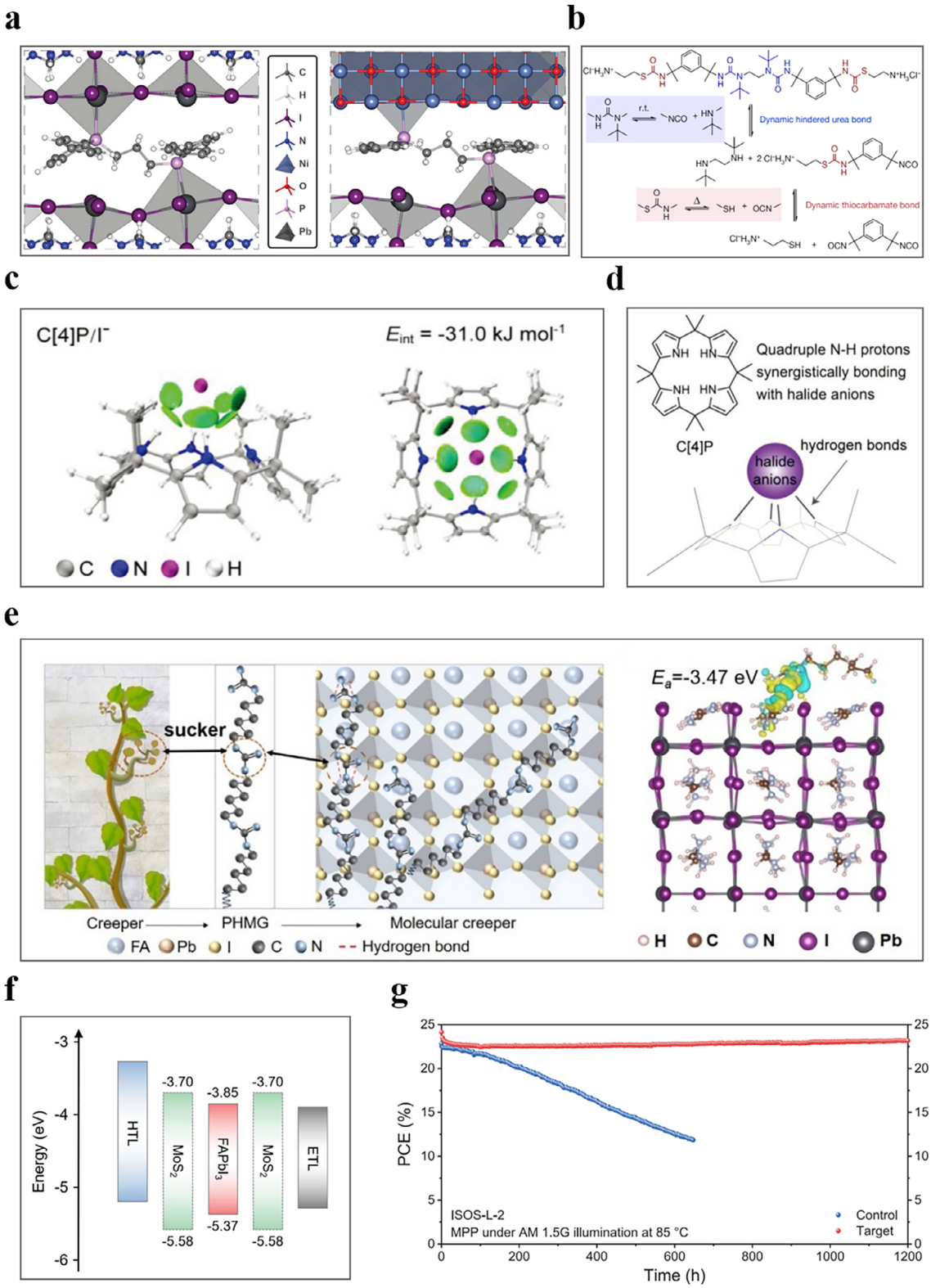


FIGURE 16 | (a) Two perovskite slabs, perovskite and NiO_x substrate through chemical-bond formation between P and Pb or Ni atoms in a Lewis acid-base reaction. Reproduced with permission [152]. Copyright 2023, The American Association for the Advancement of Science. (b) Dynamic reaction of HUBLA. Reproduced with permission [153]. Copyright 2024, Nature Research. (c) the DFT optimized geometries of porphyrin/I^- and C[4]P/I^- complex [154] d) Molecular structure of C[4]P and schematic diagram of surface halide anions complexation. Reproduced with permission [154]. Copyright 2023, John Wiley and Sons. (e) The charge density difference of the single unit of PHMG anchoring on the perovskite grain surface and schematic diagram of creeper-inspired protection strategy. Reproduced under the terms of the CC-BY 4.0 license [156]. Copyright 2024, S. Du et al. (f) Energy-level alignment between perovskite and monolayer MoS_2 [20]. (g) Tracking at MPP for encapsulated devices under AM 1.5G illumination at 85°C in the ambient atmosphere. Reproduced with permission [20]. Copyright 2025, The American Association for the Advancement of Science.

16136829, 0, Downloaded from https://onlinelibrary.wiley.com/doi/10.1002/smll.202514991 by Meicheng Li - North China Electric Power University Beijing , Wiley Online Library on [25/05/2026]. See the Terms and Conditions (https://onlinelibrary.wiley.com/terms-and-conditions) on Wiley Online Library for rules of use; OA articles are governed by the applicable Creative Commons License

This interfacial ion-blocking strategy can be further extended to grain boundaries, which are well recognized as fast diffusion channels for ion migration in perovskite films. Therefore, in addition to strategies of defect passivation, ionic anchoring and interfacial blocking, the grain boundary blocking also constitutes an important approach to inhibit ion migration [159–162]. On the one hand, grain boundaries can be directly passivated or encapsulated via additive engineering. For instance, in the work reported by Jiao et al., tributyl(methyl)phosphonium iodide (TPI) was introduced into the perovskite precursor to construct a 1D perovskite layer for grain boundary encapsulation and passivation [163]. The treated devices retained 92.2% of their initial efficiency after 1900 h of illumination at 55°C, achieving a remarkable enhancement in thermal stability. On the other hand, reducing grain boundary density via grain size regulation also serves as an indirect strategy for grain boundary engineering. For example, Zhao et al. added a triarylamine bromide trimer (TTABr) in perovskite film to enlarge the grain size through the interaction between TTABr molecules and intermediate adducts, which enables the treated devices possess an enhanced stability under thermal condition [164].

4.6 | Others

In addition to the strategies mentioned before, manipulating crystallization kinetics via the solvent engineering, anti-solvents regulation and annealing treatments to obtain high-quality perovskite films with dense morphology, low defect density also represent a feasible strategy for enhancing the perovskite thermal stability [165–168]. Notably, the design objective of such strategies is generally to achieve high photovoltaic efficiency rather than specifically addressing thermal stability issues. For instance, Wang et al. developed a green solvent-based ink system comprising γ-valerolactone (GVL), 2-methyltetrahydrofuran (2-MeTHF) and dimethyl sulfoxide (DMSO) (Figure 17a) [169]. High-quality perovskite films were fabricated via slot-die coating and vacuum drying processes under ambient air conditions, enabling the production of a 7200 cm^2 perovskite module with a certified steady-state efficiency of 17.2%. This module exhibited excellent stability under various harsh environmental conditions including thermal cycling aging (Figure 17b).

Regarding annealing processes, the most basic step is to set appropriate annealing temperatures and times based on the selected PSC system. Building upon this, researchers have explored specialized processes such as flash infrared annealing, intense pulsed light annealing, and molecular extrusion annealing. Among these, flash infrared annealing utilizes the efficient absorption of infrared light by the perovskite precursor, inducing it to transform into a crystalline state within a short time. This helps suppress the thermal volatilization or decomposition of organic cations during annealing and avoids the problem of significant residual thermal stress accumulation in functional layers during prolonged heating in traditional annealing, thus contributing to improved long-term operational stability of the thin film [170]. Intense pulsed light annealing rapidly heats the perovskite layer to its crystallization temperature using high-energy pulsed light generated by a xenon lamp, achieving a rapid annealing effect similar to flash infrared annealing. This helps maintain the stability of organic components and avoids excessive heat treatment of other functional layers [171]. Besides, Hu et al. explored a novel annealing method, molecular extrusion annealing, to address the problems of iodine loss and local lattice degradation caused by traditional thermal annealing processes. By applying pressure during the annealing process, they eliminated micropores inside the film and helped the surface passivation molecules form tighter chemical bonds with interface defects, thus alleviating the interface failure problem under subsequent high-temperature conditions [172].

In addition, thermal management technologies, including using high thermal conductivity materials, external radiative cooling layers, down-conversion approaches, etc., also can improve the thermal stability of perovskite films and PSCs. Feng et al. attempted to construct thermal conduction pathways in PSCs to achieve improved thermal stability through using g-C_3N_4 nanosheets between the perovskite layer and the electron transport layer, which significantly enhanced the thermal conduction efficiency without impeding carrier transport [135]. George et al. used a special coating to selectively reflect the sunlight absorbed by the device, minimizing the reflection of wavelengths that cannot be converted into electrical energy by the perovskite device, while simultaneously enhancing its own thermal radiation dissipation. Through experiments and simulations, researchers have shown that this treatment can effectively reduce the steady-state operating temperature of the battery without affecting power generation efficiency, thus improving the long-term thermal stability of perovskite devices [173]. Similar thermal control methods have been achieved by researchers using down-conversion materials (rare-earth-doped nanomaterials, semiconductor quantum dots, fluorescent dyes, etc.). These materials can convert high-energy photons into multiple low-energy photons, which can effectively alleviates the thermal-optical coupling degradation problem faced by perovskite materials [174]. Other researchers are exploring using the heat generated during the operation of perovskite devices to power thermoelectric generators. This integrated system design aims to improve heat management of perovskite devices and enhance overall system energy efficiency. This technological direction not only helps improve the thermal stability of perovskite devices but also holds the potential to facilitate the large-scale production of perovskite [175, 176].

Furthermore, the device encapsulation is also crucial for their thermal stability. Reliable encapsulation is an essential prerequisite to ensure that devices can withstand multi-factor synergistic aging [177, 178]. Mariani et al. developed a low-temperature stress-free encapsulation technology based on industrial lamination processes in their research on the aging resistance [179]. Low-molecular-weight homopolymer polyisobutylene (PIB) with high chemical stability and high resistivity was utilized as the main encapsulation material, leveraging its phase transition property from semi-solid to liquid within the temperature range of -40 °C to 85 °C to absorb long-term thermal stress. Meanwhile, 2D hexagonal boron nitride (h-BN) was incorporated to further enhance the thermal conductivity and barrier properties against moisture and oxygen of the encapsulation system, significantly enhancing the device stability under thermal shock tests (Figure 17c,d).

16136829, 0, Downloaded from https://onlinelibrary.wiley.com/doi/10.1002/smll.202514991 by Meicheng Li - North China Electric Power University Beijing , Wiley Online Library on [25/05/2026]. See the Terms and Conditions (https://onlinelibrary.wiley.com/terms-and-conditions) on Wiley Online Library for rules of use; OA articles are governed by the applicable Creative Commons License

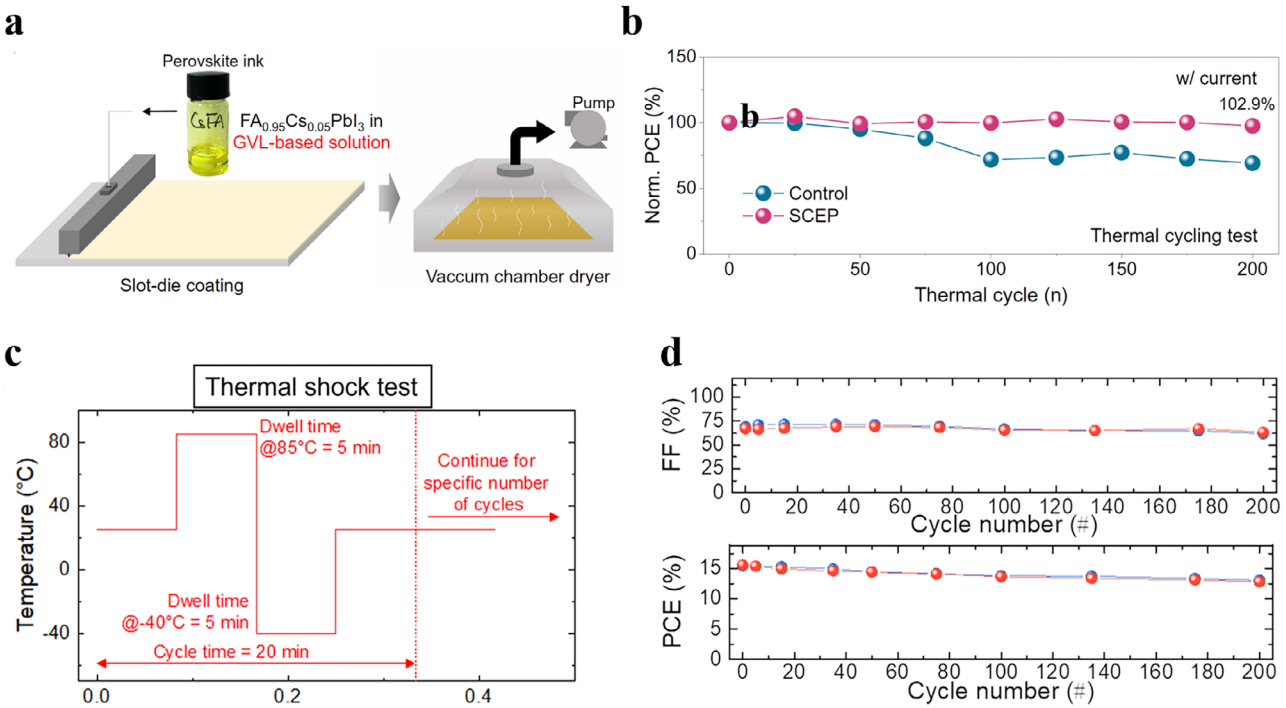


FIGURE 17 | (a) Schematic demonstrating large-scale fabrication of perovskite films with slot-die coating. Digital image of a perovskite ink composed of $FA_{0.95}Cs_{0.05}PbI_3$ dissolved in GVL/DMSO mixture [169] (b) Thermal cycling stability of perovskite module. Reproduced with permission. [169]. Copyright 2025, The American Association for the Advancement of Science. (c) Temperature profile of the thermal shock test performed on the mesoscopic n-i-p devices encapsulated with PIB and PIB:h-BN [179] (d) PV parameters of the mesoscopic n-i-p devices encapsulated with PIB and PIB:h-BN acquired over>200 cycles of the thermal shock test. Reproduced under the terms of the CC-BY 4.0 license [179]. Copyright 2024, P. Mariani et al.

5 | Conclusion and Outlooks

Perovskite solar cells (PSCs), as a rapidly emerging high-efficiency photovoltaic technology, are striving to advance toward industrialization and commercial deployment, with stability issues remaining the paramount bottleneck. As an intrinsic physical factor, heat is inevitably generated during the practical operation of PSCs, which not only directly triggers the degradation of perovskite materials, but also synergistically couples with light irradiation, humidity, reverse bias and other external stimuli to accelerate device failure. Aiming to address the critical stability challenges of PSCs, this review first briefly elaborates on the fundamental physical properties of perovskite materials, then systematically summarizes the thermal degradation mechanisms of PSCs, and further categorizes the currently effective strategies for thermal stability enhancement. We anticipate that this review will provide valuable insights for researchers in this field, facilitate the development of efficient thermal stability enhancement technologies for PSCs, and ultimately accelerate the practical deployment of PSCs and other perovskite-based optoelectronic devices.

Although remarkable progress has been achieved on the thermal stability of PSCs, numerous bottlenecks still need to be overcome in the route toward commercial applications. Therefore, further in-depth research on thermal stability is of profound scientific value and practical significance. The actual service environment of photovoltaic modules is complex and variable, where high temperature is not an isolated factor, but always acts synergistically with light irradiation, humidity, electric field and other environmental factors. Thus, future thermal stability research should follow an integrated philosophy of practical application-oriented investigation and multi-dimensional synergistic regulation. Accordingly, several specific perspectives for future research are proposed as follows:

(1) Focusing on the stability under coupled stimuli. In practical service processes, thermal effects are generally coupled with light irradiation and electric field; their synergistic action triggers an accelerated degradation effect with a superposition characteristic of "1+1>2". Current research mostly focuses on the stability of PSCs under a single thermal factor, and only a few studies have explored the coupling effects of heat with humidity or heat with light, which are insufficient to fully reflect the actual degradation behavior of PSCs. Hence, it is imperative to construct an aging test platform for the multi-field coupling of heat, light and electric field in the future, to systematically investigate the thermal degradation mechanisms under their synergistic action, further developing targeted multi-field stability enhancement strategies.

(2) Highlighting the passivation failure research. Passivation layer is indispensable for enhancing the optoelectronic performance of perovskite films, especially from the perspective of fabricating high-efficiency PSCs. Therefore, the passivation layer

16136829, 0, Downloaded from https://onlinelibrary.wiley.com/doi/10.1002/smll.202514991 by Meicheng Li - North China Electric Power University Beijing , Wiley Online Library on [25/05/2026]. See the Terms and Conditions (https://onlinelibrary.wiley.com/terms-and-conditions) on Wiley Online Library for rules of use; OA articles are governed by the applicable Creative Commons License

can be regarded, to a certain extent, as an integral component of high-quality perovskite films. Hence, it is necessary and significant to investigate the thermal-induced passivation failure and the passivator-associated perovskite degradation. At present, relatively few studies have focused on thermal-induced passivation failure; the corresponding mechanisms of thermal passivation failure, as well as the coupled decomposition mechanism between the passivation layer and the perovskite layer, remain to be further elucidated and refined. This research direction represents an underexplored yet promising direction for enhancing the thermal stability of PSCs.

(3) Developing thermo-responsive smart molecular materials for active enhancement of thermal stability. The introduction of functional organic molecules to improve the thermal stability of PSCs via defect passivation, ion anchoring and stress regulation has been proven to be an effective strategy. Nevertheless, these traditional stability enhancement strategies are mostly based on constant action pathways and enhance device stability in a passive protection manner, which are difficult to adapt to the complex and variable temperature environment during the actual operation of PSCs and the dynamic degradation mechanisms induced by temperature variation. To address this issue, utilizing thermoresponsive smart molecular functional materials is expected to be a suitable candidate strategy. Defect formation and dynamics are strongly temperature-dependent during device. Developing materials which can actively trigger responsive behaviors (e.g., structural phase transition, chemical bond recombination and ion trapping) to response temperature changes is expected to realize the dynamic regulation of defects or stress. For instance, additives with temperature-sensitive functional groups can be designed to actively bond with defects in the perovskite lattice or form a stable protective layer at high temperatures and thermally cross-linked charge transport materials can be exploited to improve their intrinsic stability and interfacial adhesion at elevated temperatures, ultimately achieving the active enhancement of thermal stability.

(4) Rationally integrating the various stability enhancement strategies. Despite the progressive advances in enhancing thermal stability of PSCs from various aspects, such as composition engineering, interface engineering, stress modulation, have been achieved, it should be noted that the optimization strategies from different research directions are not independent of each other, but highly coupled and mutually influential during the actual operation of devices. For example, the construction of low-dimensional perovskite structures can effectively suppress ion migration, but may simultaneously introduce new stress concentration issues at the heterointerfaces. Therefore, future research needs to strengthen the synergistic design of diverse strategies including composition regulation, interface modification, additive engineering and encapsulation technology, and realize the leap-forward enhancement of thermal stability through multi-strategy integration. A typical example is the combination of high-efficiency encapsulation technology with the introduction of ion migration inhibitors, which can form a dual protection mechanism of "internal inhibition & external barrier", thus synergistically enhancing the thermal stability.

Acknowledgements

This work is supported partially by the Key Research and Development Program sponsored by the Ministry of Science and Technology (MOST) (Grant nos. 2022YFB4200301), National Natural Science Foundation of China (Grant nos. 52232008, 52402254, 52102245, and 22409061), Beijing Nova Program (20220484016), Young Elite Scientists Sponsorship Program by CAST (2022QNRC001), the Fundamental Research Funds for the Central Universities (2023MS042, 2024MS036, 2023MS047, and 2024JC005) and the NCEPU "Double First-Class" Program.

Conflicts of Interest

The authors declare no conflict of interest.

Data Availability Statement

The authors have nothing to report.

References

1. NREL, Best research-cell efficiency chart 2025, https://www.nrel.gov/pv/interactive-cell-efficiency (accessed: December 2025).

2. H. Wang, S. Su, Y. Chen, et al., "Impurity-healing interface engineering for efficient perovskite submodules," *Nature* 634 (2024): 1091–1095, https://doi.org/10.1038/s41586-024-08073-w.

3. P. Cui, D. Wei, J. Ji, et al., "Planar p–n homojunction perovskite solar cells With efficiency exceeding 21.3%.3%," *Nature Energy* 4 (2019): 150–159, https://doi.org/10.1038/s41560-018-0324-8.

4. X. Xiao, N. Xu, X. Tian, et al., "Aqueous-based recycling of perovskite photovoltaics," *Nature* 638 (2025): 670–675, https://doi.org/10.1038/s41586-024-08408-7.

5. L. Yan, H. Huang, P. Cui, et al., "Fabrication of perovskite solar cells in ambient air by blocking perovskite hydration With guanabenz acetate salt," *Nature Energy* 8, no. 10 (2023): 1–10, https://doi.org/10.1038/s41560-023-01358-w.

6. A. Kojima, K. Teshima, Y. Shirai, and T. Miyasaka, "Organometal Halide Perovskites as Visible-Light Sensitizers for Photovoltaic Cells," *Journal of the American Chemical Society* 131 (2009): 6050–6051, https://doi.org/10.1021/ja809598r.

7. Z. Xiong, Q. Zhang, K. Cai, et al., "Homogenized chlorine distribution for >27% power conversion efficiency in perovskite solar cells," *Science* 390, no. 6773 (2025): 638–642.

8. G. Wang, M. Yu, H. Wu, et al., "Silicon solar cells With hybrid back contacts," *Nature* 647 (2025): 369–374, https://doi.org/10.1038/s41586-025-09681-w.

9. Z. Chu, B. Fan, Y. Zhao, et al., "Laser annealing enables rapid, degradation-free ambient processing of perovskite solar modules," *Science* 390 (6776): 905–910.

10. L. Jia, S. Xia, J. Li, et al., "Efficient perovskite/silicon tandem with asymmetric self-assembly molecule," *Nature* 644 (2025): 912.

11. Z. Liang, Y. Zhang, H. Xu, et al., "Homogenizing out-of-plane cation composition in perovskite solar cells," *Nature* 624 (2023): 557–563, https://doi.org/10.1038/s41586-023-06784-0.

12. J. Chen, X. Wang, T. Wang, et al., "Determining the bonding-degradation trade-off at heterointerfaces for increased efficiency and stability of perovskite solar cells," *Nature Energy* 10 (2025): 181.

13. J. Zhou, Z. Liu, P. Yu, et al., "Modulation of perovskite degradation With multiple-barrier for light-heat stable perovskite solar cells," *Nature Communications* 14 (2023): 6120, https://doi.org/10.1038/s41467-023-41856-9.

14. J. K. Kaldellis, M. Kapsali, and K. A. Kavadias, "Temperature and wind speed impact on the efficiency of PV installations. Experience obtained

16136829, 0, Downloaded from https://onlinelibrary.wiley.com/doi/10.1002/smll.202514991 by Meicheng Li - North China Electric Power University Beijing , Wiley Online Library on [25/05/2026]. See the Terms and Conditions (https://onlinelibrary.wiley.com/terms-and-conditions) on Wiley Online Library for rules of use; OA articles are governed by the applicable Creative Commons License

From outdoor measurements in Greece," *Renewable Energy* 66 (2014): 612–624, https://doi.org/10.1016/j.renene.2013.12.041.

15. M. K. Al-Ghezi, R. T. Ahmed, and M. T. Chaichan, "The Influence of Temperature and Irradiance on Performance of the photovoltaic panel in the Middle of Iraq," *International Journal of Renewable Energy Development* 11 (2022): 501–513, https://doi.org/10.14710/ijred.2022.43713.

16. W. Tress, K. Domanski, and B. Carlsen, "Performance of perovskite solar cells Under simulated temperature-illumination real-world operating conditions," *Nature Energy* 4 (2019): 568–574, https://doi.org/10.1038/s41560-019-0400-8.

17. J. Oh, G. Samy, and T. Mani, Temperature testing and analysis of PV modules per ANSI/UL 1703 and IEC 61730 standards in Program-35th IEEE Photovoltaic Specialists Conference. IEEE 2010, pp. 984–988.

18. N. Strevel, L. Trippel, and M. Gloeckler, "Performance characterization and superior energy yield of First Solar PV power plants in high-temperature conditions," *Photovoltaics International* 17 (2012): 148.

19. D. Faiman, "Assessing the outdoor operating temperature of photovoltaic modules," *Progress in Photovoltaics: Research and Applications* 16 (2008): 307–315, https://doi.org/10.1002/pip.813.

20. H. Zai, P. Yang, J. Su, et al., "Wafer-scale monolayer MoS_2 film integration for stable, efficient perovskite solar cells," *Science* 387 (2025): 186–192, https://doi.org/10.1126/science.ado2351.

21. Q. Li, Y. Zheng, H. Wang, et al., "Graphene-polymer reinforcement of perovskite lattices for durable solar cells," *Science* 387 (2025): 1069–1077, https://doi.org/10.1126/science.adu5563.

22. T. Zhao, M. M. Elshanawany, R. Singh, R. Guo, B. S. Richards, and U. W. Paetzold, "Accumulated structural evolution Under diurnal cycling degrades wide-bandgap perovskite solar cells," *ACS Energy Letters* 10 (2025): 4740–4748, https://doi.org/10.1021/acsenergylett.5c02064.

23. R. Azmi, E. Ugur, and A. Seitkhan, "Damp heat-stable perovskite solar cells with tailored-dimensionality 2D/3D heterojunctions," *Science* 376 (2022): 73.

24. Z. Peng, A. Vincze, F. Streller, et al., "Revealing degradation mechanisms in 3D/2D perovskite solar cells Under photothermal accelerated ageing," *Energy & Environmental Science* 17 (2024): 8313–8324, https://doi.org/10.1039/D4EE03869J.

25. Y. Zhang, Y. Bao, L. Shi, et al., "Coupled Thermodynamic and Stress–Strain Insights Into Textured Perovskite/Silicon Tandem Solar Cells," *ACS Energy Letters* 10 (2025): 3808–3817, https://doi.org/10.1021/acsenergylett.5c01282.

26. A. Raturi, P. Mittal, and S. Choudhary, "Engineering the electronic and optical properties of perovskite nanomaterials for optoelectronic applications: A review," *Materials Science in Semiconductor Processing* 203 (2026): 110250, https://doi.org/10.1016/j.mssp.2025.110250.

27. M. A. Green, A. Ho-Baillie, and H. J. Snaith, "The emergence of perovskite solar cells," *Nature Photonics* 8 (2014): 506–514, https://doi.org/10.1038/nphoton.2014.134.

28. A. K. Yadav, R. Pandey, and P. Singh, "Impedance spectroscopy in perovskite materials: From fundamentals to applications," *Inorganic Chemistry Communications* 182 (2025): 115524, https://doi.org/10.1016/j.inoche.2025.115524.

29. C. Li, M. Liu, X. Xu, and H. Mo, "Perovskite materials for multifaceted energy applications: From fundamental properties to industrialization challenges," *Materials Science in Semiconductor Processing* 202 (2026): 110199, https://doi.org/10.1016/j.mssp.2025.110199.

30. C. Zhou, H. Lin, Q. He, et al., "Low dimensional metal halide perovskites and hybrids," *Materials Science and Engineering: R: Reports* 137 (2019): 38–65, https://doi.org/10.1016/j.mser.2018.12.001.

31. K. D. Jayan and J. Aparna, "Exploring nonlinear optical properties in perovskite indoor photovoltaics: Stability and efficiency perspectives," *Materials Science and Engineering: B* 324 (2026): 118989, https://doi.org/10.1016/j.mseb.2025.118989.

32. Y.-N. Zhang, Q. Li, B. Li, and C.-X. Wang, "Insight Into structure defects in high-performance perovskite solar cells," *Journal of Power Sources* 570 (2023): 233011, https://doi.org/10.1016/j.jpowsour.2023.233011.

33. S. Tian, S. Jiang, C. Zhao, S. Wang, and L. Lin, "Surface repair strategies for Enhancing the efficiency of inverted inorganic perovskite Photovoltaics," *Chemical Engineering Science* 323 (2026): 123193, https://doi.org/10.1016/j.ces.2025.123193.

34. K. D. Devi, V. S. Pandi, R. Sundar, and G. Vishnupriya, "High-performance perovskite tandem architectures: Materials innovation, device engineering, and industrial prospects," *Materials Science in Semiconductor Processing* 202 (2026): 110149, https://doi.org/10.1016/j.mssp.2025.110149.

35. A. A. Ugochukwu, F. Ahmad, M. Khalid, et al., "Recent enhancement in photovoltaic cell efficiency performance, stability, and cost reduction: A review," *Solar Energy* 300 (2025): 113853, https://doi.org/10.1016/j.solener.2025.113853.

36. N.-K. Kim, Y. H. Min, S. Noh, et al., "Investigation of thermally induced degradation in $CH_3NH_3PbI_3$ perovskite solar cells using in-situ synchrotron radiation analysis," *Scientific Reports* 7 (2017): 4645, https://doi.org/10.1038/s41598-017-04690-w.

37. P. S. Whitfield, N. Herron, and W. E. Guise, "Structures, phase transitions and tricritical behavior of the hybrid perovskite methyl ammonium lead iodide," *Science Reputation* 6 (2016): 35685.

38. J. H. Lee, N. C. Bristowe, and J. H. Lee, "Resolving the physical origin of octahedral tilting in halide perovskites," *Chemistry of Materials* 28 (2016): 4259–4266, https://doi.org/10.1021/acs.chemmater.6b00968.

39. R. Shi, Q. Fang, A. S. Vasenko, R. Long, W.-H. Fang, and O. V. Prezhdo, "Structural disorder in higher-temperature phases increases charge carrier lifetimes in metal halide perovskites," *Journal of the American Chemical Society* 144 (2022): 19137–19149, https://doi.org/10.1021/jacs.2c08627.

40. Z. Qiu, N. Li, Z. Huang, Q. Chen, and H. Zhou, "Recent advances in improving phase stability of perovskite solar cells," *Small Methods* 4 (2020): 1900877, https://doi.org/10.1002/smtd.201900877.

41. H.-S. Kim and N.-G. Park, "Soft lattice and phase stability of α-$FAPbI_3$," *Advanced Energy Materials* 15 (2025): 2400089.

42. Z.-A. Nan, L. Chen, Q. Liu, et al., "Revealing phase evolution mechanism for stabilizing formamidinium-based lead halide perovskites by a key intermediate phase," *Chem* 7 (2021): 2513.

43. J. He, Z. Guo, and K. Liu, "Controlled Cs^+ incorporation Through organocaesium salts in α-FA–Cs perovskite solar cells With a certified efficiency of 26.61%.61%," *Nature Energy* (2026), https://doi.org/10.1038/s41560-026-02016-7.

44. D. K. LaFollette, J. Hidalgo, O. Allam, et al., "Bromine incorporation affects phase transformations and thermal stability of lead halide perovskites," *Journal of the American Chemical Society* 146 (2024): 18576–18585, https://doi.org/10.1021/jacs.4c04508.

45. J. Zhao, X. Liu, Z. Wu, et al., "Temperature-Dependent Interplay Between Structural and Charge Carrier Dynamics in CsMAFA-Based Perovskites," *Advanced Functional Materials* 34 (2024): 2311727, https://doi.org/10.1002/adfm.202311727.

46. E. J. Juarez-Perez, L. K. Ono, M. Maeda, Y. Jiang, Z. Hawash, and Y. Qi, "Photodecomposition and thermal decomposition in methylammonium halide lead perovskites and inferred design principles to increase photovoltaic device stability," *Journal of Materials Chemistry A* 6 (2018): 9604–9612, https://doi.org/10.1039/C8TA03501F.

47. W. Yang, R. Shi, H. Lu, et al., "Revisiting the thermal decomposition mechanism of $MAPbI_3$," *Physical Chemistry Chemical Physics* 26 (2024): 17999–18005, https://doi.org/10.1039/D4CP01318B.

48. J. Su, Z. Yang, X. Li, et al., "Ion migration in p-type perovskite $MAPbI_3$films Under an electric field and thin-film transistor device failure," *Chemical Communications* 60 (2024): 10930–10933, https://doi.org/10.1039/D4CC03446E.

16136829, 0, Downloaded from https://onlinelibrary.wiley.com/doi/10.1002/smll.202514991 by Meicheng Li - North China Electric Power University Beijing , Wiley Online Library on [25/05/2026]. See the Terms and Conditions (https://onlinelibrary.wiley.com/terms-and-conditions) on Wiley Online Library for rules of use; OA articles are governed by the applicable Creative Commons License

49. M. Wang, C. Fei, H. Wang, et al., "Decoupling cation segregation and volatile loss in formamidinium–caesium metal halide perovskite solar cells Under high-temperature operating conditions," *Nature Energy* (2026), https://doi.org/10.1038/s41560-026-02011-y.

50. M. Long, T. Zhang, M. Liu, et al., "Abnormal synergetic effect of organic and halide ions on the stability and optoelectronic properties of a mixed perovskite via in situ characterizations," *Advanced Materials* 30 (2018): 1801562, https://doi.org/10.1002/adma.201801562.

51. J. Liu, H. Yao, S. Wang, C. Wu, L. Ding, and F. Hao, "Origins and suppression of Sn(II)/Sn(IV) oxidation in tin halide perovskite solar cells," *Advanced Energy Materials* 13 (2023): 2300696, https://doi.org/10.1002/aenm.202300696.

52. R. Cheacharoen, N. Rolston, D. Harwood, K. A. Bush, R. H. Dauskardt, and M. D. McGehee, "Design and understanding of encapsulated perovskite solar cells to withstand temperature cycling," *Energy & Environmental Science* 11 (2018): 144–150, https://doi.org/10.1039/C7EE02564E.

53. S. Ma, J. Tang, G. Yuan, et al., "Resist thermal shock Through viscoelastic interface encapsulation in perovskite solar cells," *Energy & Environmental Materials* 7 (2024): 12739, https://doi.org/10.1002/eem2.12739.

54. A. A. Samoylov, M. Dailey, Y. Li, P. J. Lohr, S. Raglow, and A. D. Printz, "Inelastic deformation in methylammonium lead iodide perovskite and mitigation by additives During thermal cycling," *ACS Energy Letters* 9 (2024): 2101–2108, https://doi.org/10.1021/acsenergylett.4c00587.

55. L. Wu, S. Hu, F. Yang, et al., "Resilience pathways for halide perovskite photovoltaics Under temperature cycling," *Nature Reviews Materials* 10 (2025): 536–549, https://doi.org/10.1038/s41578-025-00781-7.

56. S. Qu, F. Yang, H. Huang, et al., "Redox mediator-modified self-assembled monolayer stabilizes a buried interface in efficient inverted perovskite solar cells," *Energy & Environmental Science* 18 (2025): 3186–3195, https://doi.org/10.1039/D4EE05319B.

57. L. Wang, Z. Chen, and Y. Zhang, "Advanced passivation strategies for NiO/perovskite heterointerfaces: Toward efficient and stable monolithic tandem photovoltaics," *Nano Energy* 145 (2025): 111465, https://doi.org/10.1016/j.nanoen.2025.111465.

58. Y. Wu, L. Xu, J. Lv, et al., "Nickel oxide hole transport layers for efficient and stable perovskite solar cells: Recent progress and prospects," *Solar RRL* 10 (2025): 202500789.

59. J. Ji, X. Liu, H. Jiang, et al., "Two-stage ultraviolet degradation of perovskite solar cells induced by the oxygen vacancy-Ti^{4+} states," *iScience* 23 (2020): 101013.

60. S. Wang, Z. Huang, X. Wang, et al., "Unveiling the Role of tBP–LiTFSI Complexes in Perovskite Solar Cells," *Journal of the American Chemical Society* 140 (2018): 16720–16730, https://doi.org/10.1021/jacs.8b09809.

61. Y. Zheng, T. Niu, L. Chao, Y. Xia, and Y. Chen, "Stability of hole-selective self-assembled monolayers in inverted perovskite solar cells," *Journal of Energy Chemistry* 107 (2025): 74–86, https://doi.org/10.1016/j.jechem.2025.03.032.

62. B. Feng, W. Li, Z. Cui, et al., "ITO nanoparticles to stabilize the self-assembly of hole transport layer in inverted perovskite solar cells," *Advanced Materials* 38 (2025): 202517573.

63. F. Xia, X. Lin, J. Zhang, et al., "Three-dimensional molecular engineering of fluorene-based self-assembled monolayers for high-performance inverted perovskite solar cells," *Chemical Engineering Journal* 525 (2025): 170521, https://doi.org/10.1016/j.cej.2025.170521.

64. N. Ahn, K. Kwak, M. S. Jang, et al., "Trapped charge-driven degradation of perovskite solar cells," *Nature Communications* 7 (2016): 13422, https://doi.org/10.1038/ncomms13422.

65. N. Ahn and M. Choi, "Towards Long-Term Stable Perovskite Solar Cells: Degradation Mechanisms and Stabilization Techniques," *Advanced Science* 11 (2024): 2306110, https://doi.org/10.1002/advs.202306110.

66. Q. Jiang, Y. Zhao, X. Zhang, et al., "Surface passivation of perovskite film for efficient solar cells," *Nature Photonics* 13 (2019): 460–466, https://doi.org/10.1038/s41566-019-0398-2.

67. J. Hu, P. Chen, D. Luo, et al., "Anchoring of halogen-cleaved organic ligands on perovskite surfaces," *Energy & Environmental Science* 15 (2022): 5340–5349, https://doi.org/10.1039/D2EE02698H.

68. F. Pei, S. Lin, Z. Zhang, et al., "Inhibiting defect passivation failure in perovskite for perovskite/Cu(In,Ga)Se2 monolithic tandem solar cells With certified efficiency 27.35%.35%," *Nature Energy* 10 (2025): 824–835, https://doi.org/10.1038/s41560-025-01761-5.

69. M. Wang, Z. Shi, and C. Fei, "Ammonium cations With high pKa in perovskite solar cells for improved high-temperature photostability," *Nature Energy* 8 (2023): 1229–1239, https://doi.org/10.1038/s41560-023-01362-0.

70. M. V. Khenkin, E. A. Katz, A. Abate, et al., "Consensus statement for stability assessment and reporting for perovskite photovoltaics based on ISOS procedures," *Nature Energy* 5 (2020): 35.

71. J. Zhou, Y. Gao, Y. Pan, et al., "Recent Advances in the Combined Elevated Temperature, Humidity, and Light Stability of Perovskite Solar Cells," *Solar RRL* 6 (2022): 2200772, https://doi.org/10.1002/solr.202200772.

72. G. Niu, X. Guo, and L. Wang, "Review of recent progress in chemical stability of perovskite solar cells," *Journal of Materials Chemistry A* 3 (2015): 8970–8980, https://doi.org/10.1039/C4TA04994B.

73. T. Leijtens, G. E. Eperon, S. Pathak, A. Abate, M. M. Lee, and H. J. Snaith, "Overcoming ultraviolet light instability of sensitized TiO2 With meso-superstructured organometal tri-halide perovskite solar cells," *Nature Communications* 4 (2013): 2885, https://doi.org/10.1038/ncomms3885.

74. G. Niu, W. Li, F. Meng, L. Wang, H. Dong, and Y. Qiu, "Study on the stability of $CH_3NH_3PbI_3$ films and the effect of post-modification by aluminum oxide in all-solid-state hybrid solar cells," *Journal of Materials Chemistry A* 2 (2014): 705–710, https://doi.org/10.1039/C3TA13606J.

75. N. Aristidou, C. Eames, and I. Sanchez-Molina, "Fast oxygen diffusion and iodide defects mediate oxygen-induced degradation of perovskite solar cells," *Nature Communications* 8 (2017): 15218, https://doi.org/10.1038/ncomms15218.

76. L. Zhang and P. H. L. Sit, "Ab initio study of the role of oxygen and excess electrons in the degradation of $CH_3NH_3PbI_3$," *Journal of Materials Chemistry A* 5 (2017): 9042–9049, https://doi.org/10.1039/C7TA01091E.

77. Q. Li, S. Gaastra-Nedea, D. Smeulders, and S. Tao, "Accelerated formation of iodine vacancies in $CH_3NH_3PbI_3$ perovskites: The impact of oxygen and charges," *EcoMat* 5 (2023): 12320.

78. J. He, W.-H. Fang, R. Long, and O. V. Prezhdo, "Why oxygen increases carrier lifetimes but accelerates degradation of $CH_3NH_3PbI_3$ Under light irradiation: Time-domain ab initio analysis," *Journal of the American Chemical Society* 142 (2020): 14664–14673, https://doi.org/10.1021/jacs.0c06769.

79. G. Abdelmageed, L. Jewell, K. Hellier, et al., "Mechanisms for light induced degradation in $MAPbI_3$ perovskite thin films and solar cells," *Applied Physics Letters* 109 (2016): 233905, https://doi.org/10.1063/1.4967840.

80. S. Wang, Y. Jiang, E. J. Juarez-Perez, L. K. Ono, and Y. Qi, "Accelerated degradation of methylammonium lead iodide perovskites induced by exposure to iodine vapour," *Nature Energy* 2 (2017): 16195, https://doi.org/10.1038/nenergy.2016.195.

81. B. Chen, J. Song, and X. Dai, "Synergistic Effect of Elevated Device Temperature and Excess Charge Carriers on the Rapid Light-Induced Degradation of Perovskite Solar Cells," *Advanced Materials* 31 (2019): 1902413, https://doi.org/10.1002/adma.201902413.

82. G. Abdelmageed, C. Mackeen, K. Hellier, et al., "Effect of temperature on light induced degradation in methylammonium lead iodide perovskite

16136829, 0, Downloaded from https://onlinelibrary.wiley.com/doi/10.1002/smll.202514991 by Meicheng Li - North China Electric Power University Beijing , Wiley Online Library on [25/05/2026]. See the Terms and Conditions (https://onlinelibrary.wiley.com/terms-and-conditions) on Wiley Online Library for rules of use; OA articles are governed by the applicable Creative Commons License

thin films and solar cells," *Solar Energy Materials and Solar Cells* 174 (2018): 566–571, https://doi.org/10.1016/j.solmat.2017.09.053.

83. C.-J. Tong, W. Geng, Z.-K. Tang, et al., "Uncovering the veil of the degradation in perovskite $CH_3NH_3PbI_3$ upon humidity exposure: A first-principles study," *The Journal of Physical Chemistry Letters* 6 (2015): 3289–3295, https://doi.org/10.1021/acs.jpclett.5b01544.

84. B. P. Kore, M. Jamshidi, and J. M. Gardner, "The impact of moisture on the stability and degradation of perovskites in solar cells," *Materials Advances* 5 (2024): 2200–2217, https://doi.org/10.1039/D3MA00828B.

85. R. Azmi, S. Zhumagali, H. Bristow, et al., "Moisture-Resilient Perovskite Solar Cells for Enhanced Stability," *Advanced Materials* 36 (2024): 2211317, https://doi.org/10.1002/adma.202211317.

86. Z. Song, A. Abate, S. C. Watthage, et al., "Perovskite Solar Cell Stability in Humid Air: Partially Reversible Phase Transitions in the PbI 2 -CH 3 NH 3 I-H 2 O System," *Advanced Energy Materials* 6 (2016): 1600846, https://doi.org/10.1002/aenm.201600846.

87. X. Zeng, G. Xiao, R. Song, M. Zhang, and Y. Zhang, "Engineering organic inorganic hybrid surface networks for enhanced moisture and thermal stability in perovskite solar cells," *Applied Surface Science* 719 (2026): 165019, https://doi.org/10.1016/j.apsusc.2025.165019.

88. L. Shi, M. P. Bucknall, T. L. Young, et al., "Gas chromatography–mass spectrometry analyses of encapsulated stable perovskite solar cells," *Science* 368 (2020): aba2412, https://doi.org/10.1126/science.aba2412.

89. F. Fu, S. Pisoni, Q. Jeangros, et al., "I_2 vapor-induced degradation of formamidinium lead iodide based perovskite solar cells Under heat–light soaking conditions," *Energy & Environmental Science* 12 (2019): 3074–3088, https://doi.org/10.1039/C9EE02043H.

90. B. P. Finkenauer, K. M. Akriti, and L. Dou, "Degradation and self-healing in perovskite solar cells," *ACS Applied Materials & Interfaces* 14 (2022): 24073–24088, https://doi.org/10.1021/acsami.2c01925.

91. T. Zhang, X. Meng, Y. Bai, et al., "Profiling the organic cation-dependent degradation of organolead halide perovskite solar cells," *Journal of Materials Chemistry A* 5 (2017): 1103–1111, https://doi.org/10.1039/C6TA09687E.

92. Y. Yang, S. Cheng, X. Yang, et al., "Hafnium oxide interface stabilization for efficient, photothermally stable perovskite solar cells," *Science* 391 (2026): 926–930, https://doi.org/10.1126/science.aea3339.

93. T. Burwig, K. Heinze, and P. Pistor, "Thermal decomposition kinetics of $FAPbI_3$ thin films," *Physical Review Materials* 6 (2022): 065404, https://doi.org/10.1103/PhysRevMaterials.6.065404.

94. C. Zhu, X. Guo, S. Xiao, et al., "MA-activated lattice shrinkage and bandgap renormalization advancing the stability of FA1-MA PbI3 (x=0–1) perovskites photovoltaic," *Advanced Powder Materials* 4 (2025): 100264, https://doi.org/10.1016/j.apmate.2024.100264.

95. Y. Zhang, Y. Chen, G. Liu, et al., "Nonalloyed α-phase formamidinium lead triiodide solar cells Through iodine intercalation," *Science* 387 (2025): 284–290, https://doi.org/10.1126/science.ads8968.

96. C. Yi, J. Luo, S. Meloni, et al., "Entropic stabilization of mixed A-cation ABX_3 metal halide perovskites for high performance perovskite solar cells," *Energy & Environmental Science* 9 (2016): 656–662, https://doi.org/10.1039/C5EE03255E.

97. Z. Li, M. Yang, J.-S. Park, S.-H. Wei, J. J. Berry, and K. Zhu, "Stabilizing perovskite structures by tuning tolerance factor: Formation of formamidinium and cesium lead iodide solid-state alloys," *Chemistry of Materials* 28 (2016): 284–292, https://doi.org/10.1021/acs.chemmater.5b04107.

98. S. Li, Y. Jiang, J. Xu, et al., "High-efficiency and thermally stable $FACsPbI_3$ perovskite photovoltaics," *Nature* 635 (2024): 82–88, https://doi.org/10.1038/s41586-024-08103-7.

99. D. Liu, Q. Li, and K. Wu, "Ethylammonium as an alternative cation for efficient perovskite solar cells from first-principles calculations," *RSC Advanced* 9 (2019): 7356.

100. W. Peng, X. Miao, V. Adinolfi, et al., "Engineering of CH_3 NH_3 PbI_3 Perovskite Crystals by Alloying Large Organic Cations for Enhanced Thermal Stability and Transport Properties," *Angewandte Chemie International Edition* 55 (2016): 10686–10690, https://doi.org/10.1002/anie.201604880.

101. M. Saliba, T. Matsui, J.-Y. Seo, et al., "Cesium-containing triple cation perovskite solar cells: Improved stability, reproducibility and high efficiency," *Energy & Environmental Science* 9 (2016): 1989–1997, https://doi.org/10.1039/C5EE03874J.

102. M. Saliba, T. Matsui, K. Domanski, et al., "Incorporation of rubidium cations into perovskite solar cells improves photovoltaic performance," *Science* 354 (2016): 206.

103. P. Yadav, M. I. Dar, and N. Arora, "The Role of Rubidium in Multiple-Cation-Based High-Efficiency Perovskite Solar Cells," *Advanced Materials* 29 (2017): 1701077, https://doi.org/10.1002/adma.201701077.

104. T. Duong, Y. Wu, H. Shen, et al., "Rubidium Multication Perovskite With Optimized Bandgap for Perovskite-Silicon Tandem With Over 26% Efficiency," *Advanced Energy Materials* 7 (2017): 1700228, https://doi.org/10.1002/aenm.201700228.

105. L. Flannery, J. Ogle, D. Powell, C. Tassone, and L. Whittaker-Brooks, "Voltage bias stress effects in metal halide perovskites are strongly dependent on morphology and ion migration pathways," *Journal of Materials Chemistry A* 8 (2020): 25109–25119, https://doi.org/10.1039/D0TA10371C.

106. Y. Zou, J. Eichhorn, S. Rieger, et al., "Ionic liquids tailoring crystal orientation and electronic properties for stable perovskite solar cells," *Nano Energy* 112 (2023): 108449, https://doi.org/10.1016/j.nanoen.2023.108449.

107. C. Kang, H. Rao, J. Fan, X. Zhong, and Z. Pan, "Facet orientation control enables inorganic perovskite With superior photoelectric properties," *Chemical Engineering Journal* 503 (2025): 159095, https://doi.org/10.1016/j.cej.2024.159095.

108. C. Ma, M.-C. Kang, and S.-H. Lee, "Photovoltaically top-performing perovskite crystal facets," *Joule* 6 (2022): 2626–2643, https://doi.org/10.1016/j.joule.2022.09.012.

109. F. Gao, P. Zhao, X. Qin, and Z. Zhao, "Crystal facet engineering in perovskite photovoltaics: The rise of (111)-oriented structures," *Frontiers in Chemistry* 13 (2025): 1692350, https://doi.org/10.3389/fchem.2025.1692350.

110. B. Zhou, P. Zhao, and J. Guo, "Solvent-additive cascade engineering enables single-oriented perovskite films With facet-driven performance and stability," *Energy & Environmental Science* 18 (2025): 9865–9876, https://doi.org/10.1039/D5EE04415D.

111. S. Qu, H. Huang, J. Wang, et al., "Revealing and Inhibiting the Facet-related Ion Migration for Efficient and Stable Perovskite Solar Cells," *Angewandte Chemie International Edition* 64 (2025): 202415949, https://doi.org/10.1002/anie.202415949.

112. X. Liu, X. Jiang, Y. Yin, et al., "Dominating (111) facets With ordered stacking in perovskite films," *Energy Environmental Science* 17 (2024): 6058.

113. M. Li, Y. Jiang, S. Chen, et al., "Radical Molecular Network-Buffer Minimizes Photovoltage Loss in $FAPbI_3$ Perovskite Solar Cells," *Advanced Materials* 37 (2025): 2417289, https://doi.org/10.1002/adma.202417289.

114. W. Li, S. Ding, M. Hao, L. Wang, and J. Etheridge, "Discovery of twin Defects in hybrid perovskite nanocrystals: Atomic structure and impact on photovoltaic performance and stability," *ACS Nano* 19 (2025): 35037–35049, https://doi.org/10.1021/acsnano.5c12005.

115. F. Gao, H. Li, B. Jiao, et al., "Perovskite facet heterojunction solar cells," *Joule* 9 (2025): 101787, https://doi.org/10.1016/j.joule.2024.11.004.

116. J. Li, J. Duan, C. Zhang, et al., "Facet-orientation-enhanced thermal transfer for temperature-insensitive and stable pin perovskite solar cells," *eScience* 5 (2025): 100372.

117. T. L. Leung, I. Ahmad, A. A. Syed, A. M. C. Ng, J. Popović, and A. B. Djurišić, "Stability of 2D and quasi-2D perovskite materials and devices,"

16136829, 0, Downloaded from https://onlinelibrary.wiley.com/doi/10.1002/smll.202514991 by Meicheng Li - North China Electric Power University Beijing , Wiley Online Library on [25/05/2026]. See the Terms and Conditions (https://onlinelibrary.wiley.com/terms-and-conditions) on Wiley Online Library for rules of use; OA articles are governed by the applicable Creative Commons License

Communications Materials 3 (2022): 63, https://doi.org/10.1038/s43246-022-00285-9.

118. F. Cao, P. Zhang, and L. Li, "Multidimensional perovskite solar cells," *Fundamental Research* 2 (2022): 237–253, https://doi.org/10.1016/j.fmre.2021.07.003.

119. I. C. Smith, E. T. Hoke, D. Solis-Ibarra, M. D. McGehee, and H. I. Karunadasa, "A Layered Hybrid Perovskite Solar-Cell Absorber With Enhanced Moisture Stability," *Angewandte Chemie International Edition* 53 (2014): 11232–11235, https://doi.org/10.1002/anie.201406466.

120. C. Wang, X. Dong, F. Chen, G. Liu, and H. Zheng, "Recent progress of two-dimensional Ruddlesden–Popper perovskites in solar cells," *Materials Chemistry Frontiers* 7 (2023): 5786–5805, https://doi.org/10.1039/D3QM00547J.

121. Z. Xu, Y. Zhou, C. Gong, et al., "Double amidino-mediated multiple hydrogen-bonded Dion–Jacobson perovskites enable oriented crystallization for efficient inverted FAPbI 3 solar cells and modules (642 cm 2)," *Energy & Environmental Science* 18 (2025): 8268–8279, https://doi.org/10.1039/D5EE01101A.

122. G. Chen, Y. Gan, S. Wang, et al., "Dicyandiamide-Driven Tailoring of the n-Value Distribution and Interface Dynamics for High-Performance ACI 2D Perovskite Solar Cells," *Nano-Micro Letters* 17 (2025): 305, https://doi.org/10.1007/s40820-025-01817-x.

123. L. Hu, H. Li, B. Xu, et al., "Assembling the 2D–3D–2D Heterostructure of Quasi-2D Perovskites for High-Performance Solar Cells," *ACS Applied Materials & Interfaces* 16 (2024): 42221–42229, https://doi.org/10.1021/acsami.4c08198.

124. W. Zhang, Z. Liu, L. Zhang, et al., "Ultrastable and efficient slight-interlayer-displacement 2D Dion-Jacobson perovskite solar cells," *Nature Communications* 15 (2024): 5709, https://doi.org/10.1038/s41467-024-50018-4.

125. F. Wu, Y. Gao, Y. Zeng, et al., "Quasi-pure-phase 2D perovskites for high-efficiency and stable 2D/3D perovskite heterojunction solar cells," *Chemical Engineering Journal* 523 (2025): 168799, https://doi.org/10.1016/j.cej.2025.168799.

126. Y. Xiong, M. Li, and L. Peng, "Highly Efficient and Stable 2D/3D Heterojunction Perovskite Solar Cells by In Situ Interface Modification With [(p -Fluorophenyl)ethyl]ammonium Acetate," *ACS Applied Materials & Interfaces* 15 (2023): 15420–15428, https://doi.org/10.1021/acsami.2c22212.

127. S. Tan, M.-C. Shih, Y. Lu, et al., "Spontaneous formation of robust two-dimensional perovskite phases," *Science* 388 (2025): 639–645, https://doi.org/10.1126/science.adr1334.

128. Z. Liu, B. Chang, S. Ma, et al., "Organic layer bridged 3D/2D perovskite heterojunction for efficient and stable all-perovskite tandem solar cells," *Advanced Materials* 38 (2025): 2512874.

129. X. Li, S. Aftab, S. Hussain, et al., "Dimensional diversity (0D, 1D, 2D, and 3D) in perovskite solar cells: Exploring the potential of mixed-dimensional integrations," *Journal Materials Chemistry A* 12 (2024): 4421.

130. S. Sun, M. Lu, and X. Gao, "0D perovskites: Unique properties, synthesis, and their applications," *Advanced Science* 8 (2021): 2102689, https://doi.org/10.1002/advs.202102689.

131. L. Liang, Z.-A. Nan, Y. Li, et al., "Formation dynamics of thermally stable 1D/3D perovskite interfaces for high-performance photovoltaics," *Advanced Materials* 37 (2025): 2413841.

132. Y. Shen, T. Zhang, G. Xu, et al., "Strain regulation retards natural operation decay of perovskite solar cells," *Nature* 635 (2024): 882–889, https://doi.org/10.1038/s41586-024-08161-x.

133. M. T. Mbumba, D. M. Malouangou, J. M. Tsiba, L. Bai, Y. Yang, and M. Guli, "Degradation mechanism and addressing techniques of thermal instability in halide perovskite solar cells," *Solar Energy* 230 (2021): 954–978, https://doi.org/10.1016/j.solener.2021.10.070.

134. Y. S. Shin, J. W. Song, D. G. Lee, et al., "De-doping engineering for efficient and heat-stable perovskite solar cells," *Joule* 9 (2025): 101779.

135. J. Feng, W. Shi, X. Wang, et al., "Heat-dissipation regulation for improving the thermal stability and efficiency of planar perovskite solar cells," *Journal Materials Chemical C* 13 (2025): 9632.

136. S. Tan, C. Li, C. Peng, et al., "Sustainable thermal regulation improves stability and efficiency in all-perovskite tandem solar cells," *Nature Communications* 15 (2024): 4136, https://doi.org/10.1038/s41467-024-48552-2.

137. M. Chen, Y. Dong, Y. Zhang, et al., "Stress engineering for mitigating thermal cycling fatigue in perovskite photovoltaics," *ACS Energy Letters* 9 (2024): 2582.

138. C. Liu, Y. Yang, H. Chen, et al., "Two-dimensional perovskitoids enhance stability in perovskite solar cells," *Nature* 633 (2024): 359–364, https://doi.org/10.1038/s41586-024-07764-8.

139. G. Li, Z. Su, L. Canil, et al., "Highly efficient p-i-n perovskite solar cells that endure temperature variations," *Science* 379 (2023): 399–403, https://doi.org/10.1126/science.add7331.

140. L. Ren, P. Huang, and W. Chen, "Reversible thermally driven phenyl torsion in self-assembled monolayers releases strain for heat-resilient inverted perovskite solar cell," *Angewandte Chemie International Edition* 65 (2025): 202521774.

141. Y. Tang, Z. Zhang, G. Li, et al., "Heat-Triggered Dynamic Self-Healing Framework for Variable-Temperature Stable Perovskite Solar Cells," *Advanced Materials* 37 (2025): 2420378, https://doi.org/10.1002/adma.202420378.

142. W. Yang, D. Zhong, M. Shi, S. Qu, and H. Chen, "Toward highly thermal stable perovskite solar cells by rational design of interfacial layer," *iScience* 22 (2019): 534.

143. D.-J. Xue, Y. Hou, S.-C. Liu, et al., "Regulating strain in perovskite thin films Through charge-transport layers," *Nature Communications* 11 (2020): 1514, https://doi.org/10.1038/s41467-020-15338-1.

144. S. Qu, C. Sun, F. Yang, et al., "Contextualized synthesis of phenanthroline-based isomeric linkers at heterointerfaces enables stable inverted perovskite solar cells," *Matter* 9 (2025): 102525.

145. W. Zhang, L. He, Y. Zhou, et al., "Multiple roles of negative thermal expansion material for high-performance fully-air processed perovskite solar cells," *Chemical Engineering Journal* 457 (2023): 141216, https://doi.org/10.1016/j.cej.2022.141216.

146. J. Gao, J. Wu, D. Wei, et al., "Pseudo-arch bridge-inspired stress modulation at buried interface for stable high-efficiency perovskite solar cells," *Advanced Materials* 37 (2025): 2513975.

147. H. Kim, C. A. Figueroa Morales, S. Seong, et al., "Molecular design of defect passivators for thermally stable metal-halide perovskite films," *Matter* 7 (2024): 539.

148. Z. Lan, Y. Yang, H. Huang, et al., "Interfacial electrostatic repulsion inhibits iodide ion migration for enhancing reverse-bias stability of perovskite solar cells," *Nature Communications* 16 (2025): 11407, https://doi.org/10.1038/s41467-025-66224-7.

149. Y. Zhong, J. Yang, and X. Wang, "Inhibition of ion migration for highly efficient and stable perovskite solar cells," *Advanced Materials* 35 (2023): 2302552, https://doi.org/10.1002/adma.202302552.

150. H. Zai, Y. Ma, Q. Chen, and H. Zhou, "Ion migration in halide perovskite solar cells: Mechanism, characterization, impact and suppression," *Journal of Energy Chemistry* 63 (2021): 528–549, https://doi.org/10.1016/j.jechem.2021.08.006.

151. S. Wang, A. Wang, X. Deng, et al., "Lewis acid/base approach for efficacious defect passivation in perovskite solar cells," *Journal of Materials Chemistry A* 8 (2020): 12225.

152. C. Li, X. Wang, E. Bi, et al., "Rational design of Lewis base molecules for stable and efficient inverted perovskite solar cells," *Science* 379 (2023): 690–694, https://doi.org/10.1126/science.ade3970.

153. W.-T. Wang, P. Holzhey, N. Zhou, et al., "Water-and heat-activated dynamic passivation for perovskite photovoltaics," *Nature* 632 (2024): 294.

16136829, 0, Downloaded from https://onlinelibrary.wiley.com/doi/10.1002/smll.202514991 by Meicheng Li - North China Electric Power University Beijing , Wiley Online Library on [25/05/2026]. See the Terms and Conditions (https://onlinelibrary.wiley.com/terms-and-conditions) on Wiley Online Library for rules of use; OA articles are governed by the applicable Creative Commons License

154. H. Guo, X. Wang, C. Li, et al., "Immobilizing surface halide in perovskite solar cells via calix [4]pyrrole," *Advanced Materials* 35 (2023): 2301871, https://doi.org/10.1002/adma.202301871.

155. S. Cai, J. Gao, Y. Wu, et al., "Rational Tailored Polyfluorosubstituted Amide Molecule for Stabilizing PbI 6 Framework and Inhibiting Ion Migration Toward Highly Efficient and Stable Perovskite Solar Cells," *Advanced Functional Materials* 34 (2024): 2411014, https://doi.org/10.1002/adfm.202411014.

156. S. Du, H. Huang, Z. Lan, et al., "Inhibiting perovskite decomposition by a creeper-inspired strategy enables efficient and stable perovskite solar cells," *Nature Communications* 15 (2024): 5223, https://doi.org/10.1038/s41467-024-49617-y.

157. D. He, D. Ma, J. Zhang, et al., "Universal Ion Migration Suppression Strategy Based on Supramolecular Host–Guest Interaction for High-Performance Perovskite Solar Cells," *Advanced Materials* 37 (2025): 2505115, https://doi.org/10.1002/adma.202505115.

158. S. Yang, S. Chen, E. Mosconi, et al., "Stabilizing halide perovskite surfaces for solar cell operation With wide-bandgap lead oxysalts," *Science* 365 (2019): 473–478, https://doi.org/10.1126/science.aax3294.

159. Y. Xu, S. Wang, H. Liu, and X. Li, "Microencapsulated Perovskite Crystals via In Situ Permeation Growth From Polymer Microencapsulation-Expansion-Contraction Strategy: Advancing a Record Long-Term Stability Beyond 10 000 h for Perovskite Solar Cells," *Advanced Materials* 36 (2024): 2313080, https://doi.org/10.1002/adma.202313080.

160. Z. Dong, J. Men, B. Zhang, et al., "Grain boundary defect passivation and iodine migration inhibition for efficient and stable perovskite solar cells," *Electrochimica Acta* 507 (2024): 145129, https://doi.org/10.1016/j.electacta.2024.145129.

161. N. Yadav and A. Khare, "Resolving interfacial challenges in perovskite solar cells: From defect control to energy band optimization," *Surface Interface* 56 (2025): 105593.

162. M. H. Miah, M. B. Rahman, M. Nur-E-Alam, et al., "Key degradation mechanisms of perovskite solar cells and strategies for enhanced stability: Issues and prospects," *RSC Advanced* 15 (2025): 628.

163. H. Jiao, Z. Ni, and Z. Shi, "Perovskite grain wrapping by converting interfaces and grain boundaries Into robust and water-insoluble low-dimensional perovskites," *Science Advances* 8 (2022): abg4524, https://doi.org/10.1126/sciadv.abq4524.

164. L. Zhao, P. Tang, D. Luo, et al., "Enabling full-scale grain boundary mitigation in polycrystalline perovskite solids," *Science Advances* 8 (2022): abo3733, https://doi.org/10.1126/sciadv.abo3733.

165. Y. Ma, C. Liu, M. Zhang, and Y. Mai, "Review on the effects of solvent physical properties on the performance of slot-die coated perovskite solar cells," *Surface Science and Technology* 2 (2024): 25, https://doi.org/10.1007/s44251-024-00054-5.

166. Y. Gou, S. Tang, C. Yuan, P. Zhao, J. Chen, and H. Yu, "Research progress of green antisolvent for perovskite solar cells," *Materials Horizons* 11 (2024): 3465–3481, https://doi.org/10.1039/D4MH00290C.

167. H. Wang, F. Ye, J. Liang, et al., "Pre-annealing treatment for high-efficiency perovskite solar cells via sequential deposition," *Joule* 6 (2022): 2869–2884, https://doi.org/10.1016/j.joule.2022.10.001.

168. Z. Iqbal, R. Félix, A. Musiienko, et al., "Unveiling the Potential of Ambient Air Annealing for Highly Efficient Inorganic CsPbI 3 Perovskite Solar Cells," *Journal of the American Chemical Society* 146 (2024): 4642–4651, https://doi.org/10.1021/jacs.3c11711.

169. Y. Wang, Y. Liu, X. Luo, et al., "Improved solvent systems for commercially viable perovskite photovoltaic modules," *Science* 390 (2025): 1021–1028, https://doi.org/10.1126/science.adz0091.

170. S. Sanchez, X. Hua, N. Phung, U. Steiner, and A. Abate, "Flash Infrared Annealing for Antisolvent-Free Highly Efficient Perovskite Solar Cells," *Advanced Energy Materials* 8 (2018): 1702915, https://doi.org/10.1002/aenm.201702915.

171. A. H. Ghahremani, B. Martin, A. Gupta, J. Bahadur, K. Ankireddy, and T. Druffel, "Rapid fabrication of perovskite solar cells Through intense pulse light annealing of SnO_2 and triple cation perovskite thin films," *Materials & Design* 185 (2020): 108237, https://doi.org/10.1016/j.matdes.2019.108237.

172. J. Hu, Q. Cai, Y. Lin, et al., "Molecular press annealing enables robust perovskite solar cells," *Science* 391 (2026): 164–170, https://doi.org/10.1126/science.aea8228.

173. G. Perrakis, A. C. Tasolamprou, G. Kenanakis, E. N. Economou, S. Tzortzakis, and M. Kafesaki, "Submicron Organic–Inorganic Hybrid Radiative Cooling Coatings for Stable, Ultrathin, and Lightweight Solar Cells," *ACS Photonics* 9 (2022): 1327–1337, https://doi.org/10.1021/acsphotonics.1c01935.

174. Z. Wan, R. Wei, and H. Zhao, "Thermal management technologies for improving the thermal stability of perovskite solar cells," *Nano-Micro Letters* 18 (2026): 207, https://doi.org/10.1007/s40820-025-02047-x.

175. Z. Liu, B. Sun, and Y. Zhong, "Novel integration of carbon counter electrode based perovskite solar cell With thermoelectric generator for efficient solar energy conversion," *Nano Energy* 38 (2017): 457–466, https://doi.org/10.1016/j.nanoen.2017.06.016.

176. Q. Zhao, Z. Zhao, H. Zhang, and M. Ni, "Radiative-cooling-enabled hybrid perovskite solar cell-thermoelectric system: Modeling, optimization, and performance insights," *Energy Conversion and Management* 352 (2026): 121132, https://doi.org/10.1016/j.enconman.2026.121132.

177. W. Yang, Y. Zhang, C. Xiao, J. Yang, and T. Shi, "A review of encapsulation methods and geometric improvements of perovskite solar cells and modules for mass production and commercialization," *Nano Materials Science* 7 (2025): 790–809, https://doi.org/10.1016/j.nanoms.2025.02.005.

178. S. Ma, G. Yuan, Y. Zhang, N. Yang, Y. Li, and Q. Chen, "Development of encapsulation strategies towards the commercialization of perovskite solar cells," *Energy Environmental Science* 15 (2022): 13.

179. P. Mariani, M. Á. Molina-García, J. Barichello, et al., "Low-temperature strain-free encapsulation for perovskite solar cells and modules passing multifaceted accelerated ageing tests," *Nature Communications* 15 (2024): 4552, https://doi.org/10.1038/s41467-024-48877-y.

16136829, 0, Downloaded from https://onlinelibrary.wiley.com/doi/10.1002/smll.202514991 by Meicheng Li - North China Electric Power University Beijing , Wiley Online Library on [25/05/2026]. See the Terms and Conditions (https://onlinelibrary.wiley.com/terms-and-conditions) on Wiley Online Library for rules of use; OA articles are governed by the applicable Creative Commons License